WAVE-INDUCED LOADING OF SUBMERGED CORE-LOC ARMOUR UNITS

TOMASZ KOZLOWSKI

Thesis submitted to the University of Ottawa
in partial Fulfillment of the requirements for the degree of
Master of Applied Science

Department of Civil Engineering
Faculty of Engineering
University of Ottawa

ABSTRACT

This study investigates the relationship between wave-induced hydrodynamics and the resulting loading on Core-Loc concrete armour units below the still water level in a breakwater structure.

Physical modelling experiments were performed at the National Research Council in Ottawa in which a 3D-printed 12 cm Core-Loc armour unit was instrumented and fixed in place within a rubble mound structure.

Testing featured simultaneous measurement of force on this instrumented unit, pressure head at the base of the unit, and flow velocities below the SWL. Two main scenarios were tested, the isolated unit and fully armoured scenarios, under a range of regular waves and irregular sea states.

Analysis of force development on the instrumented unit indicates that maximum slope-normal forces (both into and away from the structure) are associated with extremes in pressure head above the instrumented unit, while slope-parallel force extremes (both upslope and downslope) occur at times of the fastest change in water level. These loadings are consistent with Morison's equation and imply drag dominance in the slope-parallel direction and inertia dominance in the slope-normal direction. Significant differences in forces were observed between isolated (no neighbouring units) and embedded (with neighbouring units) armour unit test cases. The presence of the armour layer significantly increased the normal force exerted on the unit and reduced the parallel force. Irregular sea state testing shows force peaks following normal distribution.

Analysis of flow above the armour layer showed that force, flow velocity and flow acceleration are symmetrical in the slope-parallel direction, but largely asymmetrical in the slope-normal direction, with the flow velocity and force on the unit in particular experiencing large asymmetries. Wave height analysis indicated that each wave height follows a similar force development pattern with a magnitude proportional to wave height. Wave period analysis showed the formation of small secondary waves as the period increases. Wave steepness affected the peak force loading of the instrumented unit in a mostly linear fashion up to the critical Iribarren number.

ACKNOWLEDGEMENTS

I wish to express my sincere gratitude to my supervisors, Dr. Ioan Nistor and Dr. Andrew Cornett. Their persistent support, guidance, and experience were essential to the realization of this project. I am grateful for their leadership, technical expertise, and attention to detail, without which the goals of this project would not have been realized.

I would like to acknowledge as well the work of the project team that preceded me and with whom I was afforded the privilege of working alongside, including Steven Douglas, Derek Eden, Adrian Simpalean, as well as colleagues at Imperial College London.

This research was conducted at the National Research Council of Canada's Ocean, Coastal and River Engineering Research Centre. The assistance of the technical staff at NRC-OCRE is acknowledged with appreciation. This study would not have been possible without the support of Baird & Associates, as well as grant funding received for the project from NSERC-CRD.

Additionally, while not directly related to this thesis, I would like to thank Drs Hofland and Bricker for hosting me at TU Delft during the summer of 2019.

Finally, I would like to thank my friends, family, and in particular my fiancée Brenda, for their unwavering support throughout the course of this study.

Table of Contents

TABLE OF FIGURES

TABLE OF TABLES

LIST OF SYMBOLS

Symbol	Description	Units (SI)
a	Van der Meer empirical parameter	-
A	Area	m^2
b	Van der Meer empirical parameter	-
B	Crest width	m
B_t	Breakwater berm width	m
C	Characteristic length	m
C_d	Drag coefficient	-
C_L	Lift coefficient	-
C_m	Inertia coefficient	-
C_s	Surging coefficient	-

d	Water depth	m
D_n	Nominal armour unit diameter	m
D_{n50}	Nominal armour stone diameter, 50% cumulative distribution	m
F	Force	N
F_D	Drag force	
F_g	Force of gravity	N
F_i	Interlocking force	N
F_I	Inertia force	N
F_s	Seepage force	N
F_x	Slope-parallel force	N
F_y	Slope-transverse force	N
F_z	Slope-normal force	N
g	Acceleration due to gravity	m/s^2
h	Water depth	m
h_l	Breakwater leeward berm or shoulder level	m
h_t	Seaward toe level	m
H	Wave height	m
H_d	Design wave height	m
H_s	Significant wave height	m
$H_{s,toe}$	Significant wave height at breakwater toe	m
$H_{1/3}$	Statistical significant wave height	m
H_{m0}	Spectral significant wave height	m
K_C	Keulegan-Carpenter number	-
K_D	Hudson's equation empirical parameter	-
L	Wavelength	m
L_0	Deep-water wavelength	m
N	Number of waves	-
n	Number of layers	-
N_a	Packing density	$1/m^2$
N_d	Damage number	-
N_{od}	Number of displaced units per D_n	-
N_s	Stability number	-
n_v	Armour layer porosity	-
N_x	Number of units in x-direction	-
N_y	Number of units in y-direction	-
P	Notional breakwater permeability	-
p	Pressure	Pa
R_c	Crest freeboard	m
R_D	Run-down height	m
R_U	Run-up height	m
s	Fictitious wave steepness	-
S	Damage level	-
S_s, S_t	Breakwater shoulder width	m
S_{om}	Deep-water wave steepness using T_m	-
T	Wave period	s
t	Time	s
t_a	Armour layer thickness	m
t_u	Underlayer thickness	m

T_m	Mean wave period	s
T_p	Spectral peak wave period	s
u	Inline water velocity	m/s
$\dot{u}$	Inline water acceleration	m/s^2
v	Perpendicular water velocity	m/s
v_x, v_p	Velocity, slope-parallel	m/s
v_z	Velocity, slope-normal	m/s
V_A	Volume of armour unit	m^3
W	Armour unit weight	N
W'	Submerged armour unit weight	N
α	Slope angle	Degrees
Δ	Relative submerged armour unit density	-
μ	Dynamic viscosity	Ns/m^2
ξ	Iribarren number	-
ξ_{cr}	Critical Iribarren number	-
ξ_0	Deepwater Iribarren number	-
ρ_a	Armour unit density	kg/m^3
ρ_r	Rock density	kg/m^3
ρ_w	Water density	kg/m^3
σ	Surface tension coefficient	N/m
γ_a	Specific weight of armour unit	N/m^3
γ_w	Specific weight of water	N/m^3
ϕ	Packing density	-
ω	Wave frequency	Hz

LIST OF ABBREVIATIONS AND ACRONYMS

ADV	Acoustic Doppler velocimeter
CAU	Concrete armour unit
CDF	Cumulative distribution function
CLI	Concrete Layer Innovations
JONSWAP	Joint North Sea Wave Project
NRC-OCRE	National Research Council – Ocean and River Engineering Research Centre
P-P	Probability-probability
PVC	Polyvinyl chloride
Q-Q	Quantile-quantile
R	R (programming language)
SMU	Sloped multi-unit test
SSU	Sloped single-unit test
SWF	Steel wave flume
SWL	Still water level
USACE	United States Army Corps of Engineers
WG	Wave gauge

1 INTRODUCTION

Rubble-mound structures are coastal works that operate as artificial barriers to waves and wave-induced currents. These may take a wide range of shapes depending on the coastal application of the structure, such as offshore breakwaters that protect the entrance of a harbour from open ocean waves, reducing wave agitation and allowing for safe navigation, or coastal revetments that dissipate wave energy on a shoreline, reducing coastal erosion and wave-driven coastal flooding. In general, rubble-mound structures function to provide a reduced energy environment on its lee side. Figure 1-1 shows two such applications – harbour protection and shoreline erosion control.

Figure 1-1: Shore connected breakwater and rubble-mound revetment, Port St. Francis, South Africa[1]

The most critical element of a rubble-mound structure is the outermost layer, called the armour layer. This layer is comprised of natural rock or cast concrete, called armour units, which primarily rely on their mass and geometry for stability. These have historically been comprised of angular rock, but in recent decades concrete armour units (CAUs) have been developed for use when rock armouring is not appropriate, such as in high wave energy environments, or in rock-poor locations where rock armour units are not available of adequate size. Rock armour units are generally laid in at least two layers, while

[1] www.core-loc-africa.com/htm/welcome.htm

CAUs may be single or double-layered. Figure 1-2 shows the cross-section of a conventional rubble-mound breakwater.

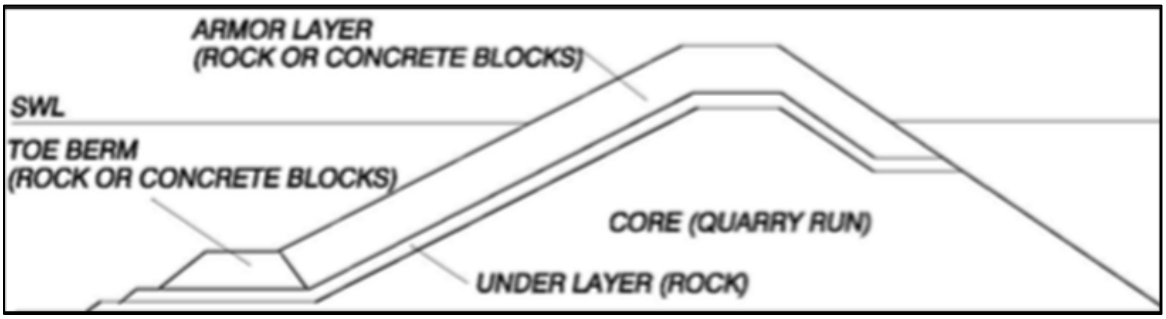

Figure 1-2. Conventional rubble mound breakwater cross-section (USACE, 2006)

Many CAUs have been developed historically. In the 1990s, the United States Army Corps of Engineers developed the Core-Loc as a replacement for, and improvement upon, the highly interlocking Dolos CAU (Melby and Turk, 1997). This CAU differs from rock armour units in its ability to provide stability not only in its weight, as with rock armouring, but due to its interlocking design as well. This interlocking allows for very high resistance to wave impacts compared to traditional rock armouring. Since its introduction, the Core-Loc has been used in thousands of projects around the world. It is the widespread usage of the Core-Loc unit that provides motivation for the present study focus.

Design of concrete armoured rubble-mound structures has followed the same process for decades: a combination of semi-empirical design formulae, engineering experience, and for important projects hydraulic model testing. Computational power has increased rapidly in recent years, as has efficiency of computational hydrodynamics. Currently there are no commercially available numerical models for the design of interlocking concrete armour units that consider armour layer hydrodynamics.

The majority of incident wave energy is dissipated within the armour layer of a rubble-mound structure. The mechanism for this dissipation is through the generation of turbulence by inducing wave breaking, flow over the rough armour layer, and flow through the armour layer void spaces. Damage and potential failure to the rubble-mound structure occurs when this flow is powerful enough to displace individual armour units, exposing the easily eroded underlayers to wave action. The complex relationship between incident wave hydrodynamics and this potentially damaging flow is not well understood. Nor is the complex destabilizing flow within an armour layer, the interaction between units, as well as between units and the under-layer. The physical environment of an armour layer under wave action is complex and estimation of the forces exerted on individual armour units is beyond current engineering capabilities.

1.1 Research Needs

The principal motivation of the current study is to develop greater understanding of wave-induced forces exerted on single-layer concrete armour units. The research is focused on the critical region of highest destabilizing outward force on these units and responds to a lack of physical modelling research considering this area. A better understanding of the forces exerted on breakwater armour units, as well as relationships between measurable sea state parameters and induced armour unit forcing, may lead to more reliable design methodologies. These improved design methodologies can become more

efficient in their use of emissions-heavy concrete construction, and in the efficiency of rubble mound structures which provide safe navigation as well as flood and erosion protection.

A secondary research motivation for the present study is in the generation of calibration data for use in future numerical models. Detailed measurements of fluid-structure interaction and armour unit forcing is crucial for the calibration of future models and the validation of their results.

Research motivation is discussed further in Section 2.4.

1.2 SCOPE

The primary objective of this research is the examination of the loading of an individual Core-Loc concrete armour unit embedded within the armour layer of a rubble mound breakwater.

To achieve this objective, a series of detailed experimental investigations were designed to investigate the hydrodynamics of Core-Loc armour units under diverse flow conditions at the National Research Council's Ocean, Coastal and River Engineering Research Centre (NRC-OCRE).

A 3D-printed Core-Loc unit was manufactured for use by the project team. Details of which can be found in Eden (2019). This unit was fixed to an artificial slope in the NRC-OCRE Steel Wave Flume (SWF) by a force transducer below the still water level (SWL). The slope was also instrumented with multiple pressure sensors and velocity was measured with an acoustic doppler velocimeter (ADV).

Tests were carried out with this setup under a variety of wave climates, and velocities, pressures and forces on the unit were recorded. The idealized breakwater conditions varied in terms of depth of filter layer from an impermeable PVC board to a layer of typical filter stone the thickness of one armour unit. Tests were also run with the instrumented armour unit embedded within an armour layer of units as would typically be constructed, as well as an isolated unit to examine the effect of the armouring on the individual unit.

This data was then analyzed to examine the loading of the instrumented unit and to determine relationships between loading and design parameters.

This research program focused on the physical modelling of a Core-Loc single-layer rubble mound structure. Limitations of the program include:

- Only one rubble mound slope was investigated. This is a typical slope found in the field, though the examination of other slopes would allow a better correlation between loading findings and Iribarren number.
- The porosity of the breakwater core is zero, where a prototype breakwater would have a low but non-zero porosity. This prevents transmission through the structure and increases the loading due to reflection.
- The scale of the instrumented unit is very large. This is beneficial for reducing scale effects but required the custom manufacture of over 100 large scale armour units. Miniaturizing of the instrumented unit would allow for standard 4 cm model armour units.

1.3 Novelty and Contributions

The novelty of this study comes from the detailed investigation of the hydrodynamic behaviour of Core-loc armour units. To the knowledge of the author, no other study involving the instrumentation of Core-loc units with load cells under wave loading has been previously performed. Similar studies have been performed in the past for rock armoured rubble mound structures, though their mechanism of stability is different.

The author joined an on-going project, which had in large measure already been planned by the project team. The main contributions of the author of this thesis includes the set up and manufacture of experimental equipment, and execution of the project program with the NRC-OCRE staff and the project team, involving hundreds of hours in the laboratory. Upon completion of the experimental program, data was divided among the project team. This thesis is concerned primarily with data collected at a location below the still water level, though other locations were investigated by other members of the project team. All analysis contained within this thesis is the work of the author.

1.4 Thesis Structure

This thesis is organized as follows:

Chapter one provides an outline of the objectives, scope, and novelty of the research presented in the thesis.

Chapter two is a comprehensive literature review related to this field of research. This chapter outlines the design methodology for rubble mound breakwater structures, as well as the hydrodynamic and structural processes affecting their loading and stability. This section also provides a foundation for the present study, as well as a motivation for it.

Chapter three presents experimental methodology for the research conducted for this thesis, including the experimental regime and setup of equipment. Experimental scenarios, manufacture of custom armour units, test conditions, experimental procedure, wave synthesis and generation, as well as data processing are discussed in this section.

Chapter four presents results, analysis, and discussion of the experimental results. This includes wave induced loading on the instrumented armour unit, force development, flow above the armour layer, a discussion of random waves, influence of wave height and stability number, and influence of wave steepness on hydrodynamic loading.

Chapter five presents conclusions of the research project and recommendations for future work.

2 LITERATURE REVIEW

2.1 RUBBLE MOUND BREAKWATERS

Rubble mound breakwaters are coastal structures designed to attenuate incident wave energy. Waves will generally break upon the slope of the structure, dissipating some of the energy as turbulence, with the remainder of the energy either reflected or transmitted through the structure. Applications of these structures include the protection of harbours from excess wave agitation for purposes of waterborne navigation, and the protection of shorelines from wave-induced erosion. Figure 2-1 shows a coastal breakwater under construction.

Figure 2-1. Breakwater under construction using Core-loc single layer system[2]

2.1.1 Breakwater Types

There are many structural options for the design of a breakwater. In function, they are generally similar, working to dissipate incident wave energy. They differ from each other in parameters such as hydraulic stability under wave action, permeability, ease of construction, aesthetics, and cost. Figure 2-2 shows many typical breakwater cross-sections.

[2] http://www.concretelayer.com/sites/default/files/147_Fujairah_UAE_2002_CORE-LOC.jpg

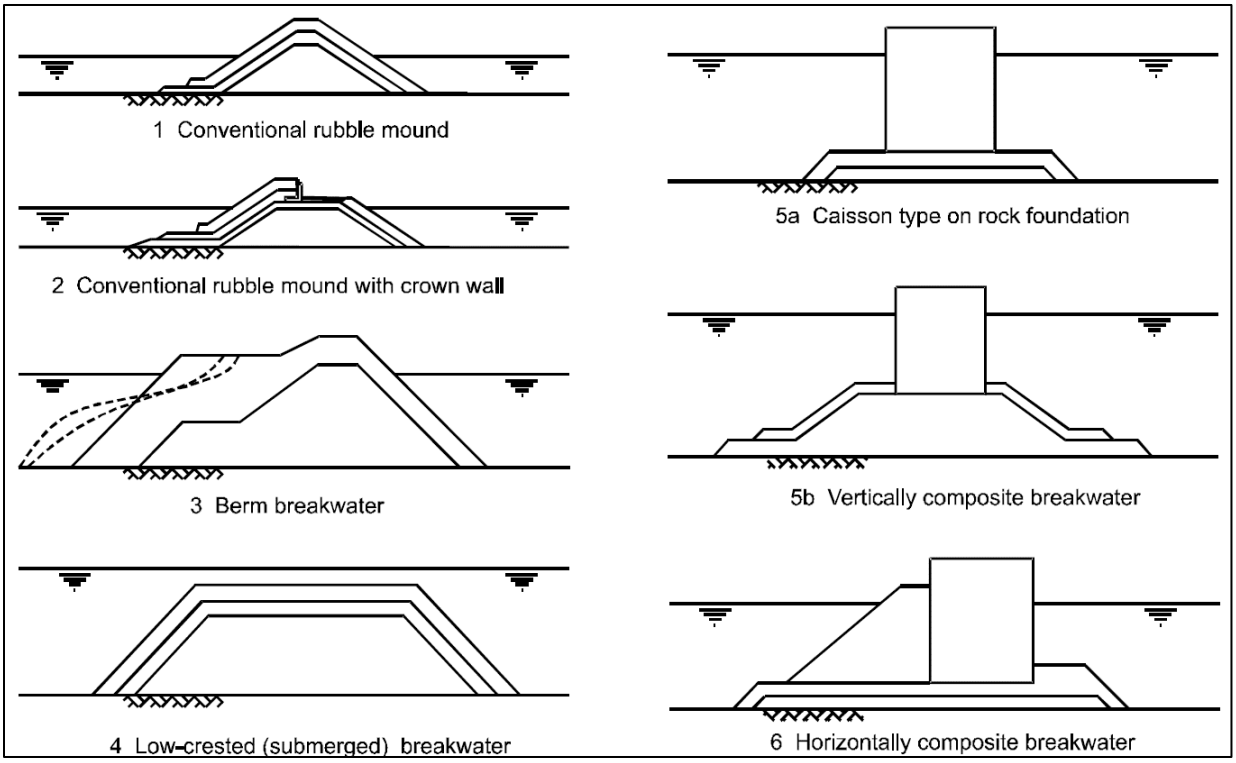

Figure 2-2. Typical cross-sections of various types of rubble mound breakwater (CIRIA, 2007)

2.1.1.1 Conventional Rubble-Mound

The focus of this study and the most typical type of breakwater is the conventional rubble mound breakwater. In its simplest form, rubble-mounds are a pile of large stones placed in the path of incident waves used to dissipate incoming wave energy. The production of stones large enough to resist wave forces is expensive, however, compared to smaller quarried material. Using only large stones would also result in a structure of high permeability, which would allow long period waves to propagate through the structure. What is conventionally done is to design breakwaters using a layered system, a schematic of which can be seen in Figure 2-3. This system uses cheaper, less permeable quarry-run material as a core. This represents the largest volume component of the structure.

To resist wave action, an armour layer of large stones (or other units such as concrete armour units) are placed on the outermost face. This reduces the volume of large expensive material required for each linear metre of breakwater.

Between the armour layer and the core is the underlayer, or filter layer. This layer acts as an intermediary and allows for the transfer of wave energy through to the foundations of the structure. This layer is comprised of small enough stones to prevent core material from being eroded through the larger voids in the armour layer. Whether the breakwater is armoured with rock or CAUs, the filter layer will be composed of rock.

A toe of the breakwater structure is also specified to prevent the undermining of the front of the breakwater from scour. The toe is typically composed of large rock or concrete armour units, generally depending on the armour layer composition.

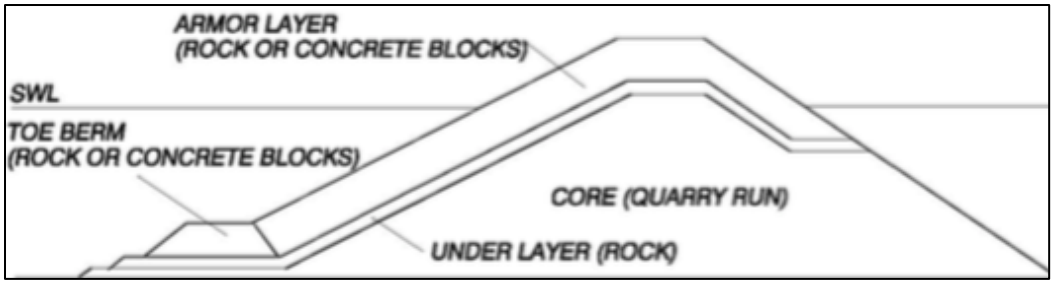

Figure 2-3. Conventional rubble mound breakwater cross-section (USACE, 2006)

2.1.2 Geometry of Breakwater Cross-sections and Typical Features

The following figure (Figure 2-4) is a drawing of a typical rubble mound breakwater, annotated with key geometric dimensions.

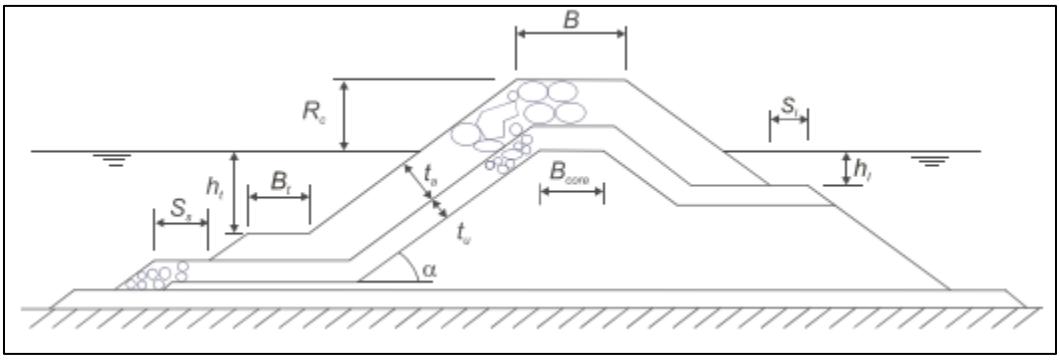

Figure 2-4. Definition sketch of rubble mound breakwater (CIRIA, 2007)

Where: R_c is the crest freeboard (m), B is the crest width (m), α is the slope angle (deg), t_a is the armour layer thickness (m), t_u is the underlayer thickness (m), h_t is the seaward toe level (m), h_l is the leeward berm or shoulder level (m), B_t is the berm width (m), S_s, S_t are the shoulder widths (m).

2.1.3 Armourstone

In the breakwater cross-section the component exposed to direct wave action is the armour layer. Several materials are possible to be used to make up this layer, though historically natural armourstone of quarried rock has been the most common. Consequently, most breakwater hydraulic research has focused on armourstone.

2.1.3.1 Concrete Armour Units

When it is impractical to source stone of sufficient size and quality to use as armourstone, it may become the most cost-effective method to substitute units made of concrete for this stone. These units are called concrete armour units (CAUs).

Many different CAUs are available on the market (Figure 2-5), with widely varied designs.

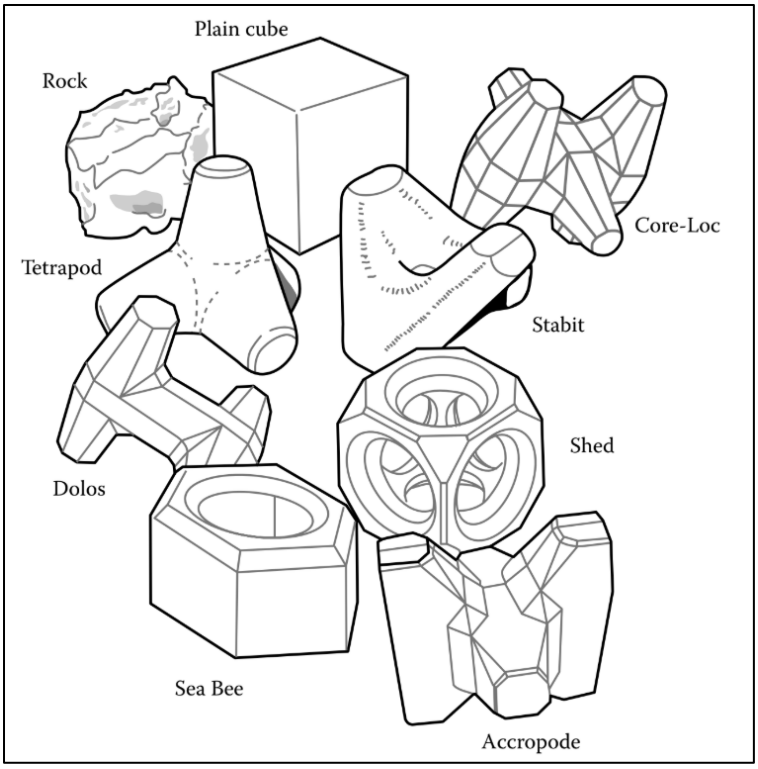

Figure 2-5: Commonly used breakwater armouring material, including rock and concrete armour units (Reeve et al., 2018)

These CAUs were developed in different countries, during different historical periods, and with a wide variety of shapes. Key factors in the selection of CAUs include structural and hydraulic stability, hydraulic performance, licensing fees, local availability of rock, fabrication and handling of units, maintenance, and appearance. Each of these factors are considered when choosing a suitable type of CAU to use for a project, or whether to use one at all over available natural material.

The following subsections will include a description of concrete armour units generally, followed by specific details of the CAUs pertinent to this investigation.

2.1.3.2 CAU Types

CAU types can be broken down into several major groupings. Distinction can be made between units that are uniformly placed on the slope of a breakwater, such as Haros or Seabees, and units that are randomly oriented on a slope, such as cubes, tetrapods, or Core-Loc.

The units can also be divided by the factor that contributes the most to the stability of the armour layer that they make up. These factors are:

- resistance primarily coming from their own weight, such as cubes or Antifers.
- resistance from interlocking between units, such as Tetrapods or Core-loc units
- resistance primarily from friction between units, such as Sheds or Seabees.

A vital aspect giving some insight into why new units are continually being developed is safety. It was found, after the failure of several breakwaters in the late 1970s and early 1980s that under intense

wave loading particularly slender structural elements of CAUs such as Dolos (Figure 2-5), are prone to breakage. There has been a trend towards bulkier, more robust units since those events.

Simultaneously, there is continual development and research into more efficient breakwater units. The building of breakwaters is expensive, and the cost of the armour layer is a significant component of that cost, so there is continuous development to attempt to reduce costs while increasing performance.

2.1.3.3 Breakage of Units

Damage or breakage of concrete armour units can be the consequence of a variety of extreme loading conditions. The most common scenario involves units in regular use under storm wave loading conditions. These wave conditions cause the units to rock once the waves have overcome the stability of the units themselves. This rocking then increases internal stresses in the unreinforced concrete and is likely to cause unit breakage. Once a unit has broken, it is now able to be picked up by wave action and thrown onto other units, which induces further cascading breakage. Other likely scenarios for inducing breakage in concrete armour units is while being manipulated or dropped during breakwater construction.

2.1.3.4 CAU Concrete

Typically, the concrete used for the construction of CAUs is unreinforced since the likelihood of corrosion is high in marine structures. The corrosion of reinforcing steel inside a concrete unit risks the likelihood of the reinforcement swelling and damaging the unit. In addition to this, the use of reinforcing steel introduces a considerable cost increase to the unit. A portion of that cost could be recouped from reduced use of concrete bulk, but typically this is not done in practice, since the potential risks outweigh the potential advantages.

The concrete used in the construction of CAUs should be of a density that is consistent with the testing that was done to determine the design formulae for hydraulic stability. This is usually a density of 2350-2400 kg/m^3.

2.1.4 Concrete Armour Layer Properties

Whereas stone armour layers are typically double layer systems, concrete armour units have been developed for both single- and double-layer systems. Concrete armour units are also developed to be laid out in a precise way, unlike rock systems which are generally placed randomly to a design thickness. The placement method for each individual concrete armour system is either published, or available from the license holder of a particular unit through a training program.

When an armour layer system of concrete armour units is to be laid out randomly, the layout will still adhere to a minimum placement density of the units, thus are said to be laid out semi-randomly. The units may also be laid out in an orderly fashion where there is both control over the minimum placement density of the units as well as the position and orientation of them.

The armour layer has a geometry dependent on several parameters. Some of these parameters are:

- Armour layer thickness, where the thickness is defined as “the distance normal to the underlayer surface, measured from the surface up to the average of the protruding points”

(CIRIA, 2007). Overall armour layer thickness is taken to be to the extreme of those protruding points.

- Placement grid, as discussed above, whereby the units are placed in such a way as recommended by the licensee of the particular type of unit.
- Layer porosity, the volume between void volume and total layer volume.
- Packing density coefficient, unlike placement grid this is a number of armour units in a nominal square diameter. This value should be between the maximum possible packing density for a particular unit, as recommended by the manufacturer or relevant literature, and the minimum density for hydraulic stability.
- Number of units per square meter, which is calculated using the packing density coefficient. This can be used to determine the volume of concrete needed for the slope design.

2.1.5 Core-Loc Armour Units

The Core-Loc single layer interlocking concrete armour unit (Figure 2-6) was developed by the United States Army Corps of Engineers (USACE) for use in the repair of damaged Dolos-based structures. These units share the same dimensions in their legs as the Dolos units but are designed with a third leg and more internal structural stability due to a reduction in slenderness. In terms of function of the units, the Core-loc units are similar to Accropodes, another CAU with which it is commonly compared, but have a slightly improved hydraulic stability, as can be seen in Section 2.2.

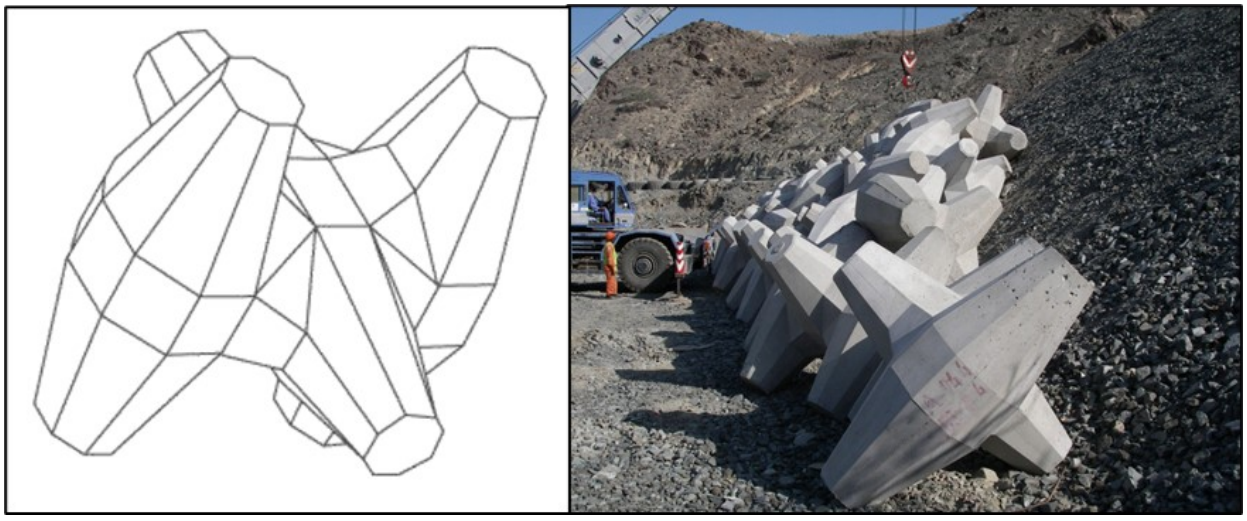

Figure 2-6: General shape of the Core-loc CAU (CLI, 2012) (left). Core-Loc CAUs deployed in breakwater project (CLI, 2012) (right).

The Core-loc unit is laid out in a single layer in a semi-random pattern, as can be seen in Figure 2-7. The placement of Core-loc units follows rules such as the maintenance of a prescribed packing density[3]; each unit shall interlock with two units in a lower row; units shall not interlock other units within the same row, etc. (CLI, 2012).

[3] Prescribed packing density varies by armour unit size, between $\phi = 0.640$ for 1 m^3 Core-Loc units, and $\phi = 0.616$ for 11 m^3 units. Placement of the number of units per nominal area is defined as: $\frac{N}{A} = \phi v^{\frac{2}{3}}$, where v is CAU volume.

Figure 2-7: Core-loc breakwater under construction (CLI, 2012)

2.1.6 Breakwater Failure Modes of Main Armour Layer

A schematic overview of the most typical modes of breakwater structural failure can be seen in Figure 2-8. This section will review the most common armour layer failure modes.

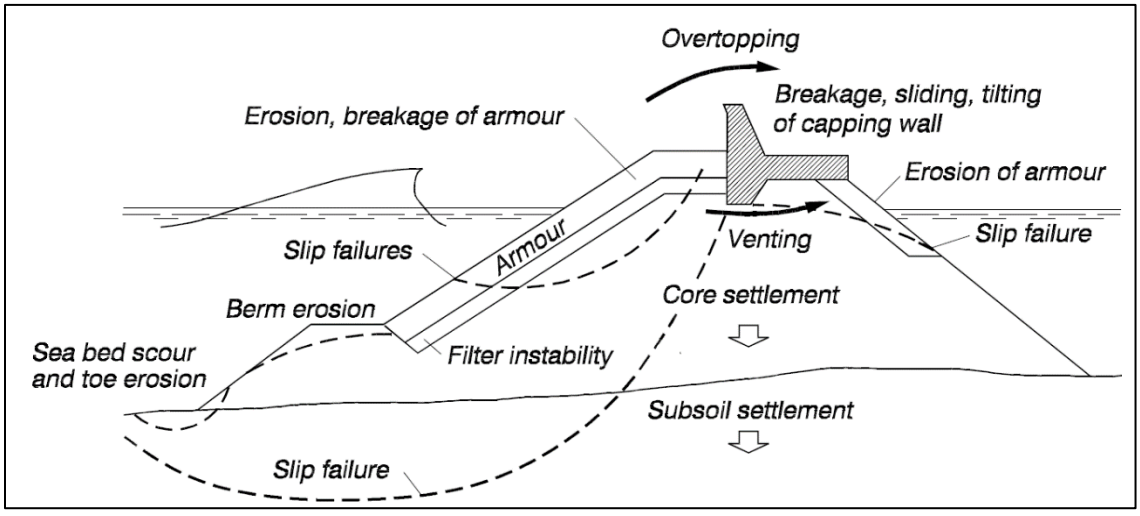

Figure 2-8. Overview of breakwater failure modes (USACE, 2006)

2.1.6.1 Double Layer Armour Layer Failure

The following figure (Figure 2-9) shows the progression of failure of a breakwater after the failure of the exterior armour layer. The first stage in this failure mode is the displacement of armour units around the SWL, where the most wave action is concentrated. Once the armour units have been displaced, the

second phase of progressive damage leave the filter layer and core are vulnerable to wave attack, causing erosion of the filter material. Following this, in the final stage, the crest of the breakwater will erode, and the breakwater elevation will be lowered and the structure will no longer function as designed.

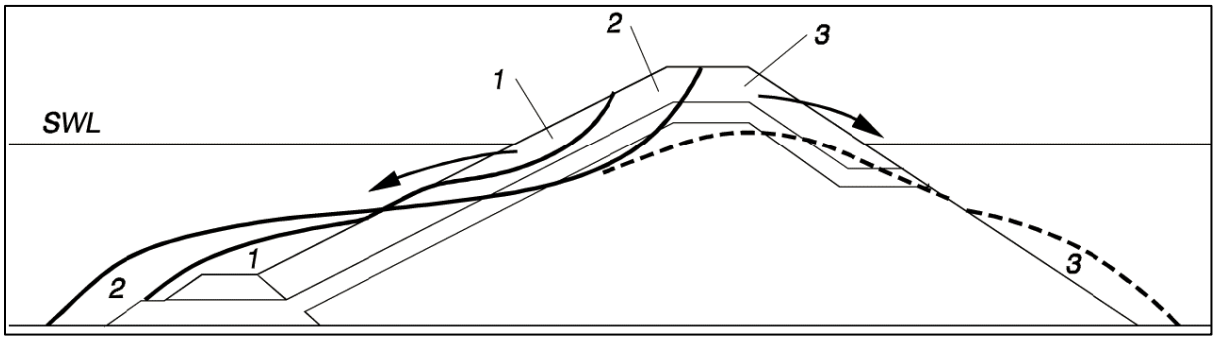

Figure 2-9. Main armour layer instability and phases of progressive damage (USACE 2006)

This failure can be resisted by proper sizing of units in the armour layer. If armour units are large enough, they will not be displaced in the area of the SWL.

2.1.6.2 Single Layer Armour Layer Failure

With single layer systems of concrete armour units, such as the Core-loc or Accropode, failure can be rapid. When an instability occurs on a steep slope (steep breakwater slopes are common due to cost reduction), the progression of failure can progress quickly to a large proportion of the armour units on the slope (Figure 2-10). After armour units have been shifted, the underlayer and core are exposed to wave action and are vulnerable to erosion. To prevent this failure mode, particular care must be taken when designing with single layer CAU systems. Single layer armouring systems are thus typically designed for zero damage, whereas conventional rock-armoured layers are designed for a small amount of damage.

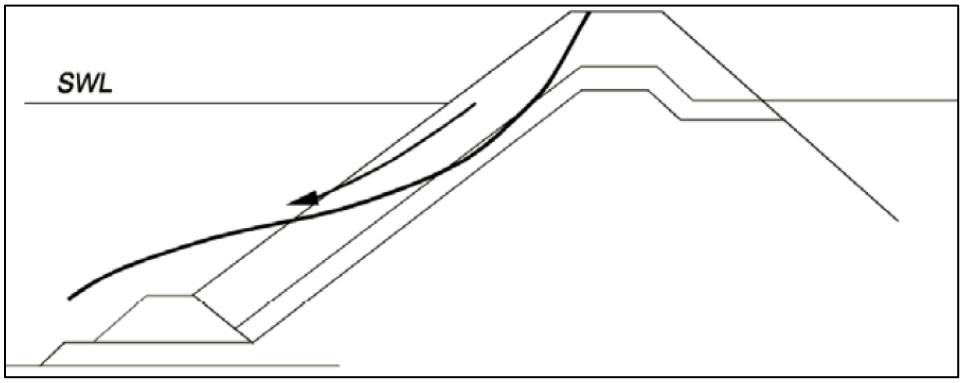

Figure 2-10. Hydraulic instability on steep slopes (USACE, 2006)

2.1.6.3 Failure of Individual Armour Units

The typical failure modes of individual armour units are shown in Figure 2-11. These modes are: rocking during uprush (Figure 2-11, a), rocking during downrush (Figure 2-11, b), the pivoting of an armour unit above an adjacent armour unit during up or downrush (Figure 2-11, c), and the sliding of several units simultaneously during downrush (Figure 2-11, d). Interlocking single-layer armour units, such as the

Core-loc, do not have the roughly spherical geometry of armour stones, and so the force required to initiate such failure is significantly larger, though the typical failure modes are similar.

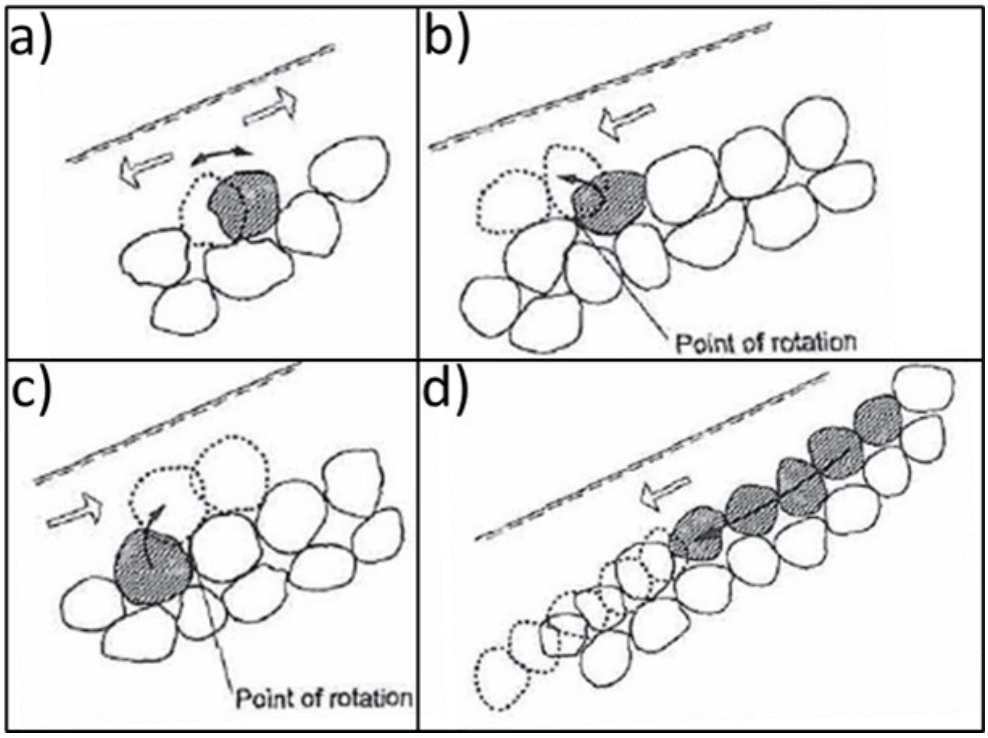

Figure 2-11: Typical rock armour layer failure modes (Hald, 1998 after Burcharth, 1993)

2.2 Armour Layer Design

With respect to the design of the armour layer using concrete armour units, there is much less rigorous study than in the use of rock for the function of the armour layer. For rock armour layers there is extensive study of the stability of the armour layer, as well as provisions and methods for studying the progression of damage. Since rock armour layers are much more common, have a longer history, and are often preferred to CAUs, there is a larger body of literature regarding the use of rock.

In general, the stability of a CAU armour layer depends on the stability of individual units. Single-layer systems are often designed with little to no tolerance for armour unit motion due to higher threat of progressive collapse after the onset of damage. A concern when attempting to size larger units for double layer systems to resist these larger waves is that, due to the slenderness of some types of units (such as tetrapods or Dolosse), they become more likely to break under the higher applied force.

When considering units typically placed in a double layer, critical failure only occurs when both layers have been displaced and the underlayer begins to be eroded. Once this occurs, however, the breakwater's damage may accelerate and lead to a relatively rapid brittle failure. In the case of a double layer system, more damage is required to the armour layer before the underlayer is exposed. This results in a more "ductile" type of failure mode for this type of armour layer. Upon initiation of damage of the double layer type systems, this damage can be identified during routine maintenance and

repaired before the ultimate failure of the breakwater, whereas with single layer systems, damage will progress rapidly upon initiation.

It is due to this method of failure, brittle vs ductile, that interlocking single layers of CAUs are typically designed for no damage. They are designed using a relatively high design stability factor, and are designed to show no damage and only minor rocking when exposed to a wave height about 20% higher than the design wave height. An advantage of single layer systems over two-layer systems is in this ability to withstand higher wave heights without damage, whereas the two-layer system would be expected to undergo damage (and subsequent repair) if the design wave height is exceeded.

One difficulty with the collection of real-world field conditions for the stability of breakwater armour layers is that the occurrence of design conditions is rare, since storms of the proper intensity are by necessity infrequent events.

2.2.1 Damage Number N_{od} and N_d

The damage to a concrete armour layer is quantifiable using the damage number N_{od} and N_d.

N_{od} is defined as the number of displaced armour units within a strip of breakwater slope with the width equal to the equivalent cube size of the unit, or nominal diameter, D_n. This measure is most used with double-layer systems such as cubes or tetrapods. Typically, damage begins at $0.2 < N_{od} < 0.5$, and failure is considered to have occurred at $N_{od} = 2$ (CIRIA, 2007).

N_d is defined as the number of displaced armour units as a percentage of the total number of armour units, usually considered in a strip of the breakwater within $\pm 1.5\ H_d$ (design wave height) of the design still water level. This measure is most commonly used with single-layer systems such as accropodes or Core-loc. Typically damage begins at $N_d > 0\%$, and failure is considered to have occurred at $N_d > 10\%$ (CIRIA, 2007).

Generally, there is a preference for the use of N_{od} when considering damage to a breakwater, since it is a measure of the actual number of units which are damaged and is less sensitive to the cross-sectional length over which it is measured (Reeve et al., 2018). For example, given an equivalent damage to two cross-sections, the shorter cross-section will have a higher N_d but the N_{od} will not change.

2.2.2 Hudson Formula

The Hudson formula was originally developed for the quantification of stability of rubble mound rock armour layers (Hudson, 1959), but has been reformulated for use in concrete armour layers. This formula relates the stability of a breakwater armour layer to commonly known physical parameters, as well as an experimentally determined coefficient. This is a commonly used and widely validated formula for the sizing of breakwater amour layer units.

$$\frac{H_s}{\Delta D_n} = (K_D cot\ \alpha\ )^{1/3} \tag{2-1}$$

Where:

H_s is the significant wave height (m). H_s is defined as the average height of the highest 1/3 of the waves (Kamphuis, 2010)

Δ is the relative buoyant density of the rock being used, i.e. $(\frac{\rho_r}{\rho_w} - 1)$. This value is approximately 1.34 for concrete in sea water.

D_n is the nominal diameter of the unit. i.e. $\sqrt[3]{V} = \sqrt[3]{\frac{M}{\rho_c}}$, where V is volume, M is mass, and ρ_c is concrete density. This represents the length of a cube of equivalent volume to the unit.
K_D is the dimensionless stability coefficient. This is generally derived from laboratory testing and has a value of close to 3 for natural quarry rock. K_D values of CAUs vary widely.
α is the angle of the breakwater with respect to the horizontal plane.

The following table (Table 2-1) is a summary of K_D values used for several types of CAU.

Table 2-1: Hydraulic stability of armour units using Hs/(ΔDn) (after CIRIA, 2007)

Armour Type	Damage Level	Stability number $H_s/(\Delta D_n)$				Slope
		Trunk		Head		
		Non-breaking waves	Breaking waves	Non-breaking waves	Breaking waves	
Core-loc	0% ($N_{od} = 0$)	2.8, $K_D = 16.0$		2.6, $K_D = 13.0$		1:1.33
Accropode	0% ($N_{od} = 0$)	2.7, $K_D = 15$	2.5, $K_D = 12$	2.5, $K_D = 11.5$	2.3, $K_D = 9.5$	
Xbloc	0% ($N_{od} = 0$)	2.8, $K_D = 16$		2.6, $K_D = 13$		

2.2.3 Van der Meer Formula

Many more sophisticated stability formulae for the sizing of rock armour units have been developed, deriving from Hudson's work as well as earlier work by Iribarren (1938). The most common of these hydraulic stability formulae, and the de-facto standard, is the Van der Meer formulae (1988). This approach considers stability differently for different types of breaking waves, specifying unique stability calculations for waves above and below the critical Iribarren number (ξ_{cri}, defined by Equation 3). This methodology was derived for use with rock armour layers.

$$\xi_m = tan\alpha / \sqrt{\frac{\left(\frac{2\pi}{g}\right) H_{s,toe}}{T_m^2}} \tag{2-2}$$

$$\xi_{cri} = \left(\frac{C_{pl}}{C_s} p^{0.31} \sqrt{tan\alpha}\right)^{\frac{1}{p+0.5}} \tag{2-3}$$

For plunging waves ($\xi_m < \xi_{cr}$)

$$\frac{H_s}{\Delta D_{n50}} = 6.2 \xi^{-0.5} p^{0.18} \left(\frac{S}{\sqrt{N_s}}\right)^{0.2} \tag{2-4}$$

For surging waves ($\xi_m \geq \xi_{cr}$)

$$\frac{H_s}{\Delta D_{n50}} = 1.0 \xi^{P} \sqrt{cot\alpha} p^{-0.13} \left(\frac{S}{\sqrt{N_s}}\right)^{0.2} \tag{2-5}$$

Where p is the notional permeability of the structure (Figure 2-12, left), N_s is the number of waves, $H_{s,toe}$ is the significant wave height at the toe of the structure. C_{pl} and C_s are plunging and surging coefficients, respectively. These were experimentally derived by Van der Meer (1988) to be 6.2 and 1.0, respectively. S is damage level[4], D_{n50} is nominal armour stone diameter assuming a 50% cumulative distribution, and C_s is the surging coefficient.

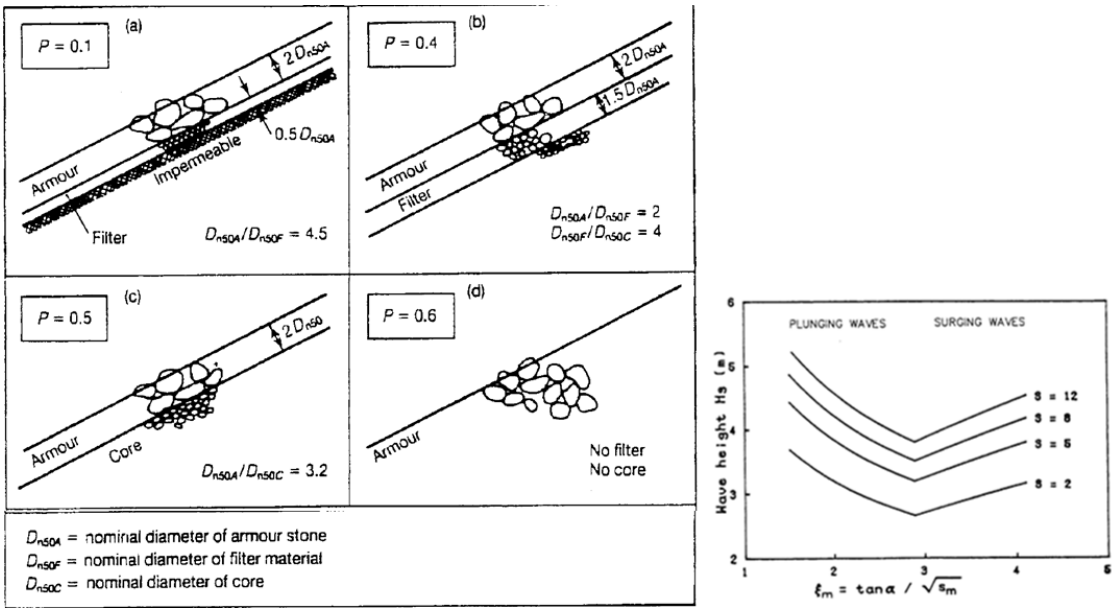

Figure 2-12: Notional permeability factor P for various structures (van der Meer, 1998) (left). Wave height versus breaker parameter, influence of damage level (van der Meer, 1998) (right)

This plunging/surging boundary is notable for sudden changes in wave behaviour, as seen in Figure 2-12 (right), as well as the differing sets of van der Meer stability equations[5] (van der Meer, 1998).

2.2.4 Accropode Stability

The behavior of single-layer CAUs, (specifically Accropodes) under wave action was found during experiments by Van der Meer (1988, a) to have a behavior that is different from that of rock as described by the Van der Meer formula. The behaviour was also different from cubes or tetrapods. Storm duration and wave period were found to have no influence on the stability of the CAU armour layer. It was also found that armour layers of Accropodes have only a small margin of safety between the start of damage and structural failure (Van der Meer, 1988, a).

Two simple equations were derived by Van der Meer using non-breaking waves on a 1:1.33 slope for the stability of Accropodes.

$$\frac{H_s}{\Delta D_n} = 3.7 \tag{2-6}$$

[4] Damage level is defined as $S = A_e/D_{n50}^2$, where A_e is the erosion area in the breakwater profile between the still water and +/- one wave height. (Reeve et al., 2018)

[5] s_m is the mean wave steepness, $s_m = \frac{H_s}{L_{o,m}}$ (Kamphuis, 2010)

This equation represents the start of damage, when $N_{od} = 0$.

$$\frac{H_s}{\Delta D_n} = 4.1 \tag{2-7}$$

This equation represents the point of failure of the Accropode armour layer, when $N_{od} > 0.5$.

These stability numbers are experimentally derived and do not include a safety factor. For design purposes, the Rock Manual recommends a safety factor of 1.5 (CIRIA, 2007). This safety factor has been incorporated in the design values included in Table 2-1. This increase in resistance from the safety factor allows the armour layers made with Accropodes to resist an overload of 20% above the design wave conditions.

The resulting equation used for design is:

$$\frac{H_s}{\Delta D_n} = 2.5 \; to \; 2.7 \tag{2-8}$$

The range of values depends whether the incident waves are breaking or not.

2.2.5 Core-loc Stability

Upon hydraulic model testing (Melby and Turk, 1997), Core-loc armour units were found to exhibit a similar behaviour to that of Accropodes. The Rock Manual recommends the use of a K_D of 16, and the following empirically derived stability formula for trunk sections. This stability formula includes a safety factor and does not vary with design wave parameters other than H_s.

$$\frac{H_s}{\Delta D_n} = 2.8 \tag{2-9}$$

The stability of Core-Loc units, as well as Accropodes, was found not to be improved on a slope less steep than 1:2. The Rock Manual recommends the reduction by 10% of the stability factors in situations with depth-limited wave heights and steep foreshore slopes. These types of units should be able to resist an overload of 20 percent above the design storm conditions without damage. Under design conditions, no damage is expected and only minor rocking.

Concrete Layer Innovations (CLI), the current license holder for the Core-loc CAU in many countries provides a design table for the sizing of the armour units for breakwater trunk sections, dependent on seabed slope and significant wave height (Figure 2-13).

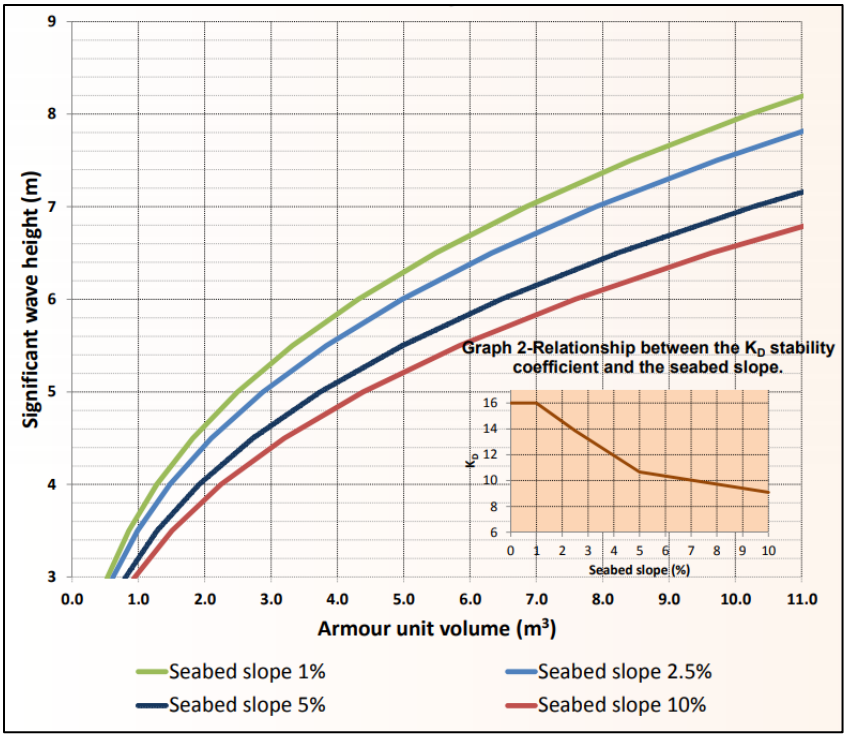

Figure 2-13: Relationship between design wave height as a function of the armour unit volume (CLI, 2012)

2.2.6 Stability Comparison of Concrete Armour Units

Figure 2-14 represents the damage curves of several types of concrete armour units commonly used in breakwater design. These values are based on the equations found in Section 2.2. For cubes and tetrapods, the values $s_{om} = 0.03$ and $N = 1000\ waves$ were used in those calculations. It can be noted that in these damage curves, the Accropodes represent a single layer system while cubes and tetrapods are double layer systems. Double layer systems are more linear in shape (particularly for the tetrapod system) and failure occurs at a much higher damage level. The implication of this figure is that the single layer systems experience a more rapid, accelerating failure mode compared to the double layer systems. The two vertical lines at approximate stability numbers of 2.5 are the design values for two common single layer systems, namely cubes and Accropodes. Since the single layer systems undergo more brittle failure, design conditions must be kept well below the failure conditions. For the double layer systems, this is less critical since the systems experience a more ductile failure mode.

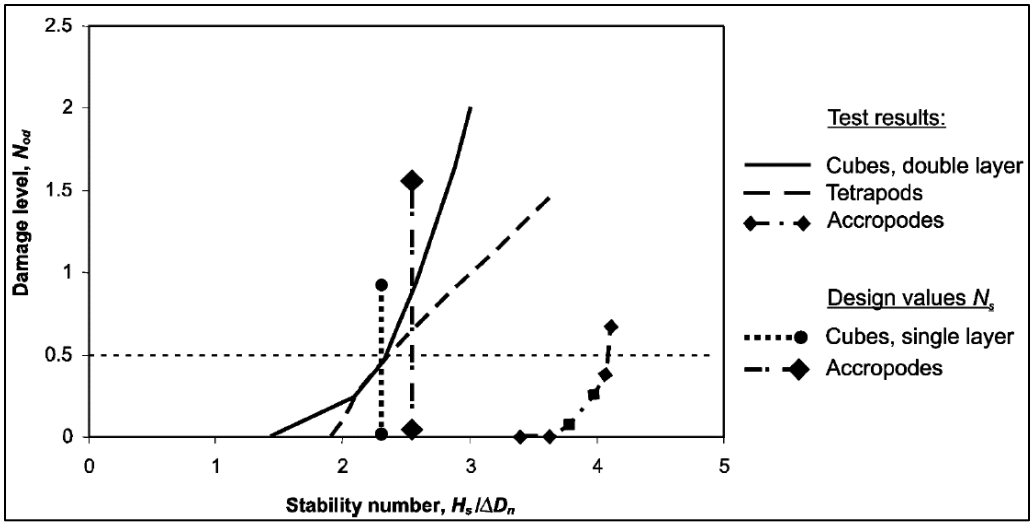

Figure 2-14. Damage curves from start of damage to failure (S_{om}=0.03 and N=1000 waves) (CIRIA, 2007)

Figure 2-15 (CIRIA, 2007) is a summary of the suggested ranges of stability numbers for common CAUs, based on the equations covered in Section 2.2. It should be noted that for design purposes, the acceptable range of stability numbers for single-layer systems (Core-loc, Xbloc, Accropode and single cubes) is much narrower than for double layer systems (tetrapods, double layer cubes).

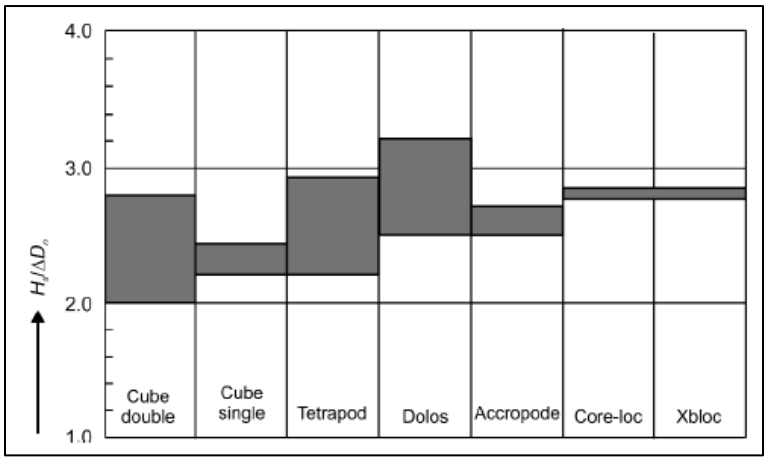

Figure 2-15. Suggested range of stability numbers for conceptual design (CIRIA, 2007)

2.3 BREAKWATER HYDRODYNAMICS

The following section describes hydrodynamics affecting CAU stability, including hydraulic conditions, breakwater flow patterns, flow velocities, flow forces, pull-out force and externally induced force on the CAU.

2.3.1 Hydraulic Conditions

The four main hydraulic aspects that will affect the structural design of a breakwater are: wave run-up, wave overtopping, wave transmission, and wave reflection. These parameters will be briefly discussed in the following subsections (Figure 2-16).

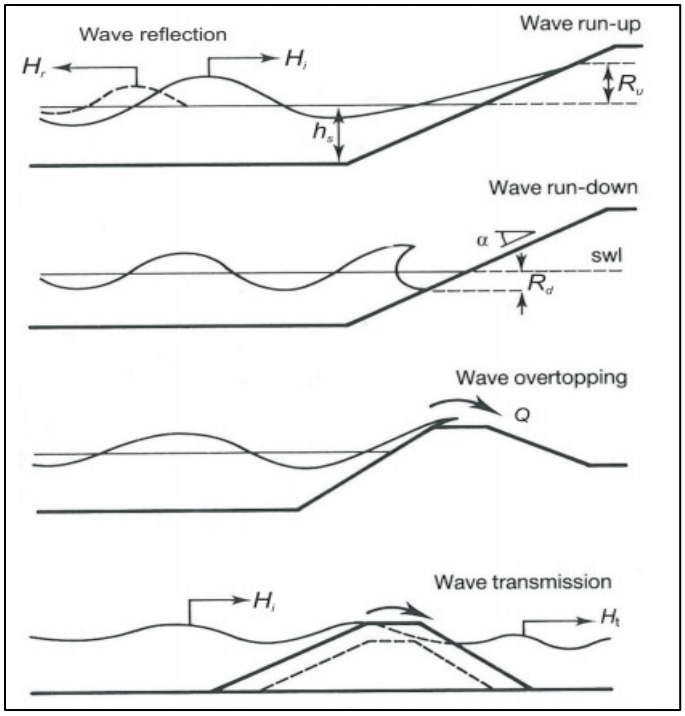

Figure 2-16. Hydraulic interactions related to waves and governing parameters (CIRIA, 2007)

A wave is generally described by the following parameters:

- incident wave height, usually considered is the significant wave height, H_s (m)
- wave period, such as the mean period, T_m (s), or the peak period[6], T_p (s)
- angle of wave attack, ß (degrees)
- water depth at the toe of the structure, h (m).

These parameters can be used to find the fictitious wave steepness, S_0, using either the theoretical deep-water wavelength, L_0, or wave period, T.

$$s_0 = H/L_0 = 2\pi H/gT^2 \quad (2\text{-}10)$$

This steepness can then, in turn, be used to find the Iribarren number (a.k.a. surf similarity or breaker parameter), ξ(-).

$$\xi = tan\alpha/\sqrt{S_0} \quad (2\text{-}11)$$

where α is the slope angle of the structure (degrees) (Figure 2-16).

The Iribarren number is useful to describe the way waves will break on a beach or breakwater, see Figure 2-17. Note that there are several versions of this number, depending on which statistical

[6] $T_P = \frac{1}{f_p}$, where f_p is defined as the frequency at which a wave spectrum displays its largest variance (or energy) (Kamphuis, 2010)

wave period or wavelength is used. These different versions are distinguished by subscript, for example $\xi_m$is the Iribarren number corresponding to mean wave period, $\mathrm{T_m}$.

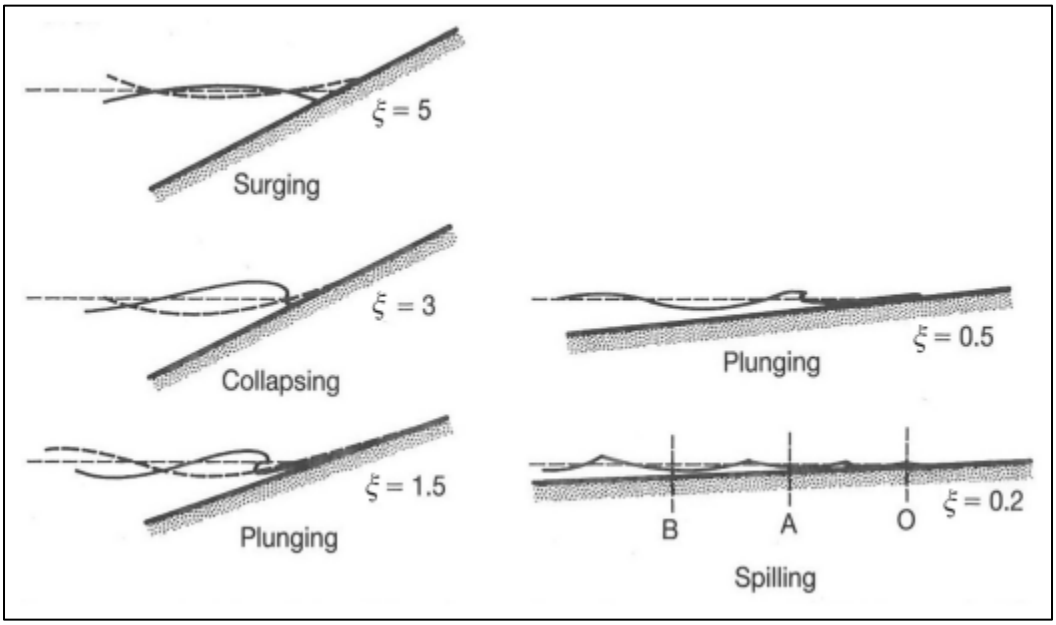

Figure 2-17. Breaker types as a function of the Iribarren number, ξ (CIRIA, 2007)

Wave breaking categorized by surf similarity parameter on steeper slopes such as breakwater armour layers is typically one of three types:

- Plunging: With $\xi < 2$, typically a plunging wave will occur. This wave is characterized by a curling forward of the wave crest.
- Surging: With $\xi > 4$, typically a surging wave will occur. This wave is characterized by a narrow or nonexistent surf zone and high uprush.
- Collapsing: This type of wave exists in the transition between plunging and surging waves.

When the slope angle, α, is held constant as in this investigation, the surf similarity parameter depends solely on wave steepness.

Fluid velocity and acceleration on the slope during uprush and downrush is strongly affected by breaking wave type. Investigation of the relationship between surf similarity parameter and water velocity as well as acceleration on the slope was performed by Sawaragi et al. (1983) (Figure 2-18). These results indicate that the highest simultaneous velocities and accelerations were observed in the range of ξ corresponding to collapsing waves. Highest accelerations occur at the plunging/collapsing boundary. Note that this experiment was performed for rock armoured slopes, not slopes armoured with CAUs.

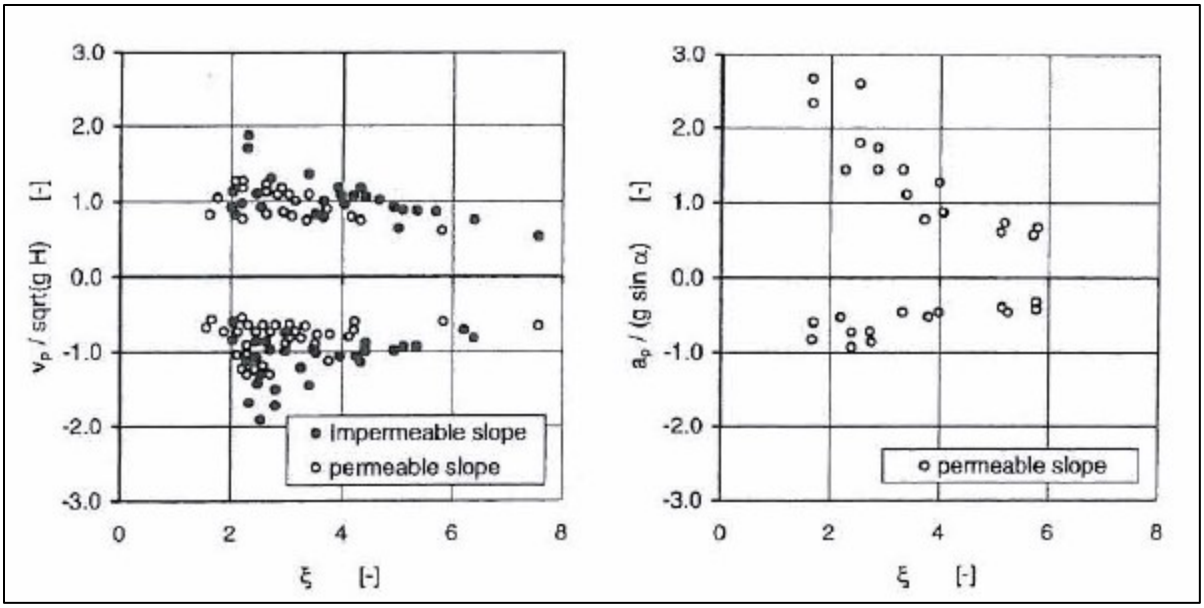

Figure 2-18: Maximum water particle velocity and acceleration (Sawaragi et al. 1983)

Plunging breakers generally produce high accelerations due to the wave impact, but correspondingly relatively low velocities when compared with surging breakers. Surging breakers show the highest flow in and out of the porous structure and have large extents of their uprushes accompanied by relatively minor velocities.

2.3.1.1 Wave Run-up

The wave run-up, R_u, and wave run-down, R_d, are measures of how far from the still water level waves will reach on a slope or structure. These values are measured as a vertical distance, in metres, from the SWL. The run-up level can be used to determine the level of the crest of a structure, and the run-down level is often the determining parameter of the lower limit of the armour layer of a breakwater.

2.3.1.2 Wave Overtopping

If run-up exceeds the height of the structure, the structure will be overtopped. Overtopping is used to determine the height of the crest of a structure as well as the geometry of the structure to ensure that the volumetric flow of overtopping remains below an acceptable design level. Similarly, the overtopping velocity will be kept below a design maximum.

2.3.1.3 Wave Transmission

Waves can be transmitted through a breakwater by one of two mechanisms. If there is sufficient overtopping of the structure, wave energy can be transmitted over and past it. If the structure has a high permeability, a long period wave can be transmitted through the structure as well. This is a concern for low-crested breakwaters, or harbour breakwaters where wave conditions in the harbour are important.

This transmission (Figure 2-16) is described using a coefficient of transmission, C_t (-), which is the ratio of transmitted to incident wave heights:

$$C_t = H_t/H_i \tag{2-12}$$

2.3.1.4 Wave Reflection

All coastal structures reflect at least part of the incident wave energy. These reflections can cause complications within a harbour, or harbour entrance, where they can interact with incident waves to produce a chaotic sea state. Reflections may also cause increased orbital peak velocities, which can cause an increase in sediment transport in the reflected area.

Wave reflection (Figure 2-16) is also described by a coefficient, C_r (-), which is the ratio of the reflected (H_r) to incident wave heights (H_i):

$$C_r = H_r/H_i \tag{2-13}$$

2.3.2 Breakwater Flow Patterns

Incident waves and the breakwater structure interact to cause the breaking of the incident waves. This broken wave will travel up and down the breakwater slope to a maximum runup location (R_u) and maximum rundown location (R_d). In a scenario involving an impermeable slope, wave runup and rundown will reach greater extents than in a permeable scenario (Figure 2-19). In the impermeable scenario, runup velocities are the highest possible and run parallel to the breakwater slope.

In the permeable scenario, the water-structure interaction is more complex. Water flows through the permeable layer at an oblique angle to the breakwater slope. The velocity vector becomes perpendicular to the breakwater slope below the SWL in the area of influence of the combined uprush of an incident wave and downrush of the preceding wave. This results in the highest slope-normal velocities, as well as rapid changes in magnitude and direction of flow velocity. This critical flow field is the location chosen for this investigation.

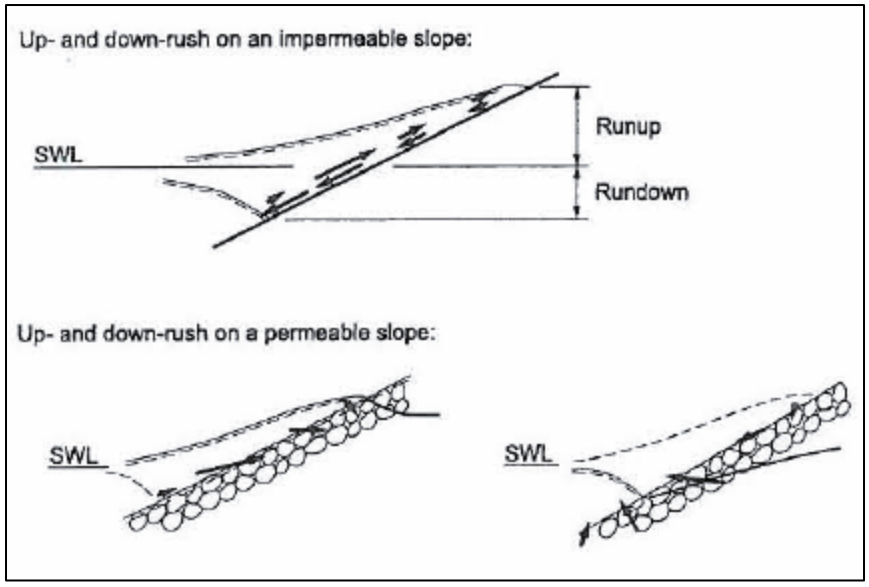

Figure 2-19: Wave structure interaction -- Runup and rundown of impermeable and permeable slopes (From Burcharth 1993)

2.3.3 Flow Velocities

While no theory exists to precisely estimate wave velocities in permeable rock or concrete armoured rubble mound structures undergoing wave breaking, Hudson (1958) assumed that the energy potential

at maximum uprush is equal to the potential at the still water level, and that this potential is proportional to incident wave height. Thus:

$$v_p = \sqrt{2gR_u} \cong \sqrt{2gH} \tag{2-14}$$

Where: v_p is the slope-parallel velocity, R_u is the run-up height, H is the incident wave height.

Internally, within the structure itself, the flow field has been modelled numerically (Figure 2-20) and physically. No simple theoretical flow model exists at this time. The flow field within the structure at rundown is the result of an interaction between the exit of the previous wave and the uprush of the incident wave. This interaction results in a slope-normal velocity vector reducing the stability of armour units below the SWL.

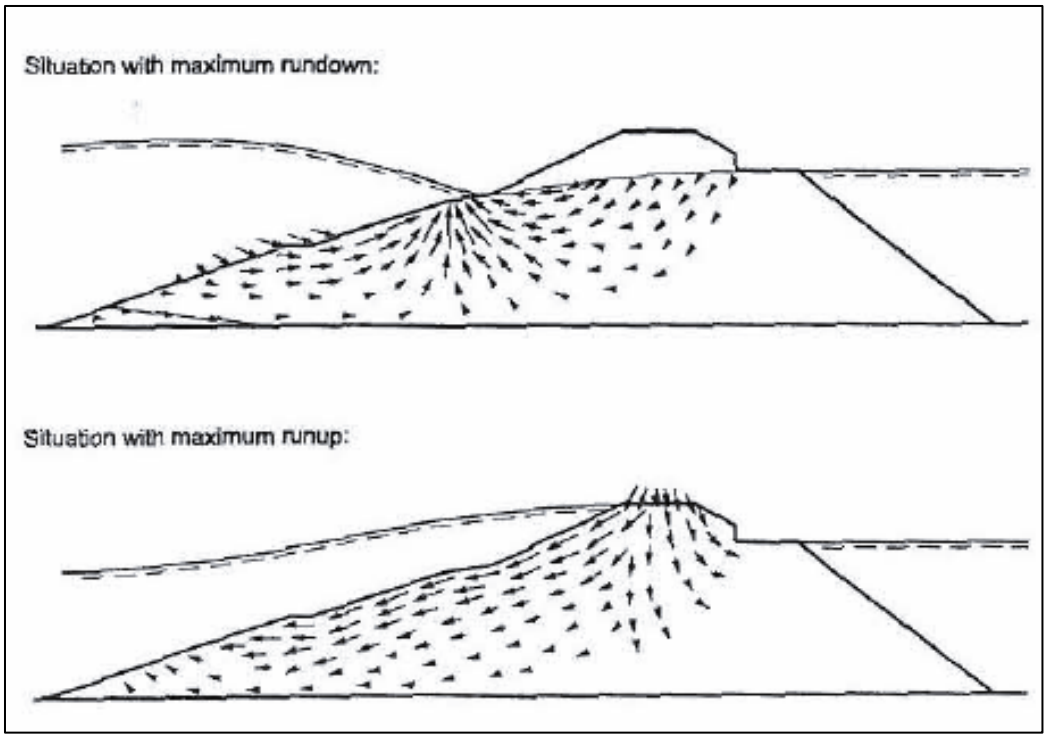

Figure 2-20: Internal flow field at maximum rundown and maximum runup (From Barendes, 1988)

2.3.4 Flow Forces

An armour unit undergoing wave loading is exposed to several forces. Flow forces resulting from the flow field are summarized in Figure 2-21.

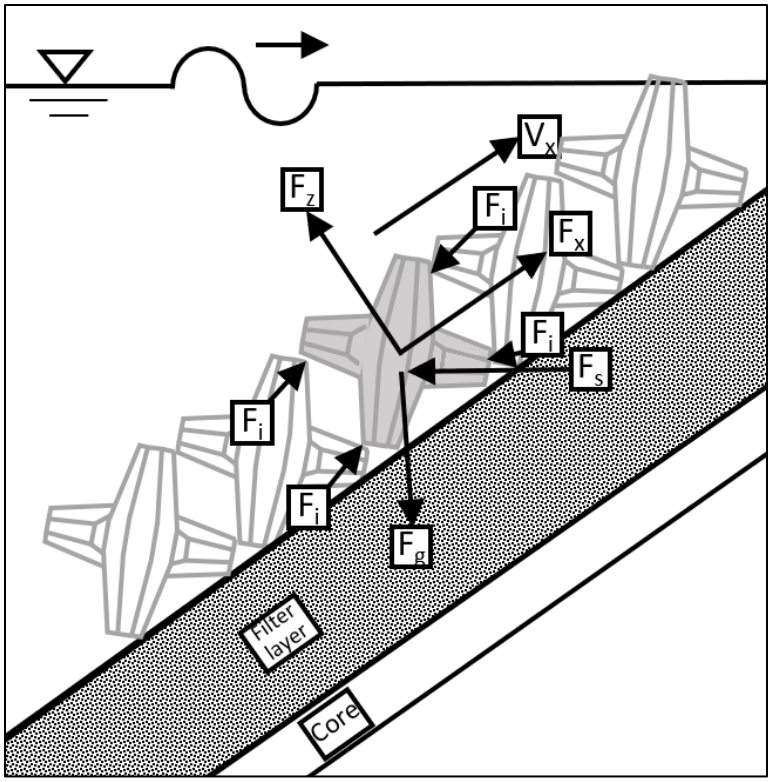

Figure 2-21: Forces present on an armour stone undergoing wave loading

Where:

F_z represents slope-normal wave force,
F_x represents slope-parallel wave force,
F_i represents interlocking force between CAUs and between CAU and filter layer,
F_s represents seepage force, or force of water emerging from the filter layer,
V_x represents slope-parallel runup velocity,
F_g represents the force of gravity.

In wave loading, the direction and magnitude of all forces are variable with time, with the exception of the gravitational force.

In a series of rock armoured breakwater tests in which an armour unit was affixed to a load cell (Hald, 1998), the parallel and normal forces acting on the unit below the SWL was measured. These results are shown in Figure 2-22.

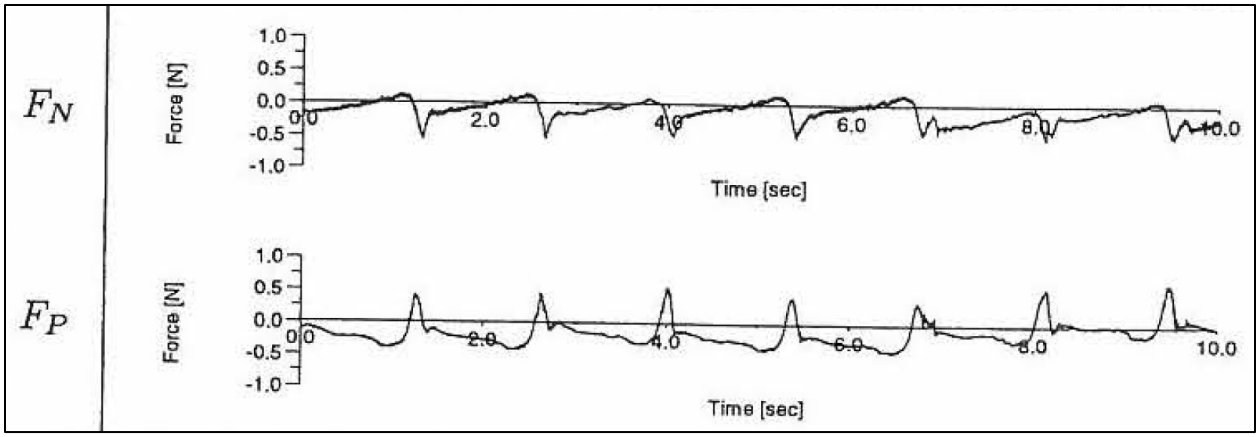

Figure 2-22: Normal and parallel force time series for s = 5% and H = 0.15 m (Hald, 1998)

In this figure, the instrumented unit experiences predominantly negative forces in both directions with sharp impulses during wave impact.

The data from the Hald experiments was also plotted as hodographs -- diagrams showing the evolution of the parallel and normal forces during a cyclical wave event (Figure 2-23).

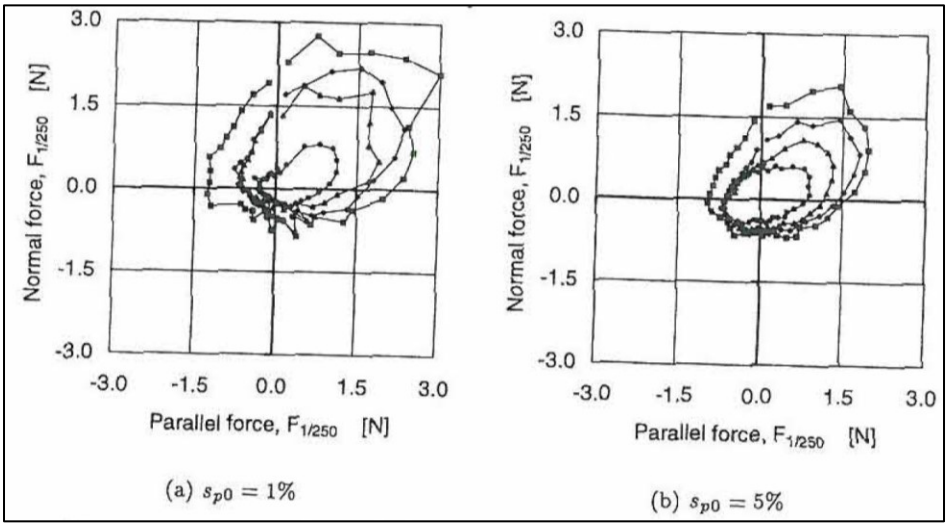

Figure 2-23: Force hodographs for rock armour instrumented testing, s = 1:3, h = 0.3 m, varying wave height and steepness (Hald, 1998)

Force in these experiments develops in a roughly oval pattern in which the largest forces are directed upward, generally occurring at an angle between 125° and 160° from the breakwater slope (Hald, 1998).

A series of instrumented armour layer experiments were also performed by Cornett (1995). These experiments examined the hydrodynamic forcing of sections of sub-SWL rock-armoured rubble-mound breakwaters. Rather than the instrumentation of individual armour stones, porous panels of welded together armour stones were instrumented. Figure 2-24 shows normalized force hodographs

from that series of tests. Wave heights greatly affect the magnitudes of forces in both directions, though the hodograph shape is generally maintained.

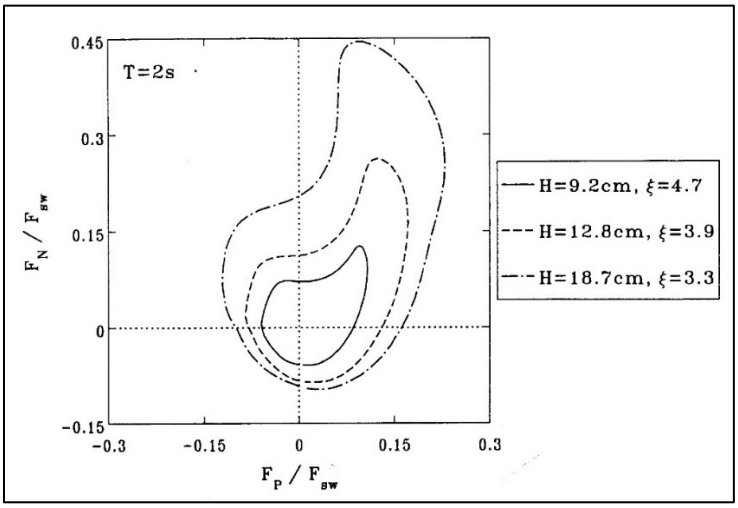

Figure 2-24: Influence of wave height on hydrodynamic forcing (Cornett, 1995)

2.3.5 Pull-out Force

Due to the interlocking design of single-layer armour units such as the Core-Loc, as well as the functionally similar Xbloc, the force required to remove an armour unit of this type from the armour layer is much higher than for rock armour units. Reedijk et al. (2005), determined the pull-out force required to remove a rock, i.e. to initiate failure of the structure, to be approximately twice the force of gravity acting on the unit. The relative force required to initiate structural failure and remove an interlocking CAU was approximately seven times the force of gravity (Figure 2-25).

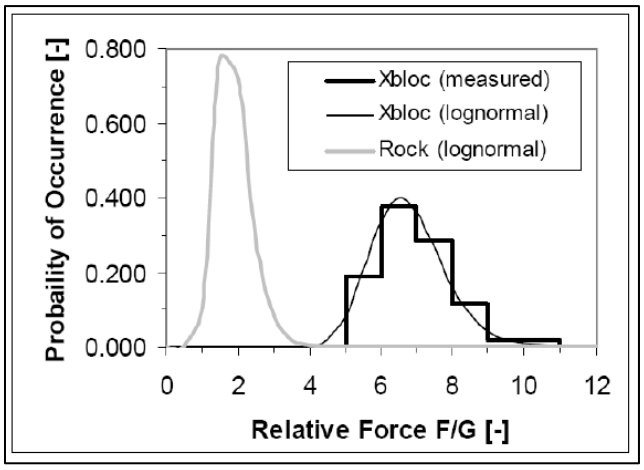

Figure 2-25: Pull-out force for single layer concrete armour unit (Xbloc) and rock (Reedijk et al., 2005)

2.3.6 Externally Induced Force

Induced wave loading on a fixed body in oscillatory flow is classically estimated with the use of the Morison equation (1950).

$$F = F_I + F_D \tag{2-15}$$

$$F_I \cong \rho_w C_m V \dot{u} \tag{2-16}$$

$$F_D \cong \frac{1}{2}\rho_w C_d A u|u| \tag{2-17}$$

where:

F is the total inline force on the body,
F_I is the inertia force,
F_D is the drag force,
ρ_w is the water density,
C_m, C_d are experimentally-derived empirical hydrodynamic inertia, drag and lift coefficients,
V is body volume,
u is inline water velocity,
$\dot{u}$ is inline water acceleration, $\frac{du}{dt}$,
v is the perpendicular water velocity,
A is cross-sectional area of the body perpendicular to the water velocity direction.

This semi-empirical equation was developed for the estimation of forces on vertical cylinders undergoing oscillating fluid flow in deep water. An armour unit embedded within an armour layer undergoes more complex flow fields than that for which the Morison equation was developed, such as the shielding of CAUs from incident flow by adjacent armour units as well as boundary layer effects.

Additionally, the lift force is similar to the drag force, but rotated perpendicular to the incident flow.

$$F_L \cong \frac{1}{2}\rho_w C_L A v|v| \tag{2-18}$$

The empirical coefficients of the Morison equation are functions of the Reynolds number (Re) and Keulegan-Carpenter number (K_C). The Keulegan-Carpenter number is defined as:

$$K_C = \frac{VT}{L} \tag{2-19}$$

where:
V is the amplitude of the flow velocity oscillation,
T is the period of the flow velocity oscillation,
L is the characteristic length scale.

Drag and inertia coefficients, C_D and C_I, for slope-parallel force were experimentally found to have values of approximately 0.35 and 0.2, respectively for rock armour (Tørum, 1994). Consistent lift force coefficients, C_L, were not found experimentally.

2.4 Motivation for Current Research

This work was inspired by previous physical modelling work done on instrumented breakwater armour units. Sakakiyama (1990) published a study involved the fixing of a model-scale tetrapod armour unit to a force gauge for the determination of hydrodynamics and loading behaviour (Figure 2-26, left).

This study focused on an instrumented double-layer tetrapod unit embedded within an armour layer and mounted at the still water level. Results of this series of experiments show that the loading of the tetrapod to be a function of wave steepness, and an examination of scale effects on CAU behaviour (Figure 2-26, right).

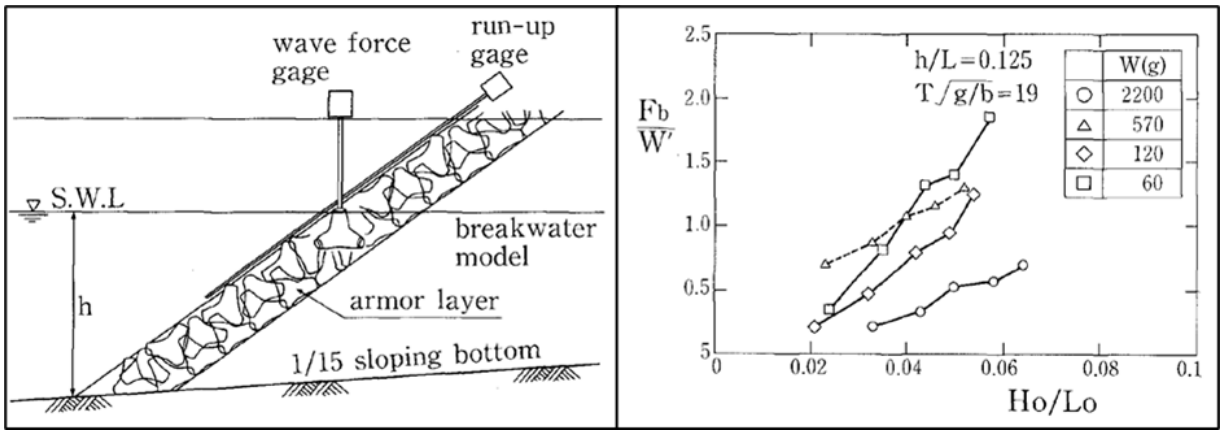

Figure 2-26: Instrumented breakwater (left). Relative wave force depending on model scale (right). (Sakakiyama, 1990)

This study also examined independently the slope-parallel and slope-normal force response of the instrumented armour unit (Figure 2-27, left) showing different force behaviour in the two orthogonal directions. Hodographs of the instrumented units show scale effects, as well as a change in hodograph shape with scale (Figure 2-27, right).

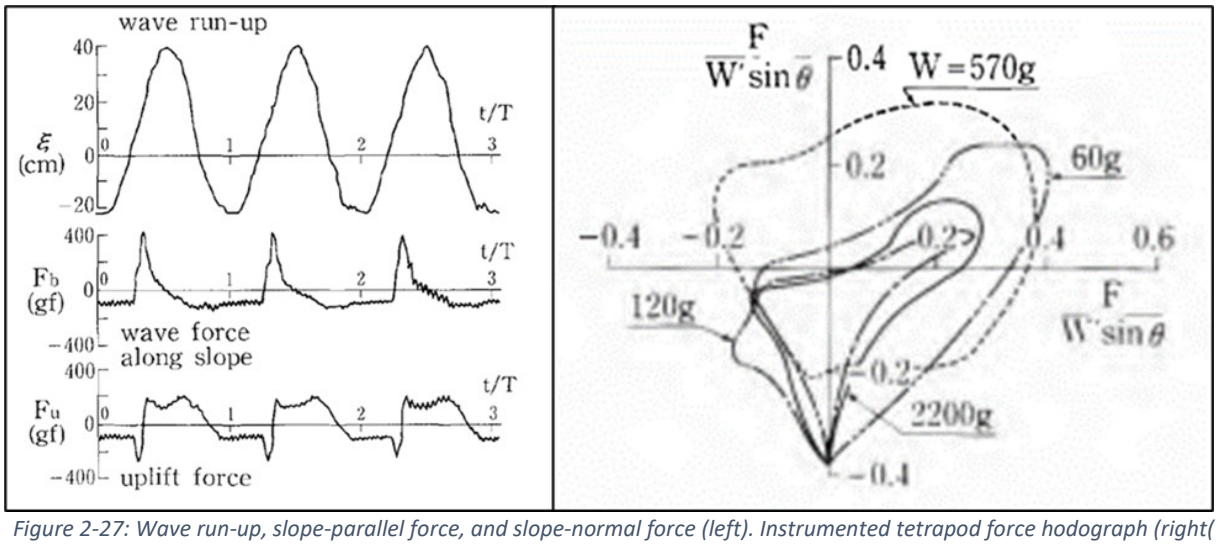

Figure 2-27: Wave run-up, slope-parallel force, and slope-normal force (left). Instrumented tetrapod force hodograph (right((Sakakiyama, 1990)

Three other studies of instrumented armour units have inspired this research: Tørum (1994), Cornett (1995) and Hald (1998). These studies involve the physical modelling of breakwater armour units that have been fixed to force transducers. In Tørum (1994) and Hald (1998), force transducers were fixed to individual armour units, whereas in Cornett (1995) several armour units were instrumented together in a panel of fused modelled armour stones. Methodologies for Tørum (1994) shown in Figure 2-28, Cornett (1995) in Figure 2-29, and Hald (1998) in Figure 2-30.

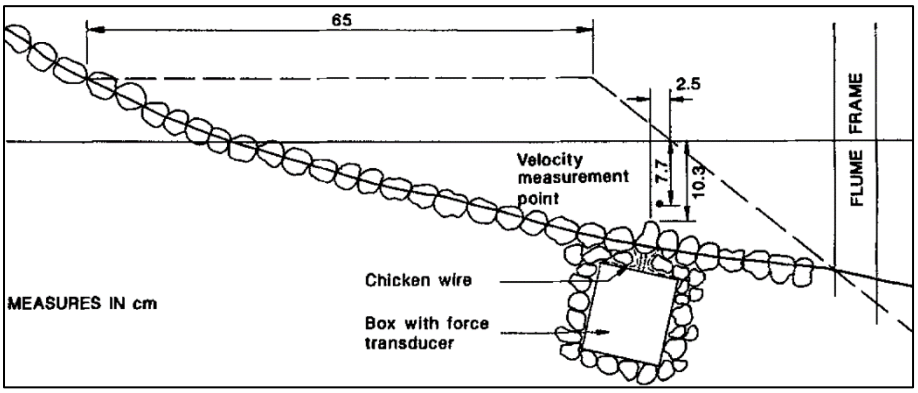

Figure 2-28: Force transducer placed in berm breakwater (Tørum, 1994)

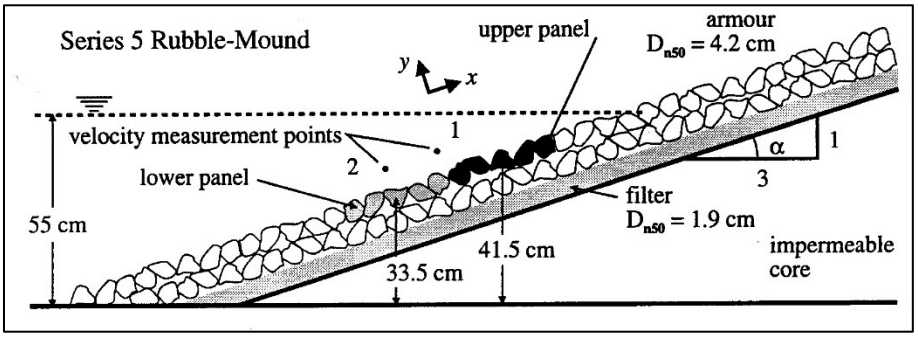

Figure 2-29: Sketch of instrumented armour panel experimental setup (Cornett, 1995)

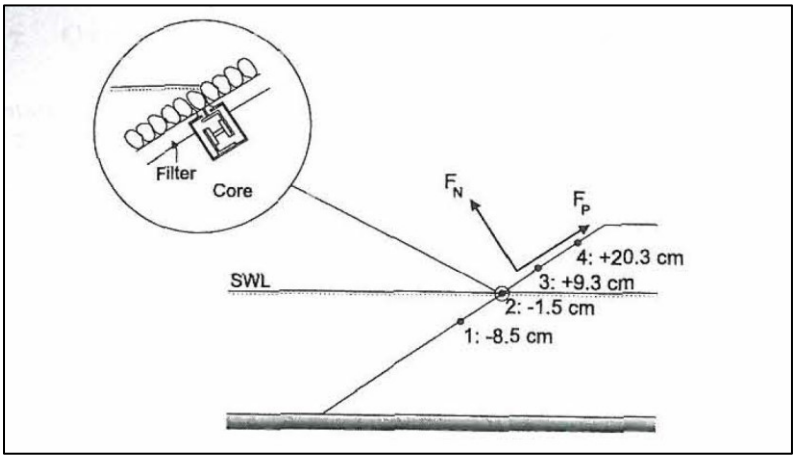

Figure 2-30: Position of force transducer in instrumented armour layer experimental setup (Hald, 1998)

Each of these studies investigated the hydrodynamic response and behaviour of rock armour units under wave loading. Tørum (1994) investigated forces on units, as well as flow velocity and acceleration, in the slope-normal and slope-parallel directions. This work examined the applicability of the Morison equation to the prediction of force response of rock armour units embedded in the flattened section of a reshaped berm breakwater. Tørum determined that the Morison equation's predictive capacity was reliable in the parallel direction, but less so in the normal direction. Slope-parallel and slope-normal experimental forces illustrated in Figure 2-31. Flow velocity and force results are shown in Figure 2-32.

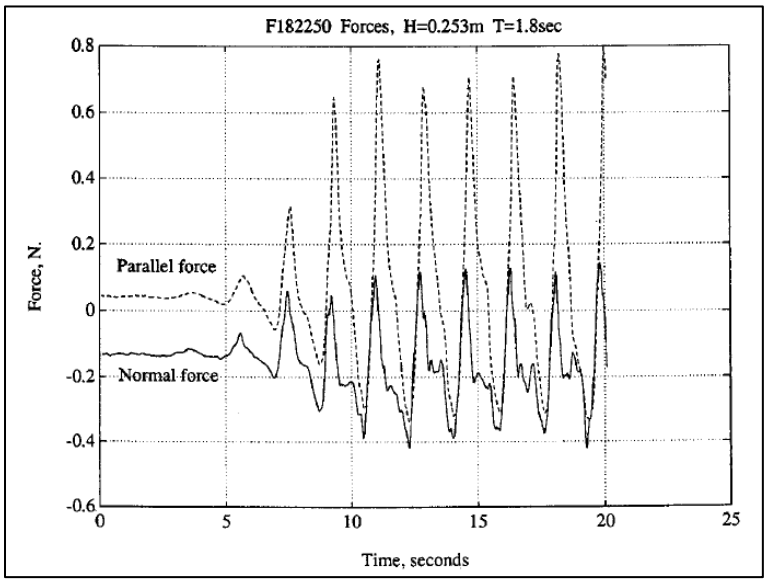

Figure 2-31: Measured parallel and normal forces on instrumented armor stone (Tørum, 1994)

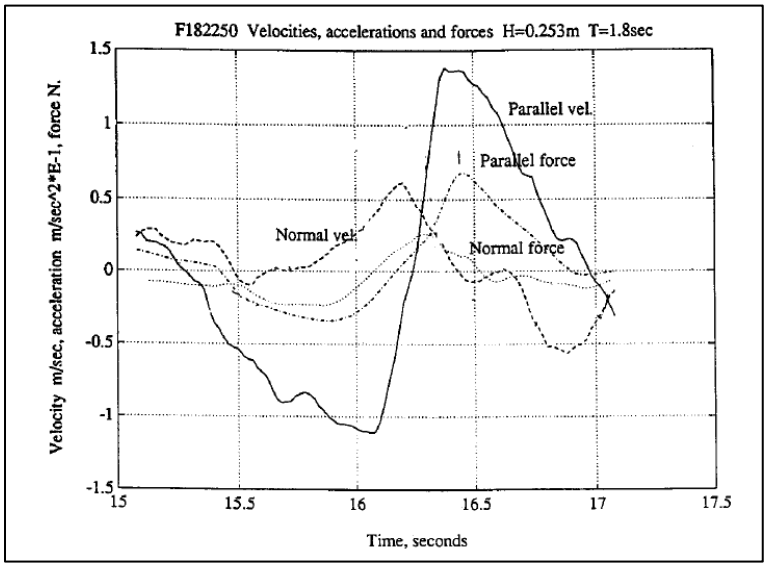

Figure 2-32: Measured velocities and measured forces (Tørum, 1994)

The force-response results of the experiments conducted by Cornett (1995) and Hald (1998) are shown in Figure 2-33 and Figure 2-34.

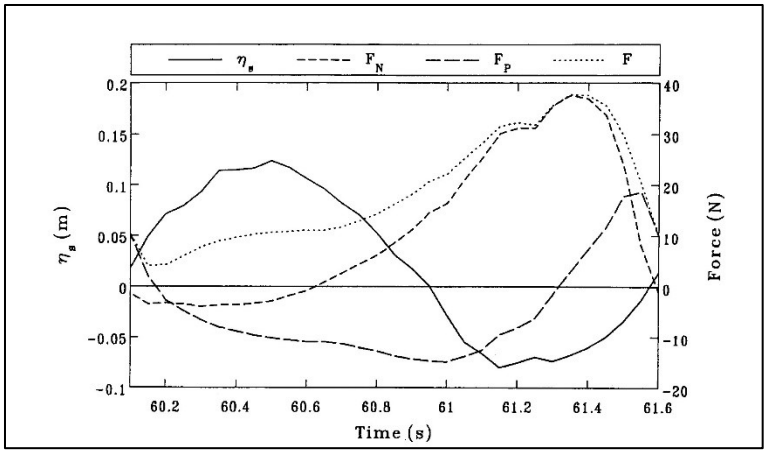

Figure 2-33: Waterline motion and hydrodynamic forces on instrumented armour panel under regular waves (Cornett, 1995)

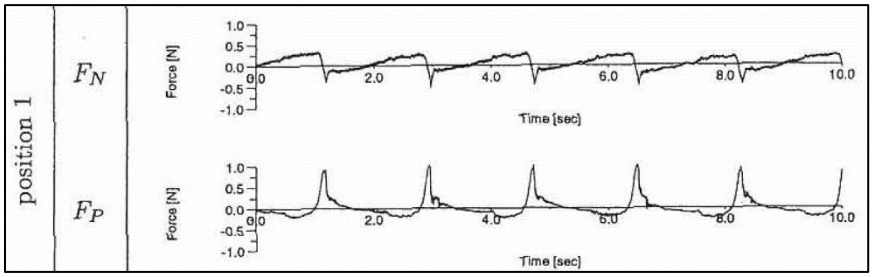

Figure 2-34: Sample normal and parallel force time series (Hald, 1998)

These physical modelling experiments were conducted on breakwaters armoured with rock. The behaviour of breakwaters armoured with concrete armour units is expected to be significantly altered, due to the effects of interlocking as well as unit geometry leading to higher energy dissipation on the armour layer compared with rock armoured breakwaters.

There has been recent development of instrumented concrete armour units, with preliminary work from Hofland (2018) showing promise in the use of independent model-scale units instrumented with small internal accelerometers (Figure 2-35. left). These accelerometers have been used to measure force and response of concrete armour units undergoing wave action (Figure 2-35, right), and are well suited to be used above breakwater failure conditions since these instrumented units are not fixed in place but can rock or be displaced as would be expected of a typical unit. Initial results of this investigation show the use of number of collisions as a proxy for armour unit or layer damage. Santos (2019) investigated antifer armoured breakwater slopes with the use of a similarly instrumented concrete armour unit, showing armour unit rocking, but the instrument used had an insufficient sampling rate for the measurement of unit translation. The use of accelerometers in physical modelling of breakwaters shows promise, though at this stage of development, much can still be discovered through the more traditonal means of directly affixing the armour unit under investigation. There is also a significant functional difference between the single-layer type armour units, such as the Core-Loc, and double-layer systems such as cubes, tetrapods or antifers.

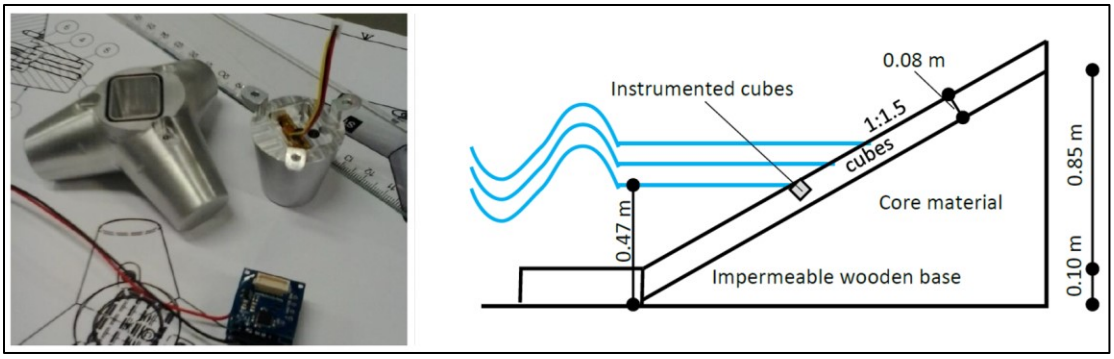

Figure 2-35: Tetrapod instrumented with accelerometer (Left). Experimental setup (Right). (Hofland, 2018)

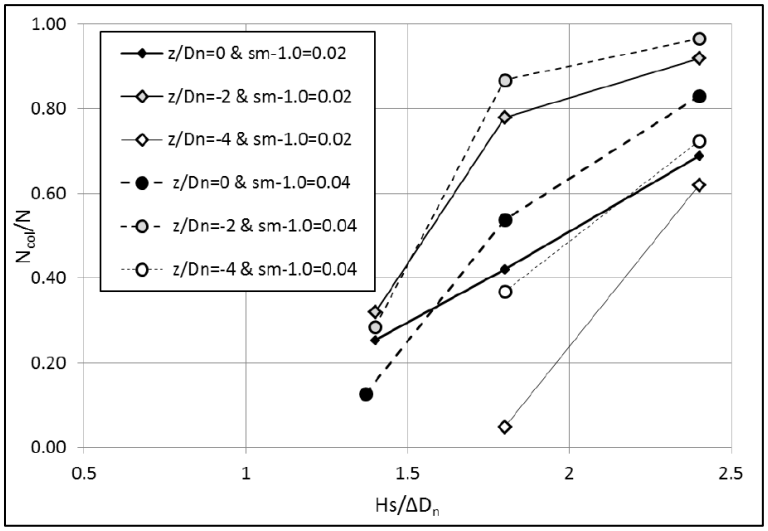

Figure 2-36: Number of collisions as a function of stability number, elevation and wave steepness . (Hofland, 2018)

There has also been, along with developments in physical modelling of breakwaters, been significant development of numerical modelling of breakwaters, for which the results of this experiment would be pertinent. The calibration and validation of numerical models of complex fluid-structure interaction, such as that in a rubble-mound breakwater, requires accurate and precise data. Physical modelling such as that done for this experiment is critical to the development of such models. Significant advances in breakwater armour layer modelling have been made by Latham et al. (2008, 2013) (Figure 2-37), in which fluid-structure interaction of Core-Loc CAUs is under development via proprietary FEMDEM methodology, such as simulation of wave breaking on fixed numerical CAUs. Altomore et al. (2014) (Figure 2-38) have published results of numerical smooth particle hydrodynamic (SPH) modelling of fluid flow through the interstitial space within antifer breakwaters, and Dentale et al. (2014) (Figure 2-39) have developed an SPH model of concrete armoured rubble-mound breakwaters in which uncalibrated and unvalidated numerical force measurements can be calculated.

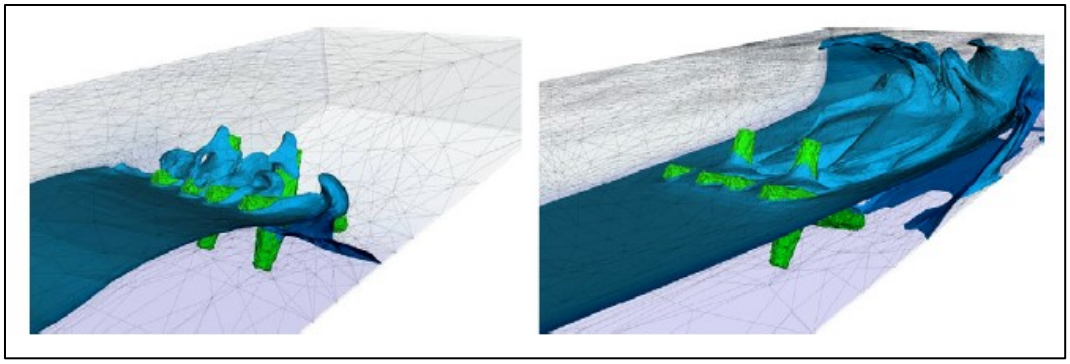

Figure 2-37: Simulated wave breaking on fixed concrete armour units (Latham, 2008)

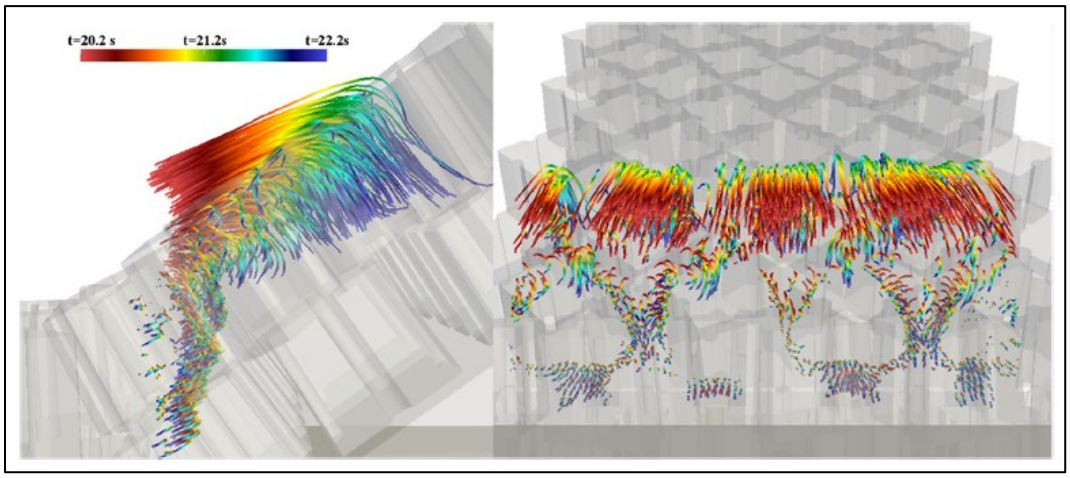

Figure 2-38: Smooth particle hydrodynamic trajectories of fluid particles within antifer breakwater (Altomore, 2014)

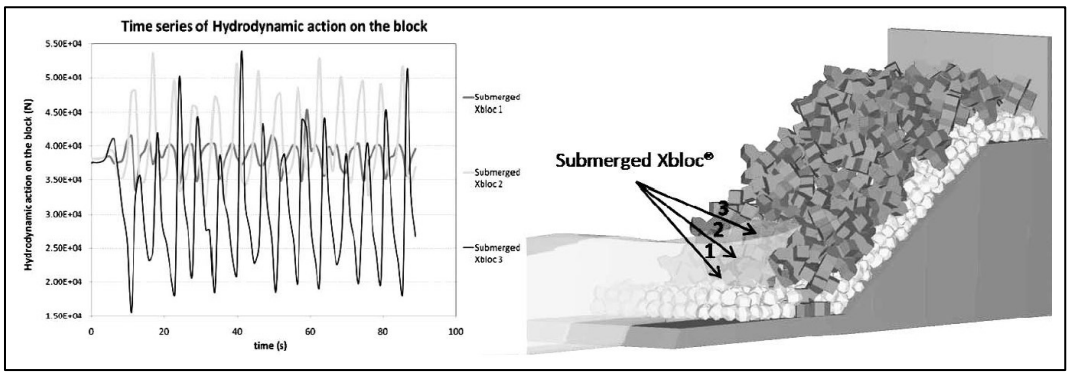

Figure 2-39: Modelled hydrodynamic forces on single submerged Xbloc armour unit (Dentale, 2014)

3 METHODOLOGY

This chapter discusses the methodology followed for this series of experiments. Experimental facility and equipment, including the manufacture of custom CAUs, experimental procedure, instrumentation as well as wave synthesis and generation are discussed. There follows a description of scale effects and the processing of acquired data.

3.1 EXPERIMENTAL FACILITY

The experiments were conducted at the National Research Council of Canada's Ocean, Coastal, and River Engineering (OCRE-NRC) Hydraulics Lab located in Ottawa, Ontario.

Under this experimental regime, a series of wave action tests were done on a Core-Loc armoured rubble mound breakwater structure. For this structure, custom Core-Loc model-scale armour units were fabricated as well as a custom sloped and instrumented breakwater core.

3.2 WAVE FLUME

The flume used for this testing was the Steel Wave Flume, measuring 64 m x 1.2 m x 1.2 m (210' x 4' x 4'). The flume is equipped with a wave generator as well as an active wave absorption system. There is also a passive wave absorption system installed at the downstream terminus of the flume, though these were unused in this series of testing due to lack of wave transmission past the testing site. A concrete foreshore was installed at a grade of 3% over a length of 7.66 m. A plan schematic (Figure 3-1), elevation schematic (Figure 3-2), and 3D photogrammetric scan (Figure 3-3) are included below.

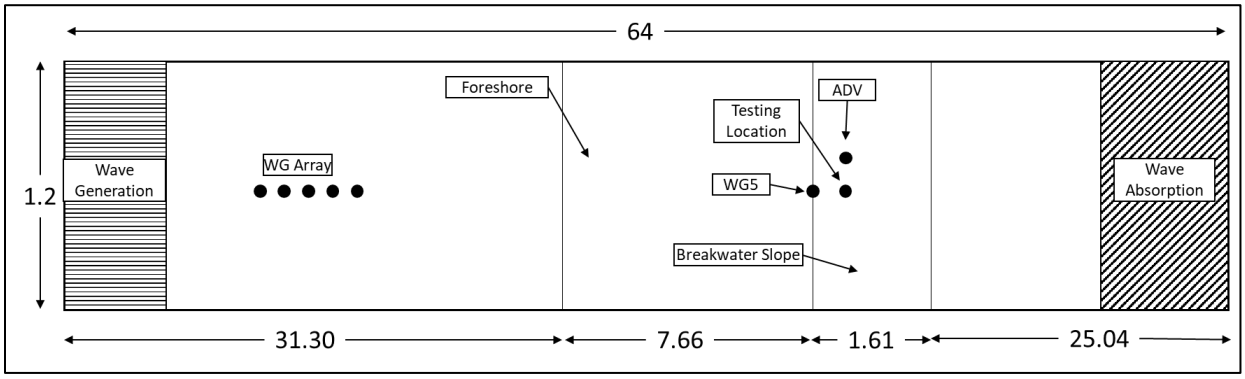

Figure 3-1. Plan schematic of steel wave flume (not to scale)

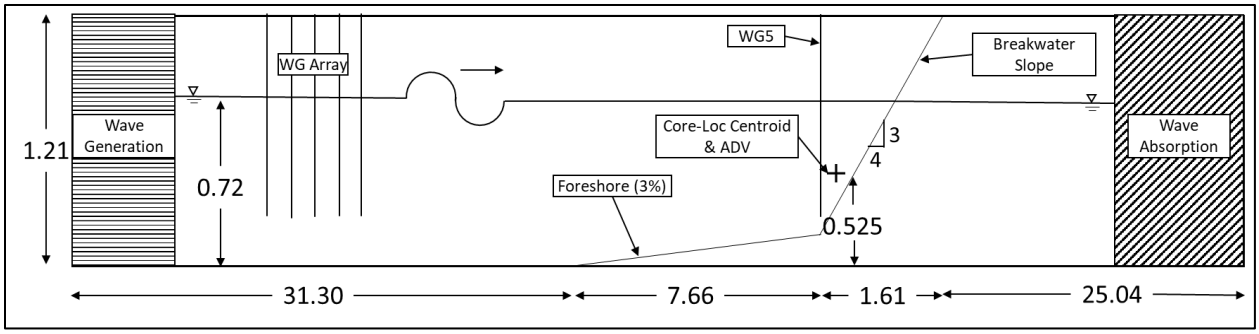

Figure 3-2. Elevation schematic of steel wave flume (not to scale)

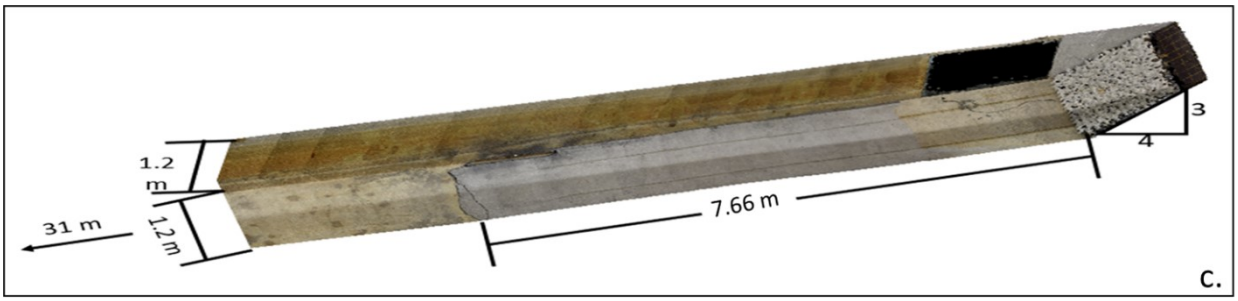

Figure 3-3. Photogrammetric scan of steel wave flume

At the top of the grade, an artificial, impermeable 15 mm thick PVC slope was installed (Figure 3-4, left). The slope has a grade of 3V:4H, typical for Core-Loc armour layers. The front face of this slope was rubberized using an aerosol rubber sealant (Rust-Oleum Leak Seal). This was done to reduce slippage of armour units or underlayer rocks on the slope as well as to allow a rougher surface for better silicone adhesion. This adhesion was necessary to prevent neighbouring armour units from interfering with the forces measured during the tests. The slope was then painted with guidelines to allow the placement of armour units at a $\phi = 0.62$ packing density (Figure 3-4, left).

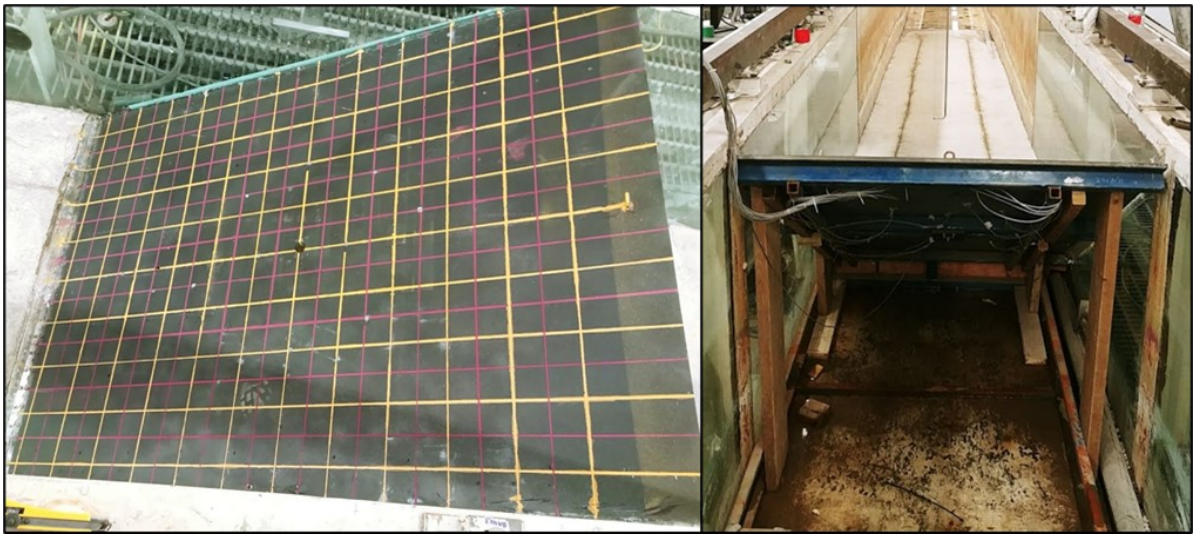

Figure 3-4: Front face of PVC slope (left). Rear of PVC slope apparatus (right).

The PVC slope is reinforced by a frame of welded 50 mm x 50 mm square steel tubing. This apparatus was held in place by a frame of 2” x 6” timber columns (Figure 3-4, right).

3.3 Concrete Armour Units

The armour units chosen for this series of tests was the Core-Loc type unit with a characteristic length[7] of 0.12 m. This length was chosen due to mechanical limitations in the construction of a custom 3D printed instrumented armour unit (Figure 3-5, left). The instrumented armour unit is counter-sunk with threaded nuts that allow the rigid attachment of the unit to a load cell (Figure 3-5, right). It is also equipped with imbedded pressure sensors that are wired to a Raspberry Pi, as well as analog-digital-converters for processing. This instrumented armour unit was used as the source of the dimensions for all further units that were to be manufactured. The instrumented armour unit itself is discussed in further detail in Eden, 2019. The ¼” rod threaded into the instrumented armour unit was then rigidly connected to a load cell (ATI Mini45 IPC68). The connection is made by a custom bracket, machined by the University of Ottawa machine shop, and held in place by two Allen keyed set screws. The load cell is fixed on a plate of 15 mm PVC. The load cell is enclosed by a tightly fitting section of 2” PVC tubing which prevented the flow of water through the hole drilled through the PVC slope for the connecting rod the instrumented unit and load cell (Figure 3-5).

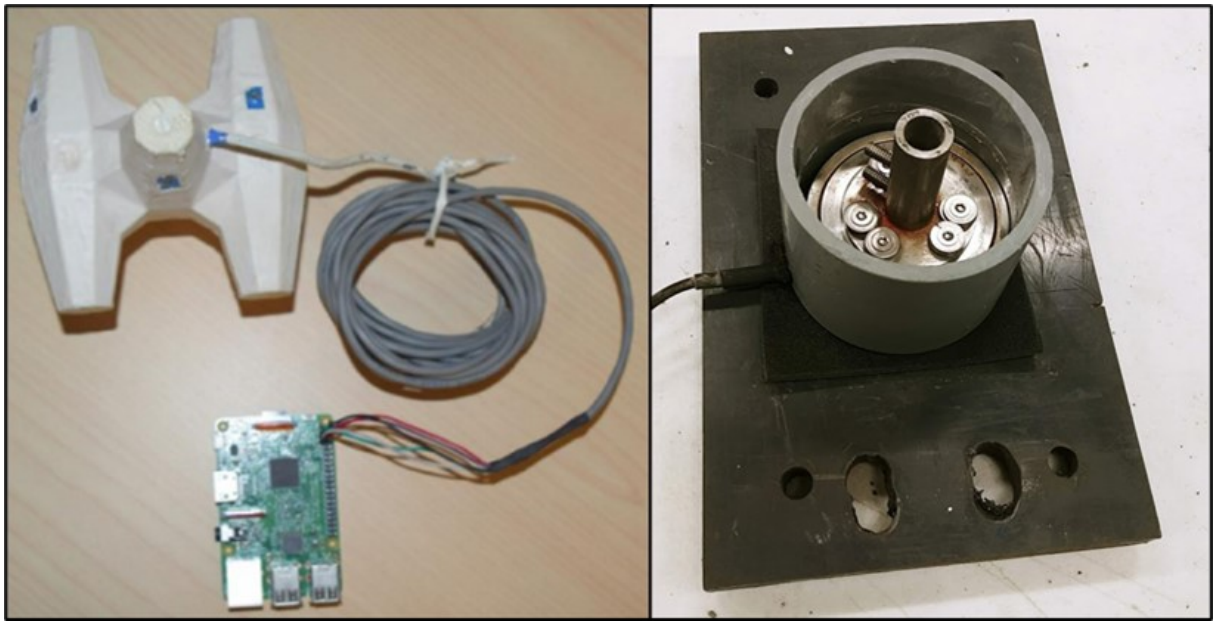

Figure 3-5. 12 cm Instrumented Core-Loc Unit (Eden, 2019 (left). Load cell and mounting apparatus (right)

This plate was then fixed to the artificial core slope either by being bolted directly to the frame for a load cell location close to the still water level, or by being bolted to a piece of wood fixed to the

[7] Characteristic length or armour unit height is calculated using the shape coefficient, by $C = \left(\frac{V_{CAU}}{K_s}\right)^{\frac{1}{3}}$, where C is the characteristic length, V_{CAU} is armour unit volume, and K_s is shape coefficient (with a value of $K_s = 0.2211$ for Core-Loc units) (CLI, 2012)

reverse side of the slope for the lowest testing locations. (Figure 3-6, left) In order to facilitate the repeated decoupling and reassembly of the instrumented armour unit from the load cell, a connection was made between two sections of threaded rod – between the instrumented unit and the load cell. This connection used a section of sheet copper that has been fixed to the threaded rod by two hose clamps (Figure 3-6, right).

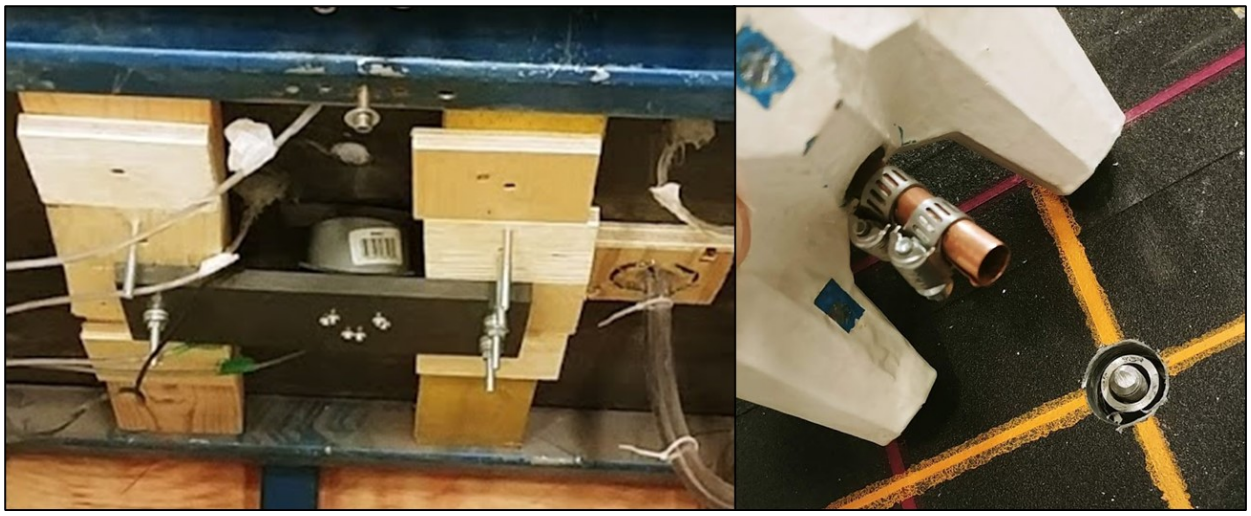

Figure 3-6: Load cell mounted to PVC slope (left). Threaded rod connection between load cell and instrumented armour unit (right).

When attached to the load cell, the output cable of the instrumented armour unit was secured to the underlying geogrid for the porous series of tests (Figure 3-7, left), and to the rod holding the ADV in place in the impermeable series of tests (Figure 3-7, right).

Figure 3-7: Top of filter layer, geogrid, and instrumented unit (left), Instrumentation wire, ADV connection, and pressure sensor apparatus mounted through PVC board (right)

Since the laboratory facility had only the typical 0.04 m characteristic length Core-Loc units on hand, the concrete armour units for the embedded testing phase needed to be manufactured. The need for a 0.12 m characteristic length for all these units was established by the 3D printed instrumented armour unit.

The concrete armour units were constructed from poured concrete grout using SIKA 212 HP grout. This is a “high performance, non-shrink, fluid, cementitious grout with silica fume” with a 28-day compressive strength of 62 MPa. The units were constructed by pouring the grout into plaster of Paris molds. The molds themselves were created by pressing a 3D-printed half-unit into the wet plaster. Model units were made one half-unit at a time and connected by either a bolt or loop of wire (Figure 3-8 ,left).

Figure 3-8. Model scale concrete armour unit manufacturing process (left). Finished, painted, custom concrete armour units (right).

Once cured, the molds were struck, and the model units cleaned with a rasp and painted. The purpose of the paint was to allow for a more uniform surface of the units, since there were rough sections where excess material had been removed. The paint also reduces the skin friction on the units and would reduce the effect of scale. (Figure 3-8, right). In total, 170 such units were manufactured for this series of experiments.

The armour units were placed on the slope along the guidelines for a 0.62 packing density. As the units were placed, they were fixed at their intersection points with a bead of silicone. They were both fixed to each other and to the slope. The instrumented unit, when installed in a Core-Loc armour layer was allowed freedom of motion by preventing the nearby units from coming into contact with it. This arrangement ensures that any forces imparted onto the instrumented armour unit will be transferred to the load cell and recorded. The influence of interlocking forces (F_i) is therefore eliminated ($F_i = 0$). Figure 3-9 shows this arrangement.

Figure 3-9. Typical setup of units in Core-Loc armour layer (instrumented unit at centre)

3.4 TEST CONDITIONS

The armour layers of the tested breakwater were built under four regimes:

1. Impermeable slope with an isolated instrumented armour unit (Figure 3-10)
2. A permeable filter layer, atop an impermeable slope (core) with isolated instrumented armour unit (Figure 3-11)
3. Impermeable slope with the instrumented armour unit embedded in a full armour layer of Core-Loc units (Figure 3-12)
4. A permeable filter layer, atop an impermeable core with the instrumented armour unit embedded in a full armour layer of Core-Loc units (Figure 3-13).

Experimental scenarios used during this suite of testing are summarized in Table 3-1.

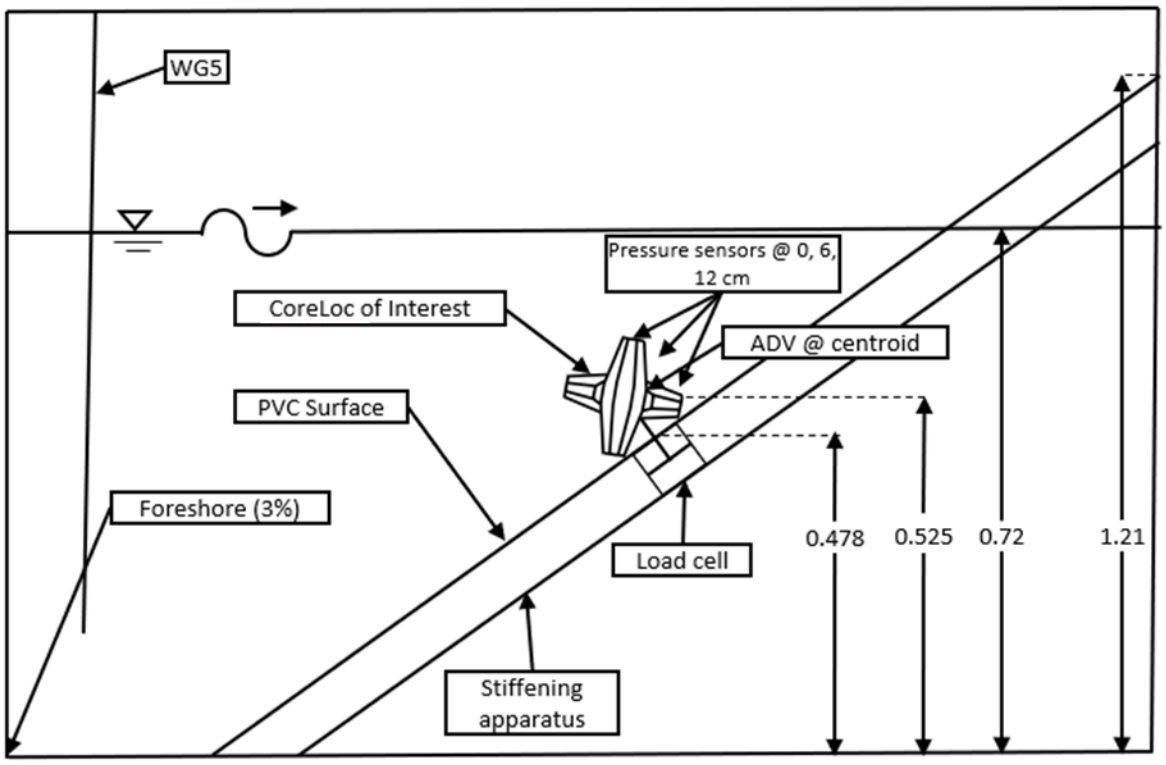

Figure 3-10. Impermeable, isolated single-unit testing setup

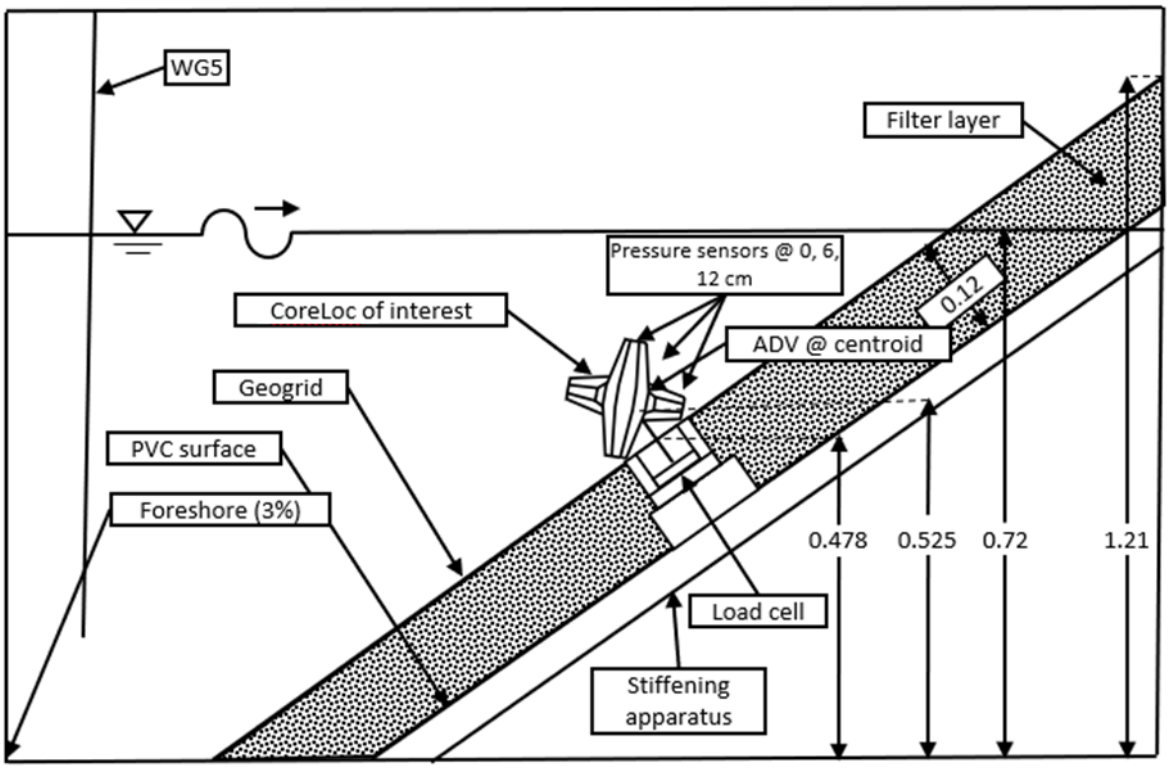

Figure 3-11. Isolated unit setup with porous filter layer

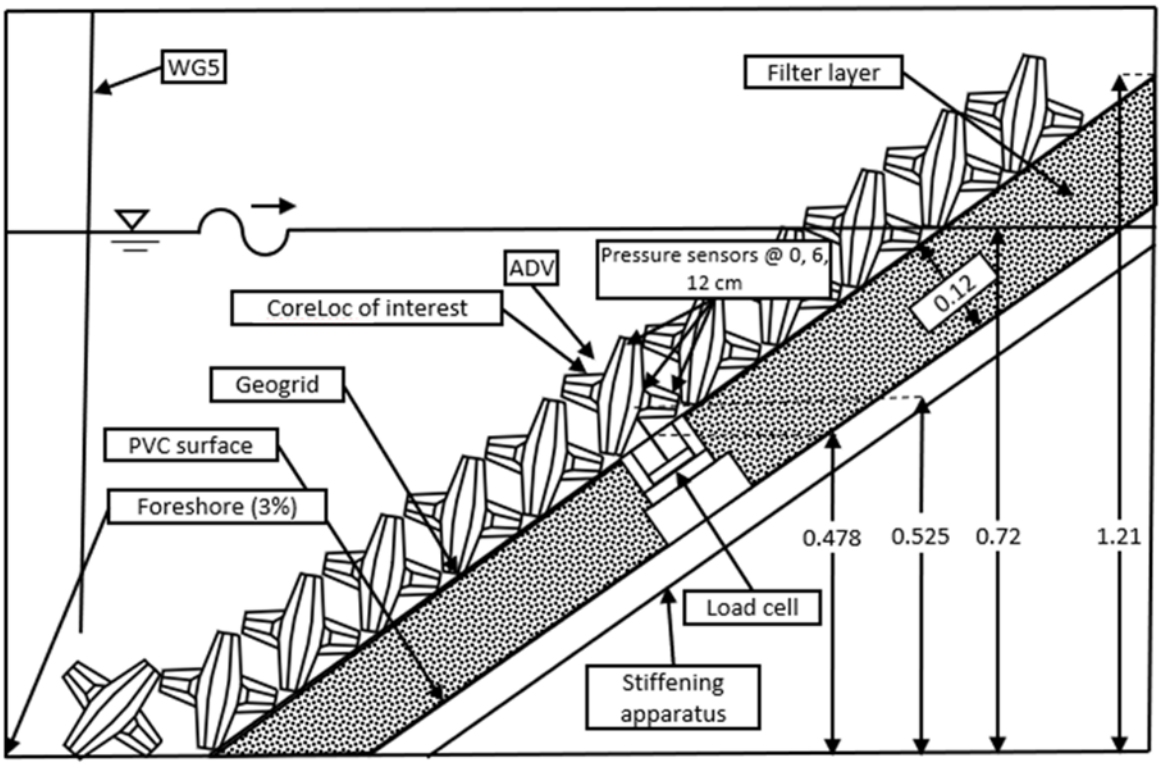

Figure 3-12. Instrumented unit embedded within concrete armour layer with porous filter layer setup

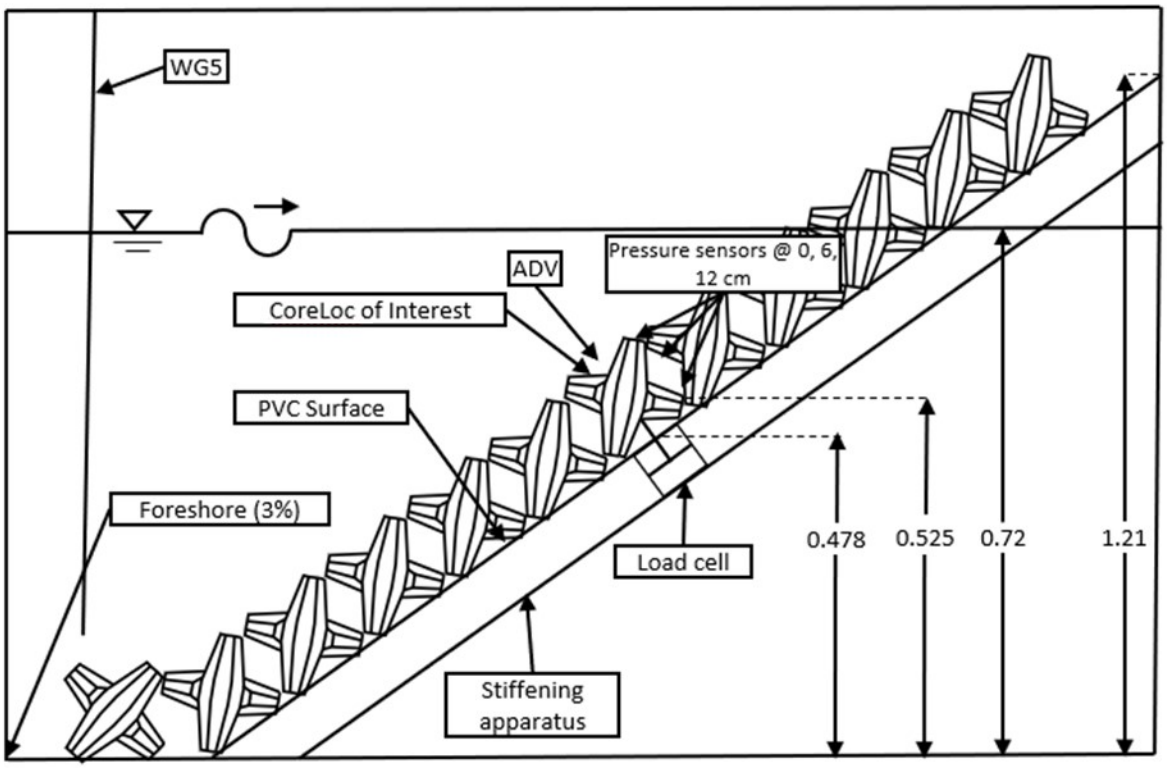

Figure 3-13. Instrumented unit embedded within concrete armour layer with impermeable filter layer setup

Table 3-1. Four experimental scenarios used as part of this suite of tests

Experimental Setups	Front View	Profile View
• Isolated armour unit • No filter layer • Impermeable core		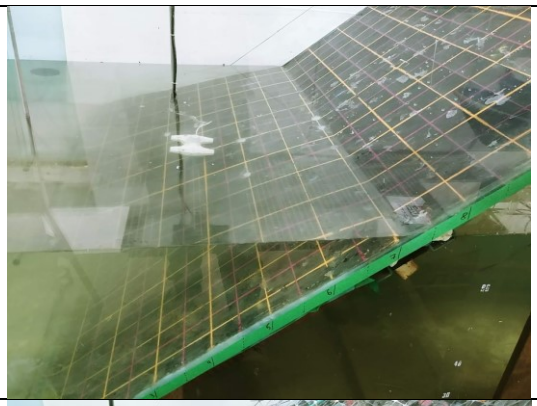
• Isolated armour unit • 12 cm permeable filter layer • Impermeable core		
• Embedded armour unit • No filter layer • Impermeable core		
• Embedded armour unit • 12 cm permeable filter layer • Impermeable core		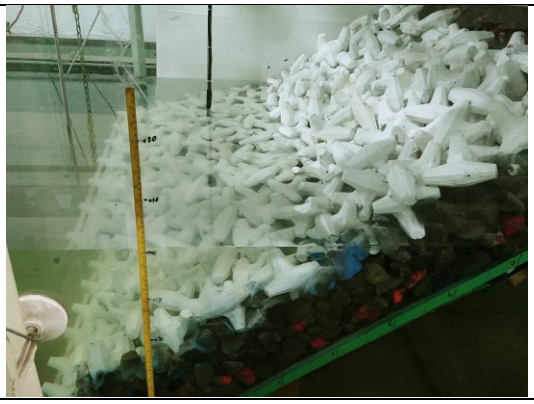

3.5 Experimental Procedure

For each day of testing, the following procedure was followed:

- Fill the wave flume to 72 cm with fresh water $\left(\rho \cong 1000 \frac{kg}{m^3}\right)$
- Calibrate 6 wave gauges using 3 known points and NRC's NDAQ software
- Calibrate the load cell to read zero while submerged in hydrostatic conditions
- Ensure full range of motion for the instrumented armour unit
- Using wave signals that have been calibrated to produce the prescribed significant wave height at the toe of the structure, run the waves via NRC's proprietary wave signal software.
- Collect data via the NDAQ system. Force data from the load cell, pressure data from the pressure sensors, water velocity data from the ADV, and wave gauge elevations are collected this way. Data was collected at 1000 Hz, with the exception of wave gauge data which was collected at 50 Hz.
- Record video of the testing with a Nikon D5300 DSLR camera, running at nominal 60 FPS. The camera was remotely triggered to avoid disturbance.
- Allow the water in the flume to settle
- Repeat testing for all wave conditions

Setting a new armour layer setup required the dismantling of the previous armour layer, and the assembly of the new layer by the guidelines provided by the Core-Loc manufacturer, CLI (CLI, 2011) . This includes the packing density target of 0.62 as well as the interlocking behavior of units. For example, each unit must have an orientation different from its neighbours and must interlock at least two units below it. After armour layer assembly, the units were then fixed together using a bead of silicone (GE 100% waterproof gutter silicone) to ensure they would not move excessively during testing. This silicone was allowed 24 hours to cure before each new round of testing.

3.6 Instrumentation

Forces on the instrumented armour unit were collected with a load cell (ATI Mini45 IP68[8]). This is a six degree of freedom force transducer, though only forces in three dimensions were recorded. Moments built up in the system were disregarded.

Honeywell TBF-Series pressure sensors[9] were imbedded in the PVC slope by drilling a hole through the slope of the diameter of the sensor's diaphragm. The sensor was then epoxied into the hole. A flexible tubing apparatus designed to take pressure readings at three vertical locations (0 cm, 6 cm, 12 cm) was also mounted on the slope within the same row as the instrumented armour unit. The vertical locations correspond to elevations at which the armour unit rests (filter layer or core), the midpoint of the concrete armour unit, and the top plane of the armour layer (Figure 3-14). The pressure sensors were fitted to the end of 1.2 m of Tygon tubing which was filled with water. In this way, the

[8] Compact force sensor rated for submersion in fresh water to a depth of 4 m. High signal to noise ratio. Sensing ranges: Fz = 290 N, Fx & Fy = 145 N. Force resolution: Fz, Fx & Fy = 1/16 N. https://www.ati-ia.com/products/ft/ft_models.aspx?id=Mini45+IP65%2FIP68

[9] Analog, compensated, unamplified flush diaphragm pressure sensors. Internally temperature compensated and calibrated. ±0.15 %FSS resolution. https://sps.honeywell.com/us/en/products/sensing-and-iot/sensors/force-sensors/basic-tbf-series

wiring and electronics of the sensor could be kept dry above the water surface with the diaphragm remaining exposed to pressure fluctuations at the location of interest.

Figure 3-14: Flexible tubed pressure sensor apparatus

Six capacitance type wave gauges were employed along the length of the flume. Five of these gauges were arranged in an offshore array. The sixth wave gauge was installed at the toe of the structure.

A Nortek brand acoustic doppler velocimeter[10] (ADV) was used to record the velocity timeseries of the tests. The ADV was oriented facing the centroid of the instrumented armour unit and measured a sample volume approximately 0.05 m away from the instrumented unit itself at the same elevation during single unit tests. During embedded testing, the ADV was mounted 0.02 m above the armour layer and recorded readings in the same horizontal location as during the single unit tests.

Data was recorded through an IMC Cronos Compact DAC system[11], and the NRC proprietary NDAQ data acquisition system. During most tests, the data was acquired at 1000 Hz, though some tests were run at 200 Hz.

3.7 Wave Synthesis and Generation

The following wave conditions (Table 3-2) were tested during this series of tests. Each of these tests was performed in both an embedded armour unit setup as well as a setup with a single isolated concrete armour unit. Figure 3-15 shows the tested wave heights and periods.

[10] Nortek Vector – 300 m. High accuracy single-point current meter with small sampling volume. 64 Hz maximum sampling rate. Accuracy of ±0.5% of measured value ±1 mm/s. https://www.nortekgroup.com/products/vector-300-m

[11] Imc CRONOScompact 400-11. 400 kHz maximum sampling rate. https://www.imc-tm.com/products/daq-systems/imc-cronoscompact/overview/

Table 3-2. Testing conditions run in both isolated and embedded scenarios

Test	Period - T (s)	Wave height - H (s)	Iribarren number - ξ (-)	Wave Steepness – s (-)
1	1.4	0.12	3.79	0.065
2	1.8	0.12	4.87	0.032
3	2.2	0.12	5.95	0.026
4	2.6	0.12	7.03	0.022
5	3	0.12	8.12	0.049
6	1.4	0.15	3.39	0.030
7	1.8	0.15	4.36	0.024
8	2	0.15	4.84	0.017
9	2.4	0.15	5.81	0.012
10	2.8	0.15	6.78	0.009
11	3.2	0.15	7.74	0.007
12	3.8	0.15	9.19	0.049
13	1.4	0.2	2.93	0.007
14	2	0.2	4.19	0.039
15	2.2	0.2	4.61	0.024
16	2.4	0.2	5.03	0.011

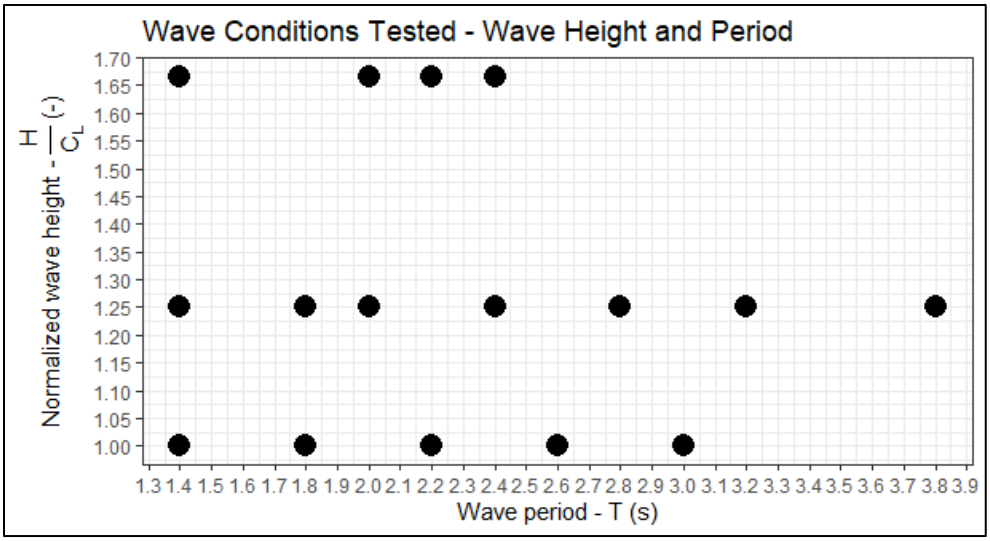

Figure 3-15: Wave conditions tested, for fully armoured and isolated armour unit scenarios

Along with these regular wave conditions, three random waves were tested, using JONSWAP parameters. All random waves were programmed for a significant wave height of Hs = 0.15 m and three peak periods were tested: Tp = 1.8 s; 2.2 s and 2.6 s.

3.8 Scale Effects

The concrete armour units used in this series of testing are much larger than those typically used for hydrodynamic testing. Typical armour units have a characteristic length of 0.04 m, whereas those used in this study are of 0.12 m. The relationship between Core-loc length and volume/mass is cubic ($V = 0.2236C^3$)(CLI, 2011). Therefore, this threefold increase in length will cause a 27-fold increase in mass and volume. This increase in scale reduces laboratory and scale effects traditionally observed with physical model testing, such as a reduction of the influence of viscosity and surface tension. As a result, these larger scale tests have a greater degree of reliability than those performed with typical 0.04 m model units.

3.9 Data Processing

3.9.1 Load Cell Signals

Raw data collected from the load cell can be seen in Figure 3-16. Instrument noise can be seen in the periods of calm water before and after the wave train has arrived at the structure. The noise was removed by passing the signal through through a lowpass Butterworth filter.

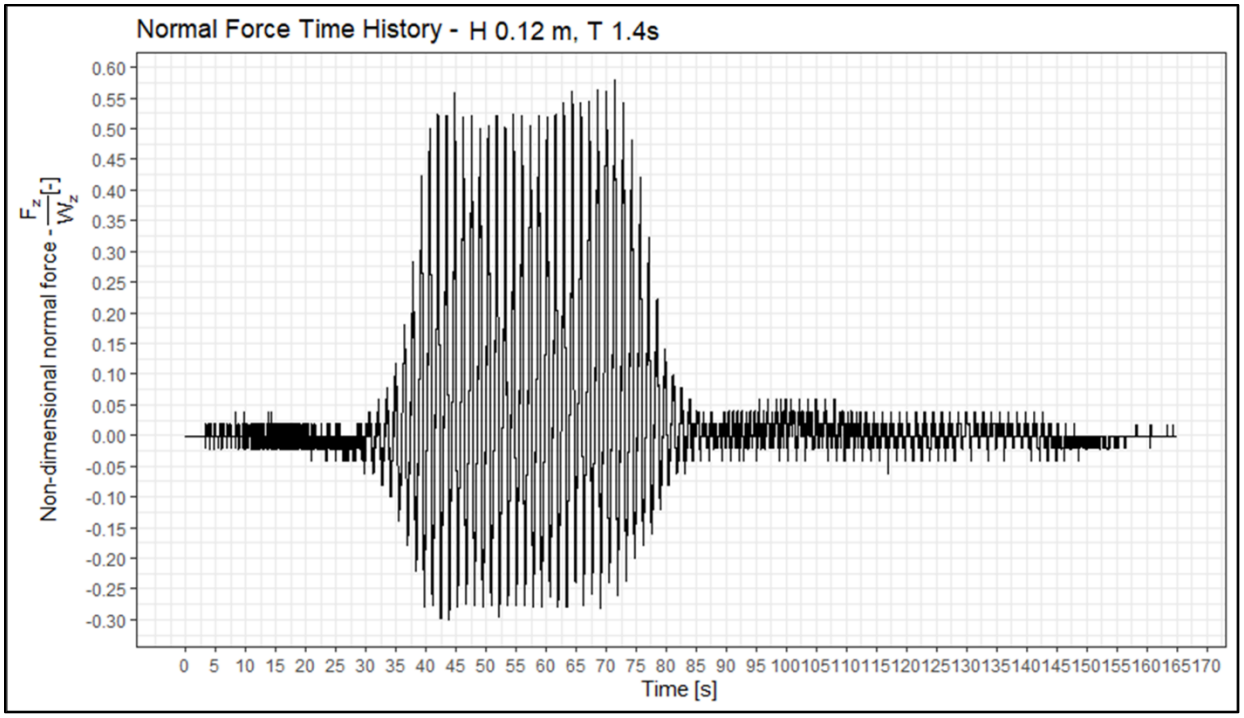

Figure 3-16: Typical load cell signal (Normal force, fully armoured scenario, h = 0.12 m, T = 1.4 s)

3.9.2 Signal Processing

Data collected via load cell and ADV was low-pass filtered with a 15 Hz Butterworth filter via the R 'Signal Processing' package. 15 Hz was chosen to retain as much signal as possible, while reducing noise. This distinction can be seen in Figure 3-17 and Figure 3-18. The velocity peak of Figure 3-17 has been slightly attenuated by the signal filtering. Since these are peaks caused by regular wave loading, large discontinuities are not likely to occur and are much more likely to be signal noise, and were thus removed from the signal. Figure 3-20 depicts the spectra of the horizontal velocity (v_x) signal before and after application of the Butterworth filter. Influence of high frequency noise has been greatly reduced by filtering.

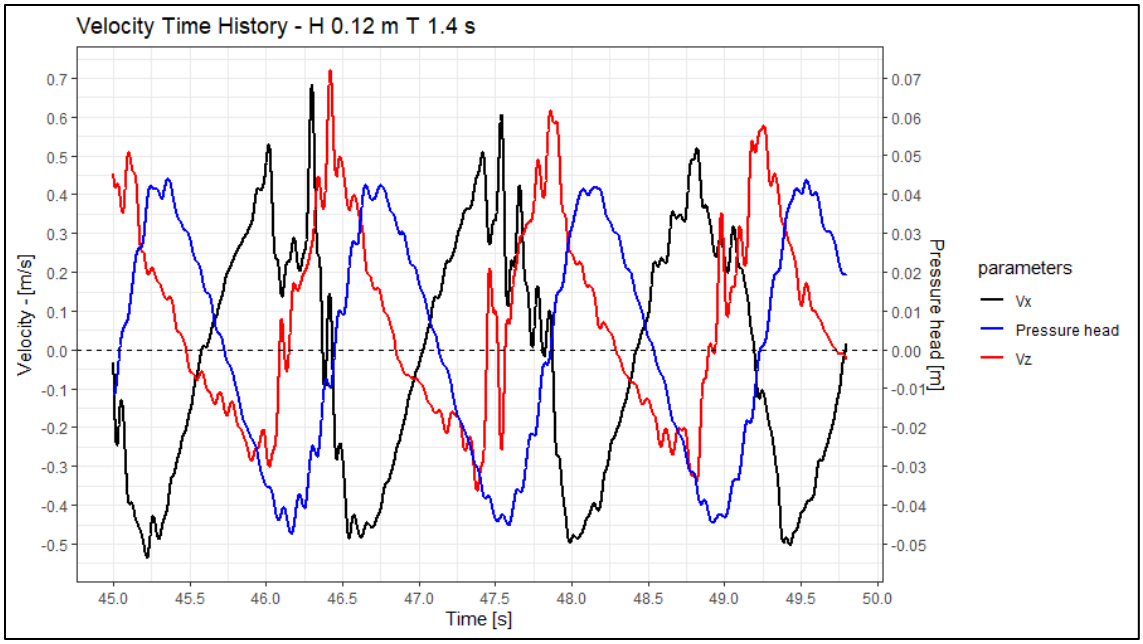

Figure 3-17: Velocity and pressure head time history, embedded armour unit (no filtering)

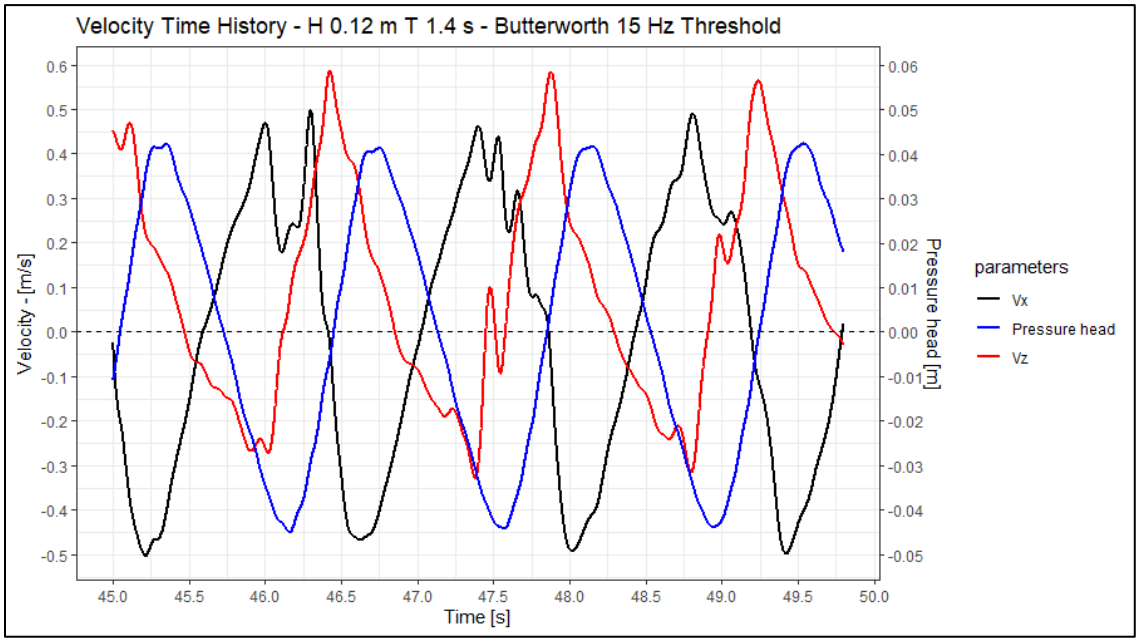

Figure 3-18: Velocity and pressure head time history (15 Hz Butterworth filter)

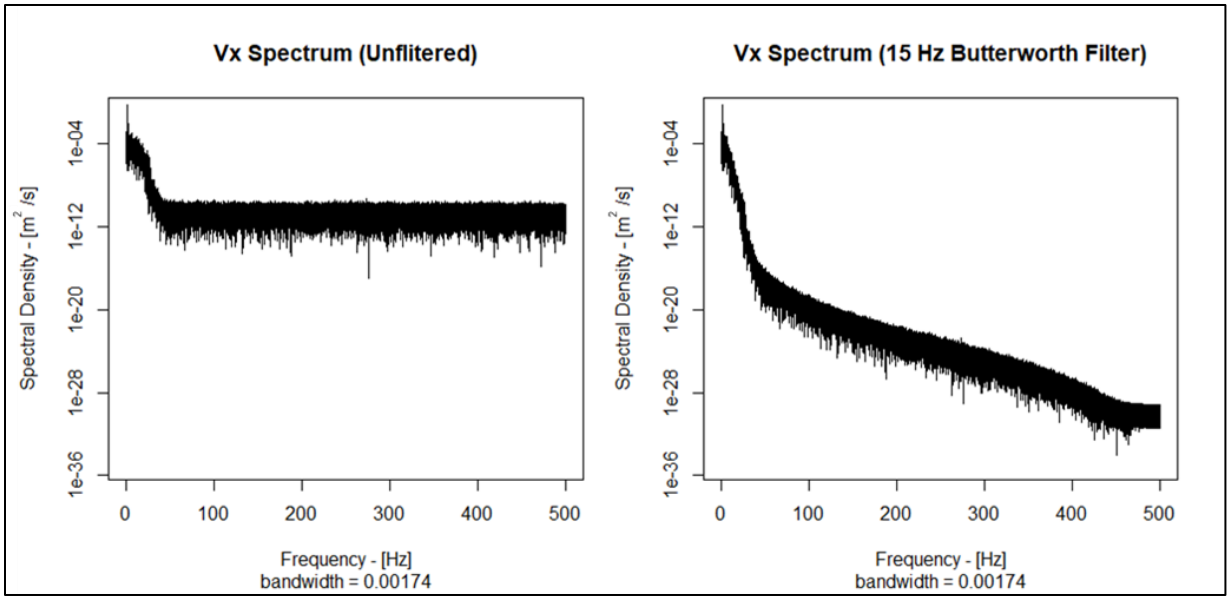

Figure 3-19: Frequency domain plot of x-direction velocity as captured by ADV (left) and after Butterworth filtering (right)

3.9.3 Non-Dimensionalization

Parameters under investigation for this study were non-dimensionalized where possible. This non-dimensionalization was conducted for the time-history of the force data by dividing the component of the force by the corresponding component of the submerged weight of the armour unit. E.g.:

$$F_{\frac{x}{W_x}} = \frac{load\ cell\ reading\ in\ slope-parallel\ direction}{slope\ parallel\ weight\ of\ armour\ unit}$$
$$= \frac{load\ cell\ reading\ in\ slope-parallel\ direction}{V_{CAU} \times g \times (\rho_{concrete} - \rho_{water})}$$

3.9.4 Pressure Head

Pressure head is calculated by the total pressure observed at the base of the instrumented concrete armour unit, less the hydrostatic pressure. Therefore, at still-water the pressure head at the armour unit will be set to zero. This pressure head is composed of primarily hydrostatic pressure above the instrumented unit and can be thought of as a proxy for water surface elevation at the unit itself. There is also an unknown component of this pressure arising from dynamic pressure in the interstitial space between the armour units and in the armour layer, and thus the total pressure head is not an exact measurement of water surface elevation. Motivation for the use of this pressure sensor data to approximate water surface elevation was due to the fine temporal nature of the data and the wave transformation caused by the structure itself. No capacitance wave gauges were able to be deployed directly above the instrumented armour unit without compromising the flow field. The closest wave gauge was installed at the toe of the structure.

3.9.5 Extraction of Peak Values

Peak values were extracted from time series data by the 'findpeaks' function in R. The accuracy of this method can be seen in Figure 3-20. The data used for peak extraction was a 10 second wave signal after

waves had reached the structure. The peaks found during this time period were averaged via the mean to find the average max (or min) force during a test.

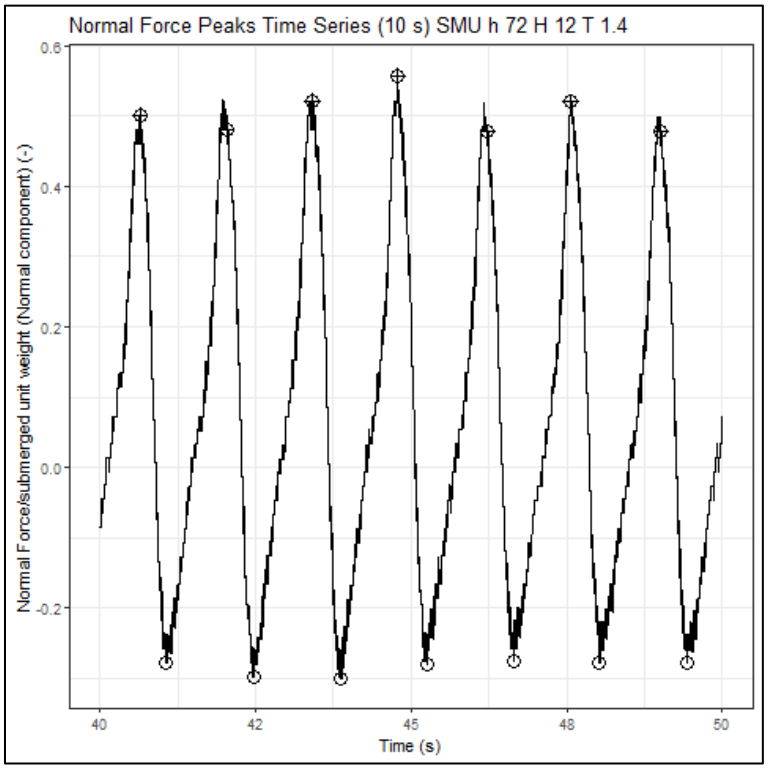

Figure 3-20: Normal force peaks, found via the 'findpeaks' function

3.9.6 Armour Unit Buoyancy

The force data used for this analysis is taken via load cell fixed to an instrumented armour unit. This unit is found, at its highest point, to be 0.15 m below the still water level. Due to wave transformation across the armour layer, incident waves even of 0.2 m at the toe of the structure do not expose the submerged armour unit. If during testing of the largest waves, the instrumented unit is exposed, it is only momentarily, as can be seen in Figure 3-21. The effect of partial buoyancy, induced by the partial emergence of the instrumented armour unit, has thus been neglected in this analysis.

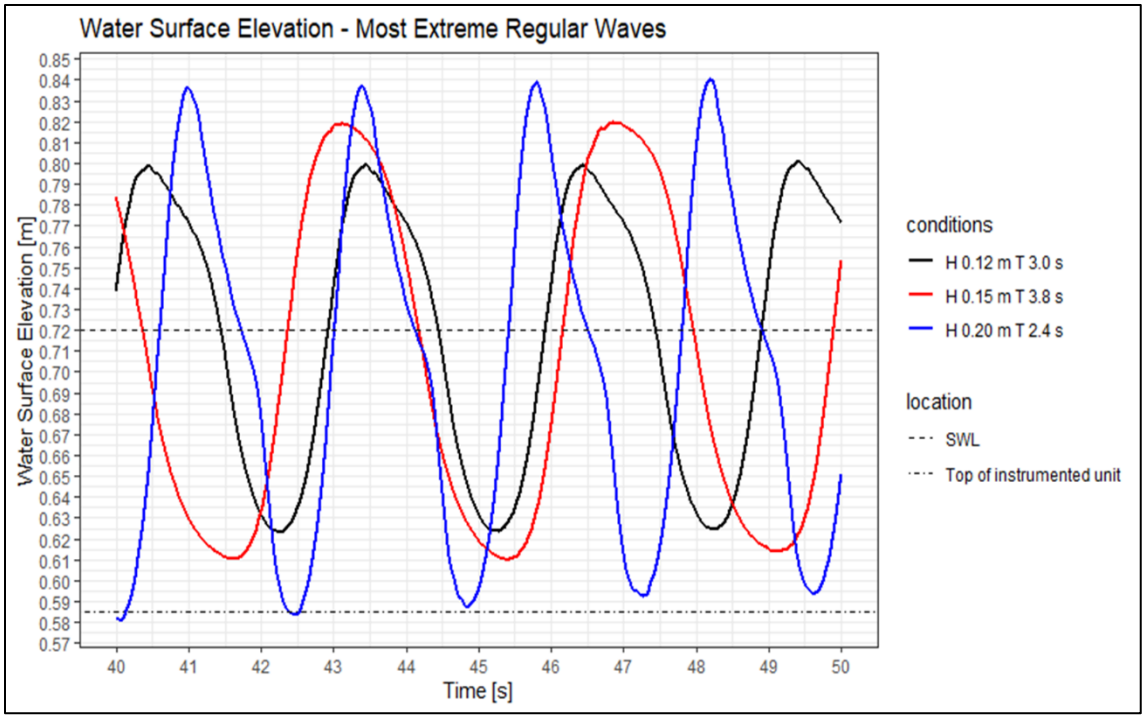

Figure 3-21: Pressure head as proxy for water surface elevation and the emergence of the instrumented armour unit. Isolated armour unit scenario.

4 Analysis and Discussion

The following chapter discusses the results of the study, including discussion of wave-induced loading on the instrumented armour unit, influence of random or irregular wave trains on the individual armour unit, as well as the influence of sea-state parameters such as wave height, period, and steepness.

4.1 Representative Wave Cycle

The flow follows four main phases under regular wave action, as outlined in Figure 4-1 these are:

1. the downward crossing of the SWL, when the water surface elevation is at its neutral position,
2. rundown, where the wave flow will continue decreasing until new incident wave energy causes the water direction to reverse,
3. the upward crossing of the SWL, where the surface elevation reaches neutral for the second time,
4. runup, where the wave will rush up the armour layer, dissipating its energy and being brought down again by gravity.

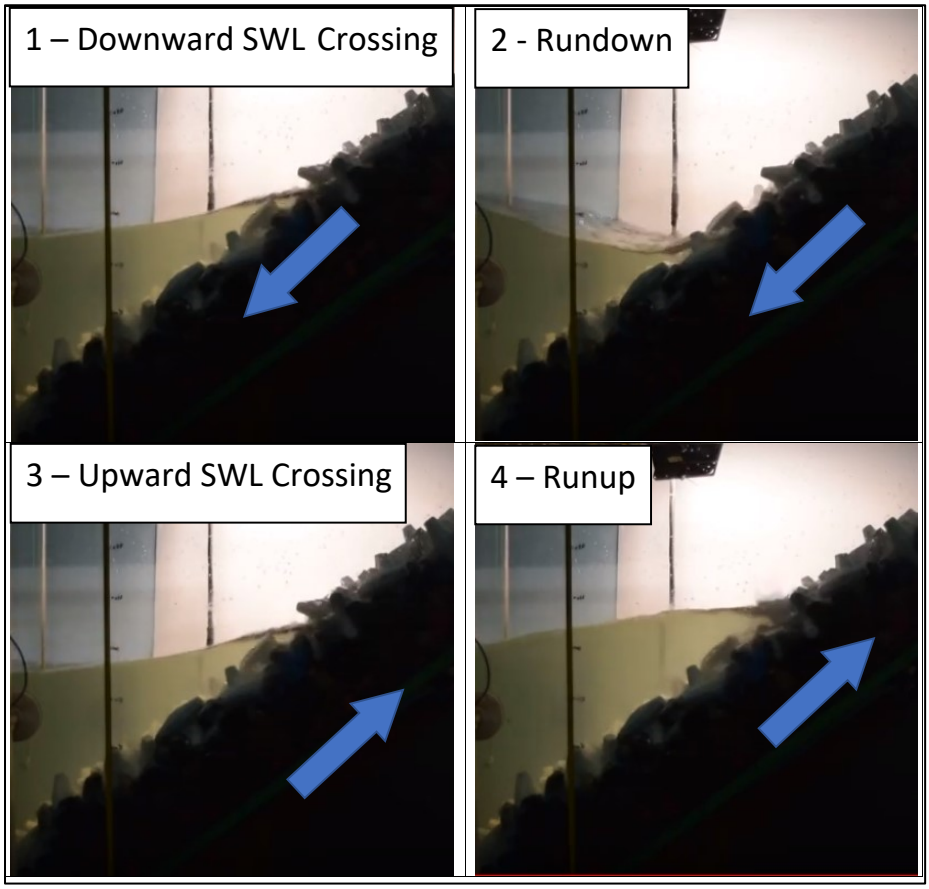

Figure 4-1: Stages of wave action on experimental apparatus. Wave front direction of change in blue.

4.2 Force Development on Instrumented Unit

In a typical regular wave cycle, whose force history is represented by Figure 4-2, the following phases have been identified:

1. The downward crossing of the water level coincides with the maximum negative parallel force and negligible normal force,
2. The lowest point of the water level coincides with very small parallel force and approximately with the peak normal force in the positive direction (outward of the structure),
3. The upward crossing of the SWL coincides with the maximum positive parallel force and negligible normal force,
4. The highest point of the water level coincides with negligible parallel force and maximum negative normal force.

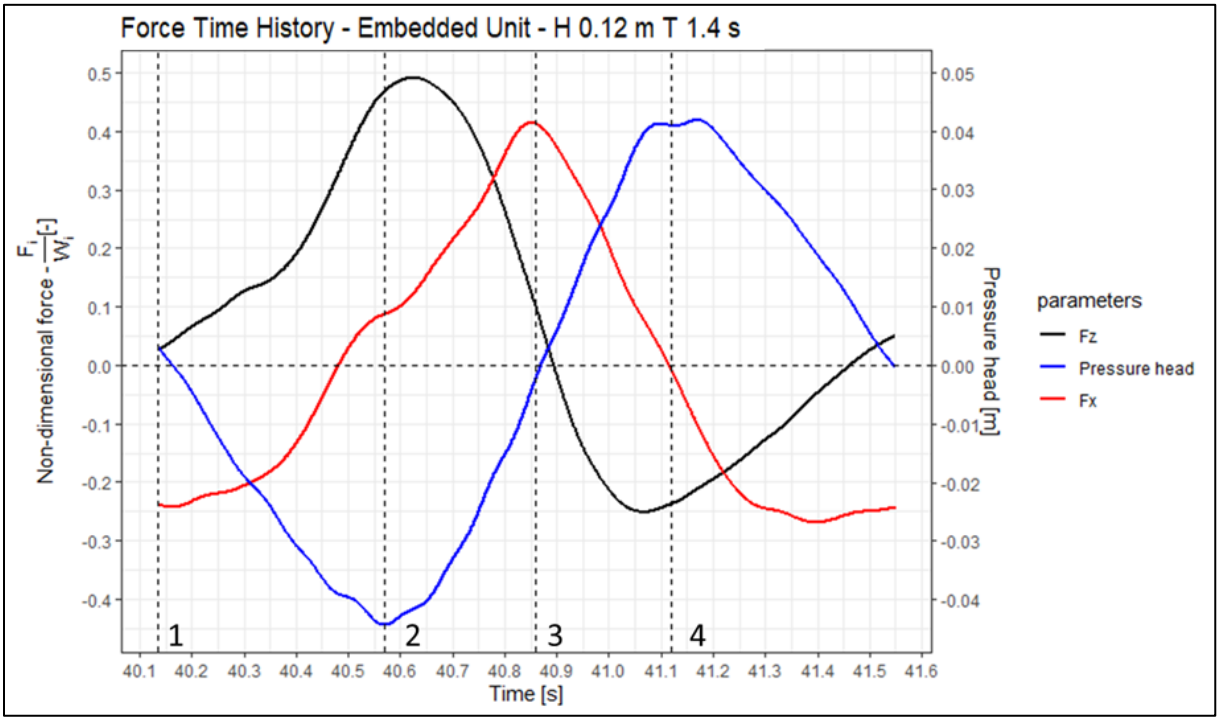

Figure 4-2: Typical regular wave cycle, including parallel and normal forces. Force time history, fully armoured scenario (H = 0.12 m, T = 1.4 s)

As the pressure head changes, corresponding with changes in the free water surface, force on the instrumented unit directly responds. Increases in pressure head cause an increase in downward normal force response of the instrumented unit. A decrease in the water level will cause a negative (uplift), force on the instrumented unit. This behaviour is possible due to the complex flow patterns within the armour layer itself, with water flowing upwards through the layer as it rushes downslope and is redirected by the random orientation of adjacent armour units as well as the arrival of the next incident wave, as seen in Figure 2-20.

The highest velocity of water corresponds with a low flow acceleration and imparts a high parallel force but a weak normal force. Conversely, when the flow experiences high acceleration but low velocity, a high normal force is imparted with a weak parallel force. The force development is mostly symmetrical about the x-axis in runup and in rundown, though higher positive forces are recorded than negative.

These findings are consistent with the trends of Morison's equation, expressed as

$$F = \rho C_m V\dot{u} + \frac{1}{2}\rho C_d A u|u| \tag{4-1}$$

Where the $\rho C_m V\dot{u}$ component represents the inertial force, a function of flow acceleration, and the $\frac{1}{2}\rho C_d A u|u|$ component represents the drag force, which is a function of on flow velocity. (Morison, 1950)

The Keulegan-Carpenter number is a dimensionless number that describes the relative importance of inertial or drag forces in a flow. It is defined as:

$$K_C = \frac{VT}{L} \tag{4-2}$$

Where V is the flow velocity, T is the period of oscillation, and L is a characteristic length (taken to be the characteristic length of the concrete armour units in this case). At low K_C, inertia forces dominate the flow, and at high values of K_C, drag forces dominate.

Parallel force maxima occur while the water surface is quickly crossing the SWL. The flow at that time has high velocity and low acceleration. This corresponds to an induction of lower inertial force and higher drag force. The Keulegan-Carpenter number is at its highest at this point.

Normal force maxima occur at the maximum extents of runup and rundown, corresponding to the highest flow acceleration, but low flow velocity. This induces a higher inertial force, but a lower drag force. At this point, the KC number is at its minimum.

The following figures show force development on the instrumented unit over a longer timeframe, showing a 5 second interval rather than one wave cycle. As expected, maximum normal forces in the negative direction (into the structure) occur at the maxima of the pressure head, and the maxima of the parallel force in the positive direction (upslope) occurs when the pressure head crosses the still water level ($z = 0m$) , both in the upward and downward directions.

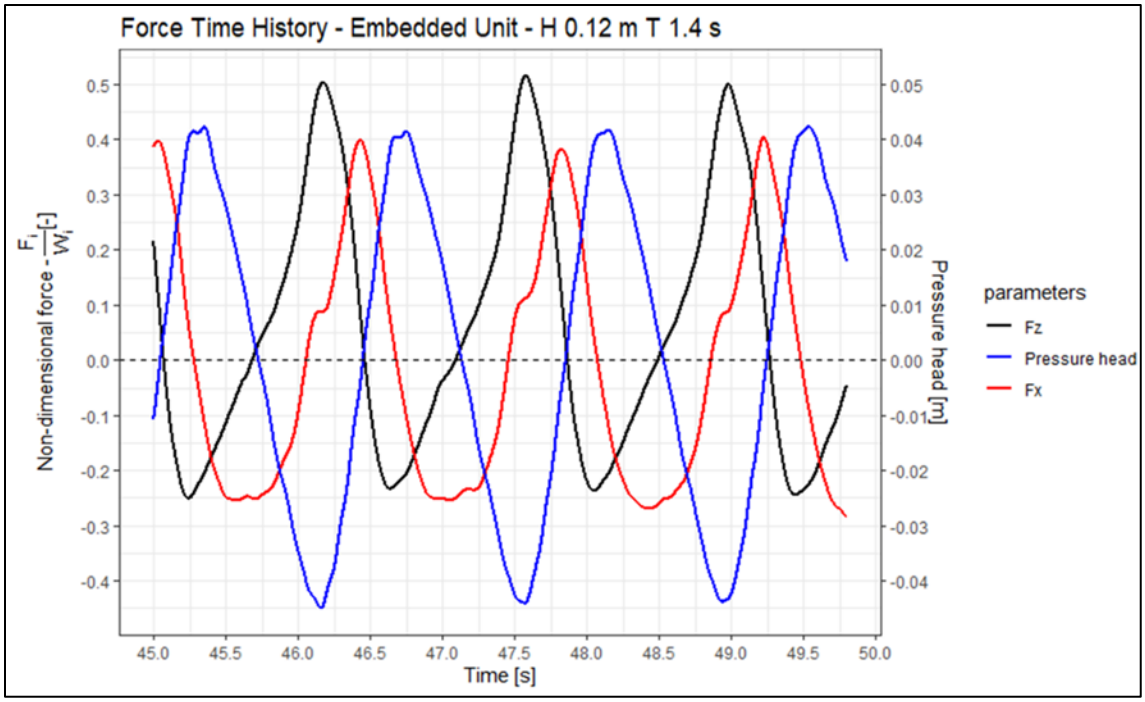

Figure 4-3: Force time history of fully armoured layer (H= 0.12 m, T = 1.4 s)

Figure 4-4 shows the force development in a single armour unit that is not packed within an armour layer. In contrast to the embedded armour unit, slope-parallel forces on the isolated armour unit are significantly more pronounced relative to the normal forces. This force redistribution is due in part to an increase in normal force from the redirection of flow within the armour layer which does not occur during isolated unit testing. Normal force is also affected by an increase in flow away from the armour layer during the downrush as the slope-parallel flow speed is reduced due to the presence of the adjacent armour units. This causes a stagnation of the wave crest during downrush with subsequent increase in water pressure pushing upward normally away from the filter layer. Normal forces oscillate regularly along with the incident wave energy, with upward normal forces exceeding downward forces by approximately 33%. This is similar to the exceedance of change of pressure head in the uprush of approximately 33% over the change of pressure head during the downrush. Conversely, parallel forces are much stronger in the upslope direction, exceeding downslope forces by approximately a factor of 3.

Interference of the armour units and complex flow behaviour within the armour layer channel uprush flow and shelter the instrumented unit during wave uprush.

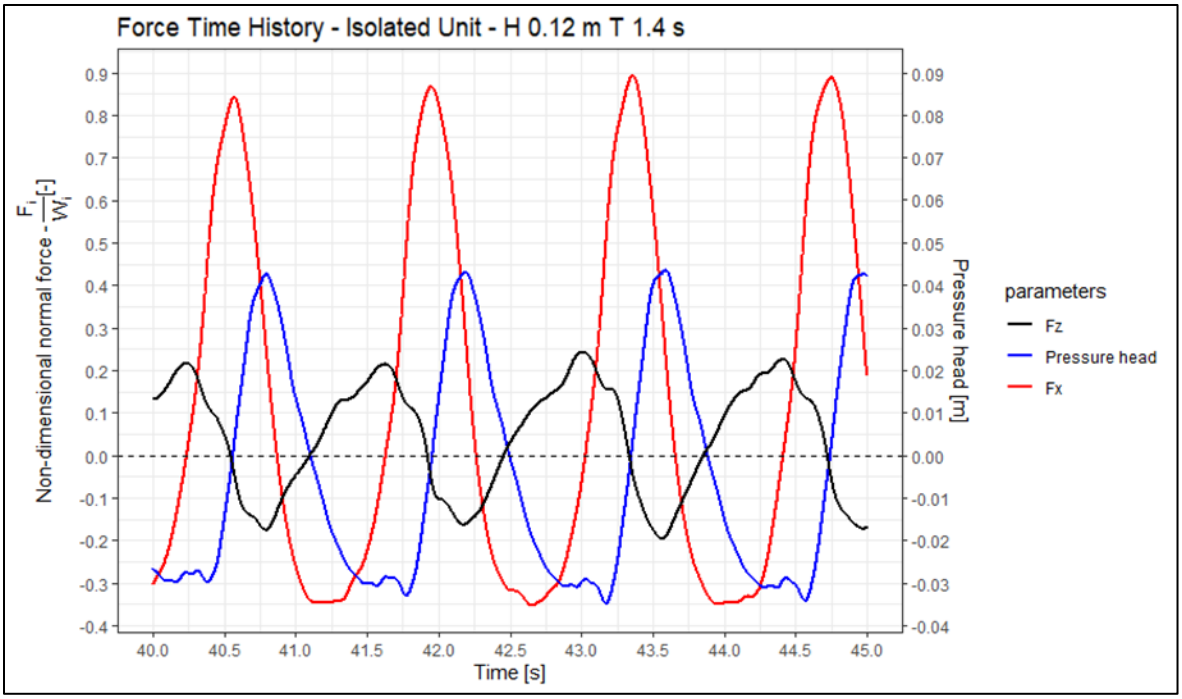

Figure 4-4: Force time history on isolated armour unit (H = 0.12 m, T = 1.4 s)

Figure 4-5 depicts normal force loading differences between an isolated armour unit and embedded armour unit. The peaks have been time shifted to allow easier comparison.

Normal forces developed in fully armoured tests are in the range of double the magnitude of the upward normal forces exerted on the isolated unit. In the downward direction (into the armour layer), the forces on the embedded unit were higher than those recorded on the isolated unit by approximately 66%. The wave signal observed in the fully armoured testing is smoother than that observed in the isolated unit testing. This effect is most pronounced at the upper maxima of the isolated unit testing, coinciding with the lowest pressure head. The truncated shape of this force signal may be due to interference of the incoming wave crest with the rundown of the previous wave. Rundown is slowed by the existence of the armour layer, and the location at which this interference occurs would be affected by this. Thus, the instrumented unit in the fully armoured scheme will be submerged further at the lowest water level and would experience a different force behaviour.

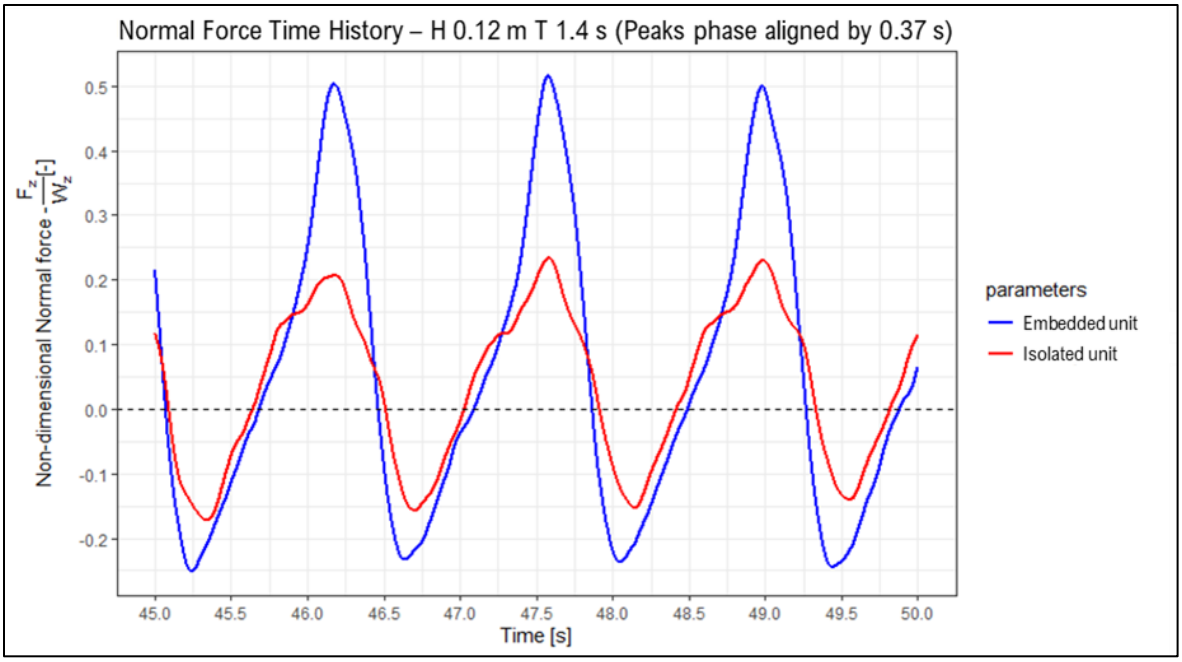

Figure 4-5: Normal force time history (H = 0.12 m, T = 1.4 s) (Force peaks aligned by shifting 0.37 s)

Figure 4-6 shows the orthogonal direction, with a phase-aligned comparison of parallel forces.

The effects of sheltering on the instrumented unit are more significant in the upslope direction. This plot shows a large increase in parallel force sustained on the isolated unit which does not have the benefit of sheltering. Upward parallel forces are approximately twice the recorded level in an embedded test for similar wave conditions. Downward parallel forces on the isolated unit, associated with the downrush, exceed those recorded on the embedded unit by approximately 30%.

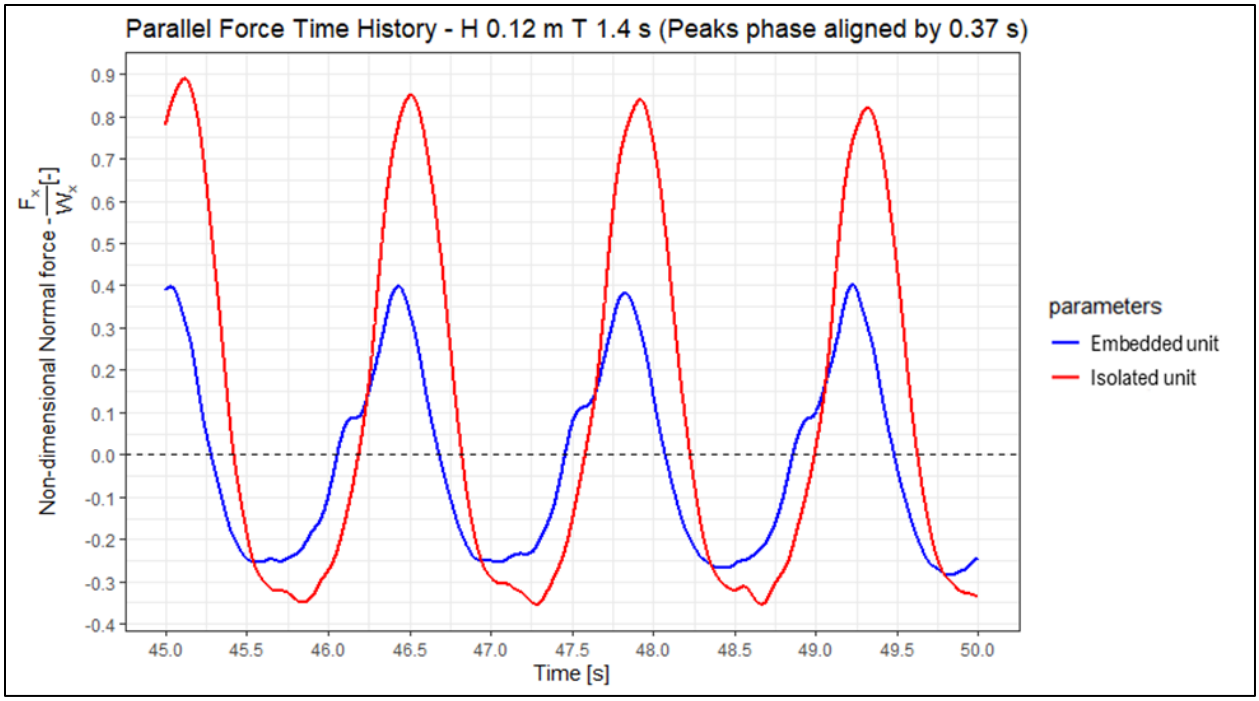

Figure 4-6: Parallel force time history (H = 0.12 m, T = 1.4 s) (Force peaks aligned by shifting 0.37 s)

For both cases comparing an isolated unit to the fully armoured scenario, most of the difference in force signal is found in the positive force direction, corresponding to the upward and up-slope directions. Relatively little difference is found in the downward and down-slope force directions. This result may be due to the effects of sheltering and force redirection being more prominent during the uprush compared to the rundown.

4.3 Flow Above The Armour Layer

Velocity measurements above the armour layer were taken via ADV. Results are depicted in the following figures.

Figure 4-7 shows velocity measurements in the slope-parallel and slope-normal directions, as well as the pressure head above the instrumented unit with hydrostatic pressure removed[12]. These results show the transfer of influence from parallel to normal velocity as the water level increases around the instrumented unit – parallel velocities are highest when pressure-head is inflecting, corresponding to the inflection points of the water surface elevation. Both up-slope and down-slope velocities are roughly equivalent (within 10%). Slope-normal velocities are highest during periods of increasing water-levels with water surface elevation below the SWL. Vertical uplifting velocity peaks are significantly higher than negative slope-normal velocity peaks (increase of approx. 250%).

[12]Conversion to absolute pressure would require the simple reintroduction of hydrostatic pressure when the system is at rest, which accounts for an additional 0.242 m of pressure head.

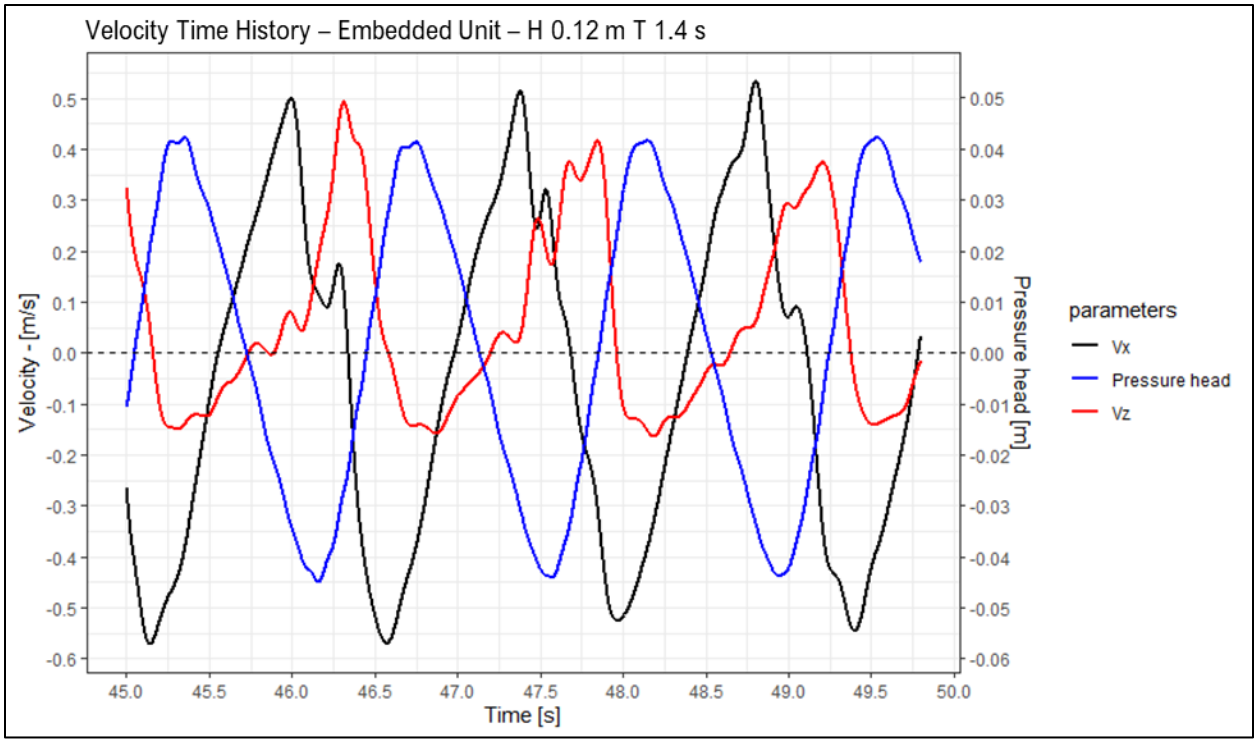

Figure 4-7: Velocity time history comparing slope-normal and slope-parallel directions, embedded.

Figure 4-8 shows the comparison of slope-parallel forces between a fully armoured layer and an isolated armour unit. The first thing to note is the phase-lag between the velocity peaks. This may be due to slight differences in ADV location between fully armoured and unarmoured tests, with the unarmoured testing having the ADV in line with the centroid of the instrumented armour unit and above the armour layer in the same direction for the fully armoured testing. The peak values of slope-parallel velocity for both the fully armoured scenario and isolated unit scenario are within 0.1 m/s of each other. Potentially this difference can be accounted for by proximity to the boundary layer, with the isolated unit's velocities measured slightly closer to the boundary layer. Both positive and negative peaks are of roughly equal magnitude for both test cases, showing similar velocities in the uprush and downrush phases. Counterintuitively, the velocity peaks for the embedded test case are slightly higher than for the isolated unit test case – the increase in friction caused by the armour layer would predict a reduction in flow velocity. This difference may also be due to the change in ADV measurement location between test cases, with the isolated testing recording velocity closer to the boundary layer and as a result recording slightly slower velocities than the embedded test case.

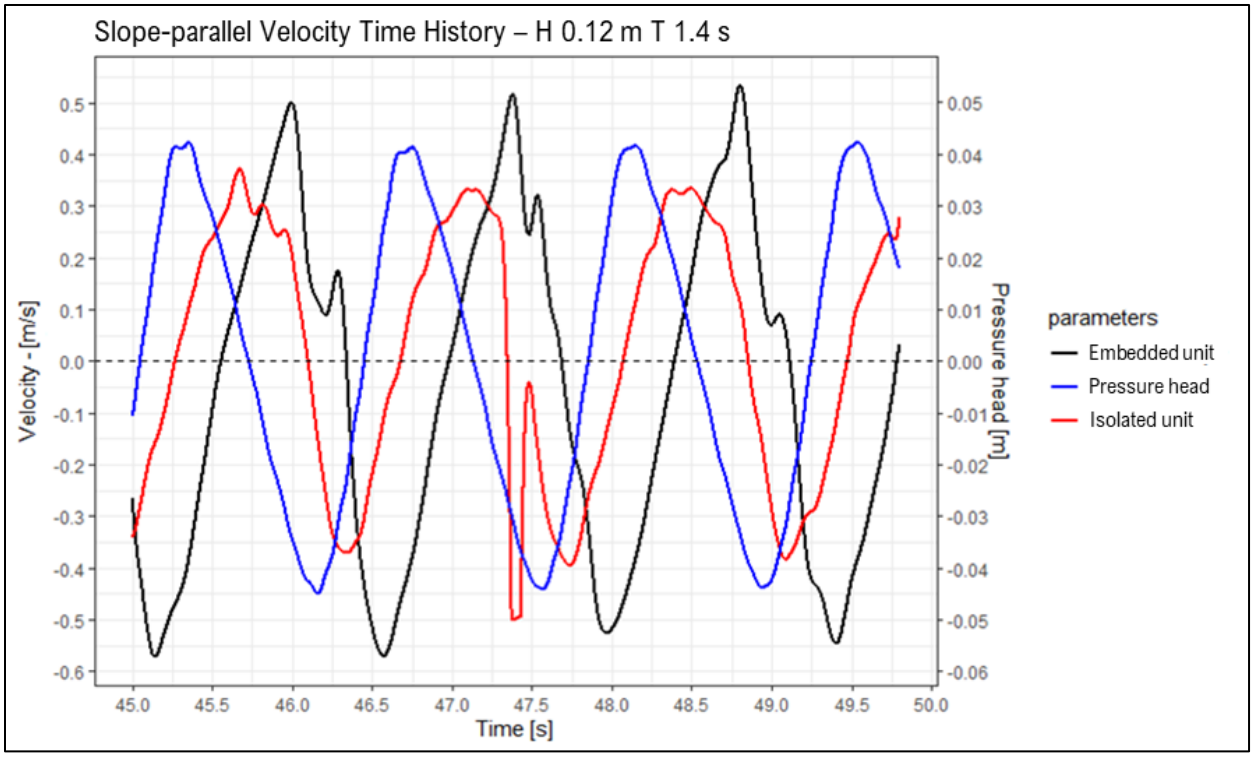

Figure 4-8: Slope-parallel velocity time history, fully armoured and isolated unit scenarios

Contrary to the relative similarity between velocity signals in the parallel direction, the plot in Figure 4-9 shows a significant difference between the slope-normal velocities in the fully armoured and unarmoured state. In isolated unit testing, the peaks in positive and negative directions are both roughly equal (despite some noise in the isolated testing signal around 47.5 s). The fully armoured velocities show far greater upward velocities during the uprush of water from the lowest rundown point than the isolated unit test case. Downward velocities are similar in both test cases. This upward velocity is likely caused by influence of the armour layer – disrupting the flow pattern and directing water upwards.

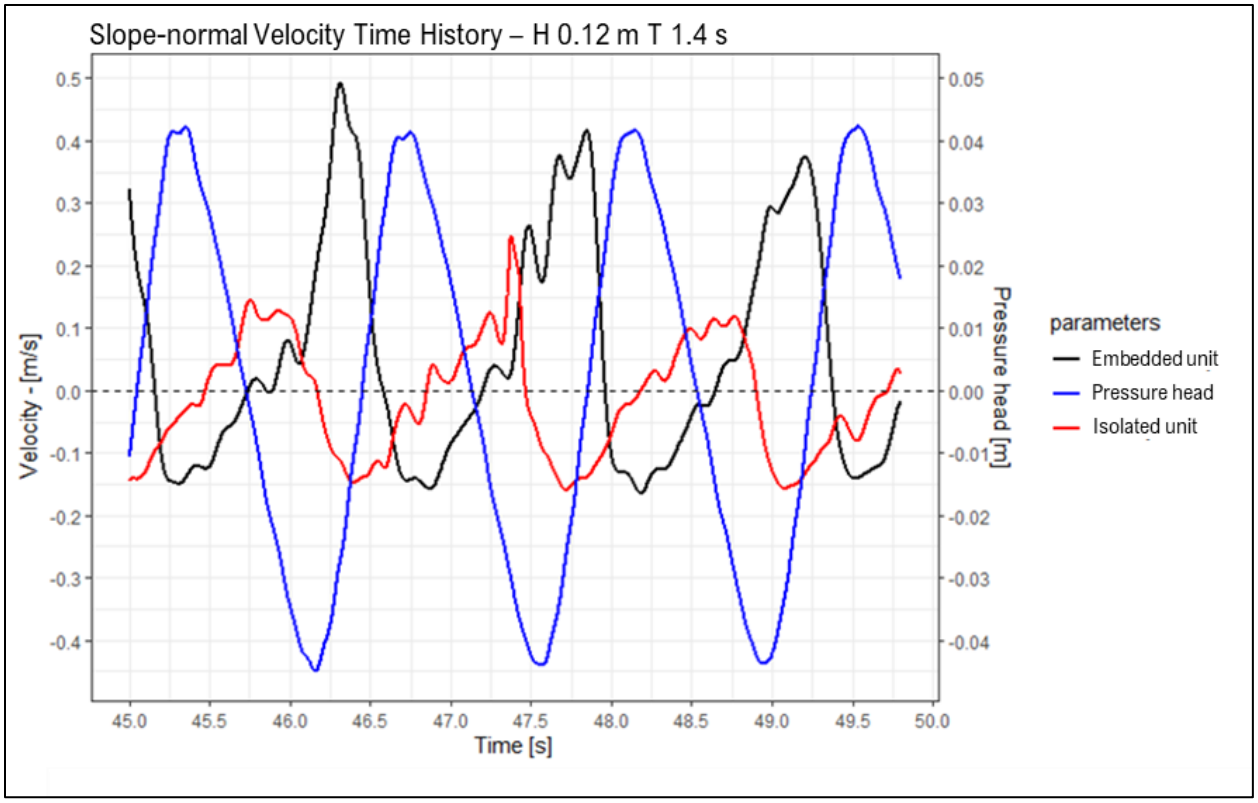

Figure 4-9: Slope-normal velocity time history, fully armoured and isolated unit scenarios

The behaviour of flow acceleration is depicted in the following two figures. Figure 4-10 shows slope-normal flow velocity, flow acceleration, and force measured on the instrumented unit for the embedded test case.

This signal in the slope-normal direction shows generally coincident phases of force, flow velocity, and flow acceleration. The greatest force coincides with peak acceleration, though not with peak velocity. Peak velocity occurs during a time of decreasing force. Peaks of velocity, acceleration and force signals are higher in the upward slope-normal direction than in the downward.

Figure 4-11 shows velocity, acceleration, and force in the slope-parallel direction. This shows similar behaviour to the slope-normal direction in that the peak forces are coincident with peak acceleration. There is much less difference between upward and downward peaks in the slope-parallel direction, however. Force follows acceleration more closely than it does velocity, with peak velocity coinciding with very small forces.

The distinguishing change between the slope-normal and slope-parallel directions is that force, flow velocity and flow acceleration are much more symmetrical in the slope-parallel direction, with the flow velocity and force on the unit in particular experiencing large asymmetries. Flow velocities are in the range of 4 times higher in the upward than downward direction. Force on the instrumented unit is approximately double in the upward direction than in the downward.

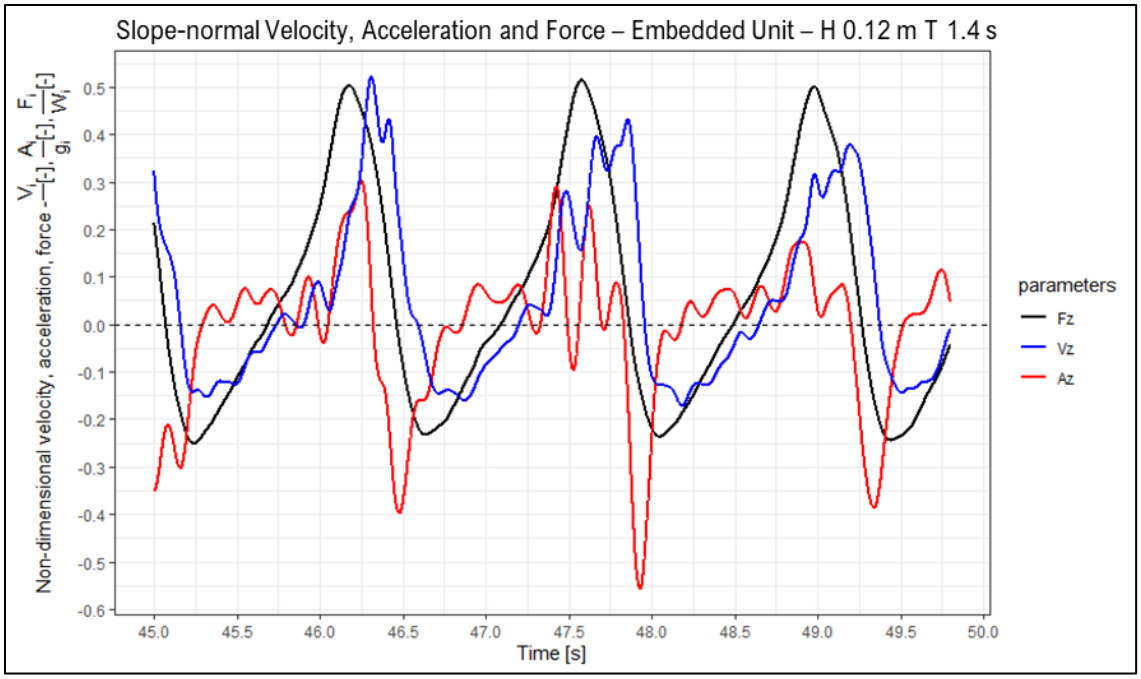

Figure 4-10: Slope-normal velocity, acceleration, and force in fully armoured scenario (H= 0.12 m, T = 1.4 s)

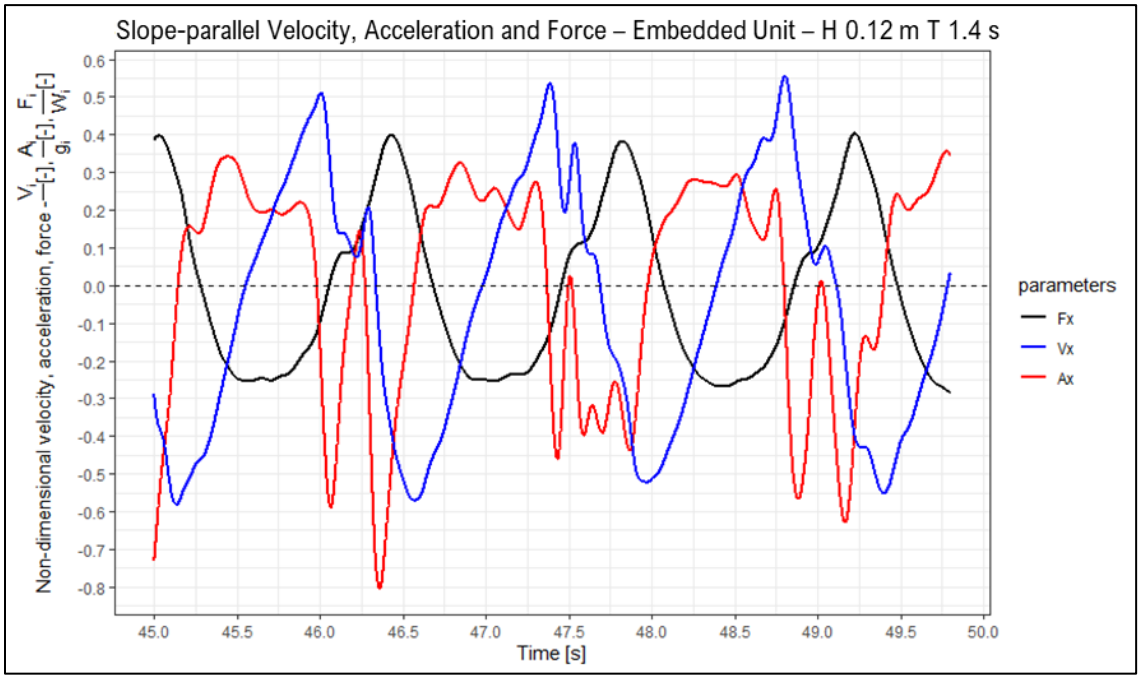

Figure 4-11: Slope-parallel velocity, acceleration, and force in the slope-parallel direction

4.4 RANDOM WAVES

It is essential to consider the behaviour of the armour units under irregular waves as well as regular waves. The force time history of a test run of random waves for an Hs of 0.15 m and a T_p of 1.8 s is shown in Figure 4-12. In this figure, the pressure head above the base of the unit can be seen with the

blue line, demonstrating the approximate position of the water surface. Slope-wise normalized force can be seen with the red line, and slope-normal normalized force can be seen with the black line. These results illustrate a similar relationship between force and water surface – as the water surface is at its peak, the slope-normal force is at its peak as well. Upward forces are in general higher than downward forces. This phenomenon is likely due to the influence of the armour layer itself causing a redirection of flow as well as the seepage of water through the filter and armour layers at the end of a wave cycle, pushed upwards by the next incident wave front. The slope-parallel forces show their peaks as the water surface crosses the still water level, corresponding to the highest velocity but lowest acceleration of flow. In general, the force behaviour noted for regular waves is retained for random waves.

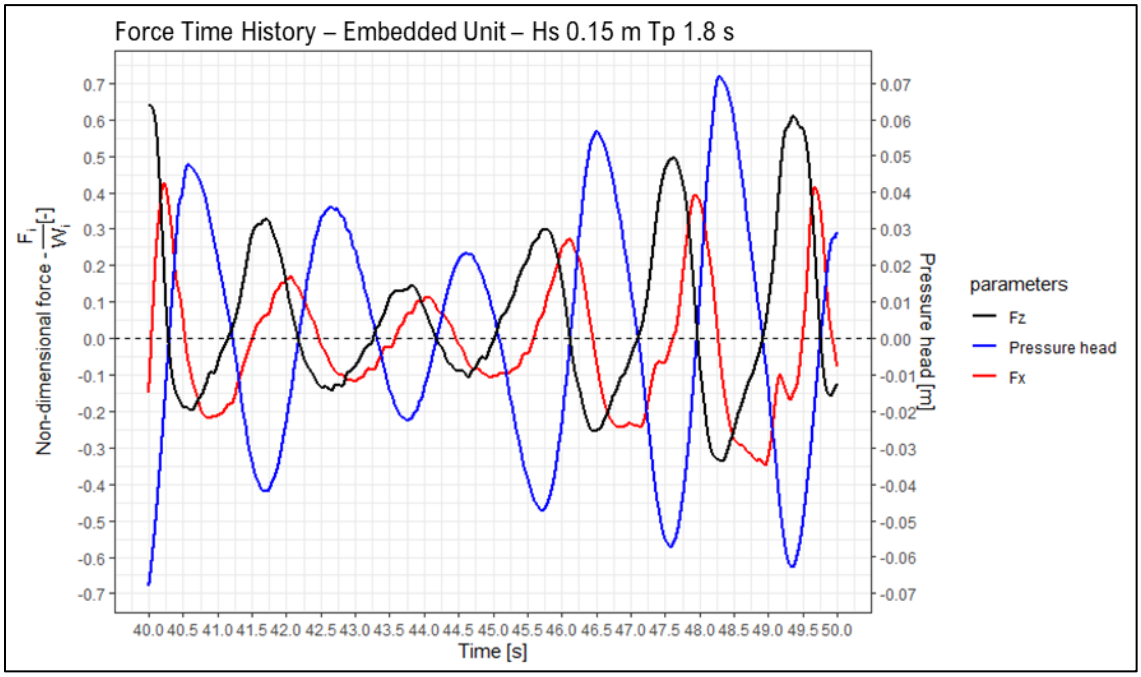

Figure 4-12: Force time history, Embedded, Hs = 0.15 m, Tp = 1.8 s

4.4.1 Statistical Fit of Slope-Normal Forces Exposed to Random Waves

The slope-normal and slope-parallel force peaks for one set of random waves were extracted using the R *findpeaks* function. Slope-normal results are shown in Figure 4-13, slope-parallel results are shown in Figure 4-14. These force results have been normalized by the slope-normal and slope-parallel components of the unit weight of a concrete unit.

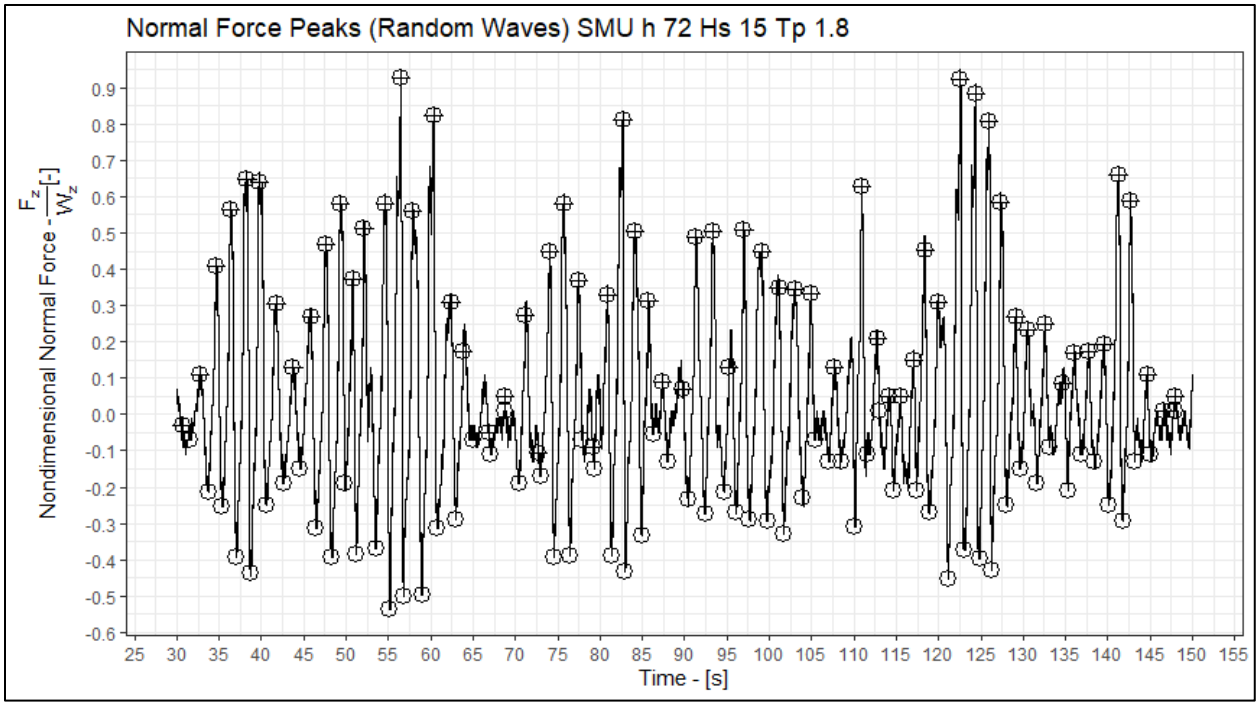

Figure 4-13: Slope-normal force peaks (Random Waves), embedded instrumented unit, Hs =0.15 m, Tp = 1.8 s

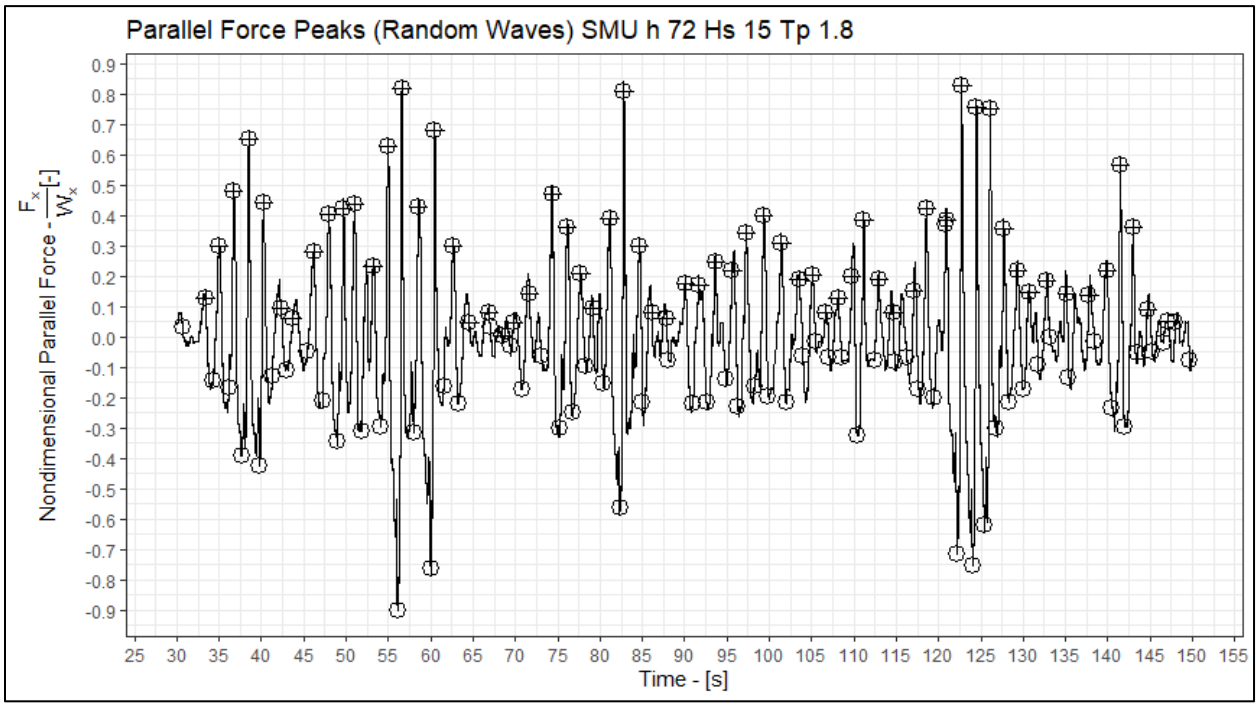

Figure 4-14: Slope-parallel force peaks (Random Waves), embedded instrumented unit, Hs =0.15 m, Tp = 1.8 s

The probability density distribution of these force peaks was calculated in R. Parallel forces show in Figure 4-15 and normal forces in Figure 4-16. The skewness of the normal forces is significantly higher than for the parallel forces. It is likely that these density plots would have smoother transitions between

bins if longer random wave testing was completed, e.g. in the order of 600 s per test or longer rather than 120 s. This would also lead to more reliability of these statistical results.

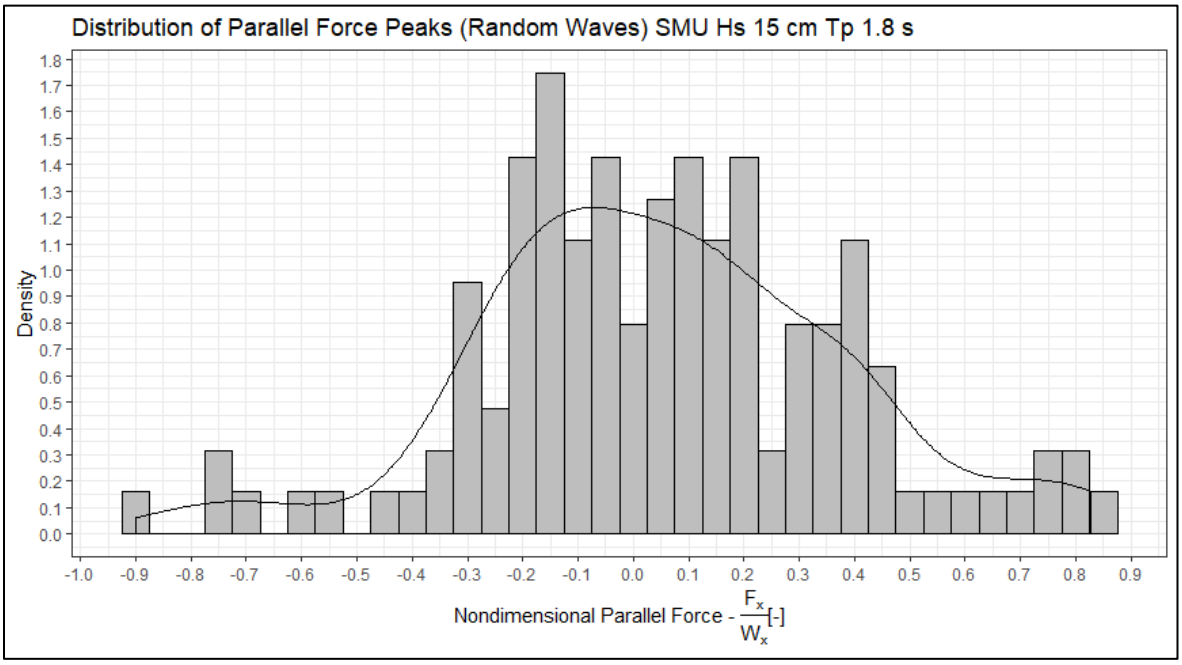

Figure 4-15: Distribution of parallel force peaks (Random waves), embedded instrumented unit, Hs = 0.15 m, Tp = 1.8 s

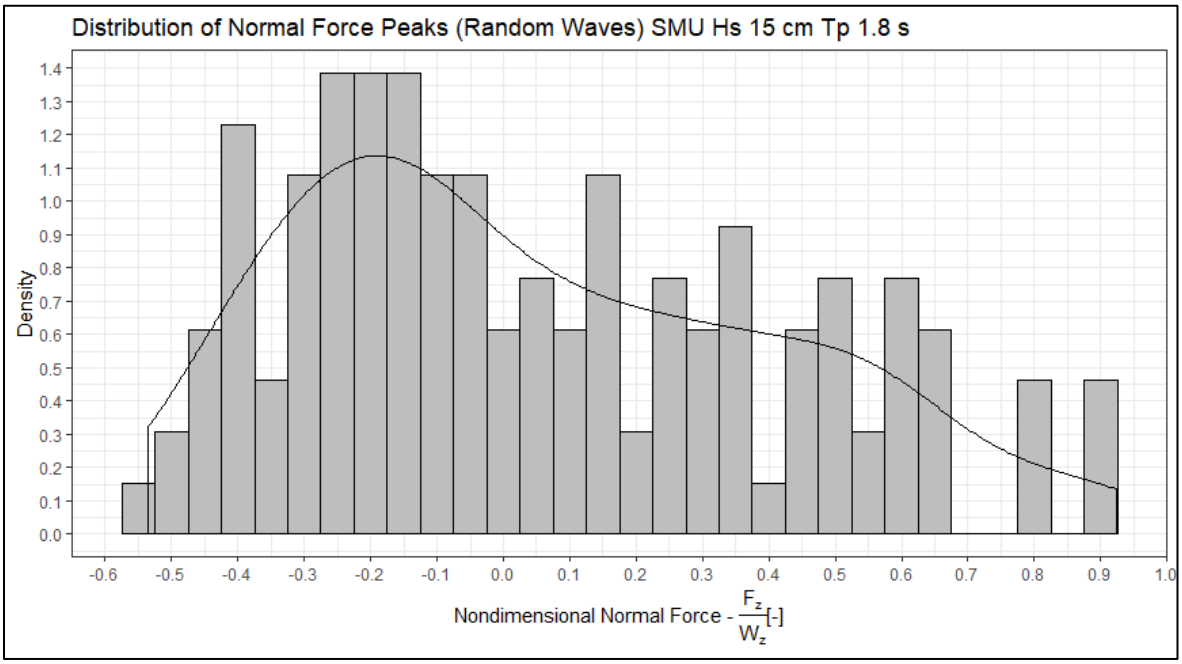

Figure 4-16: Distribution of normal force peaks (Random waves), embedded instrumented unit, Hs = 0.15 m, Tp = 1.8 s

Figure 4-17 shows the comparison of the probability density functions of the parallel and normal force peaks. This figure shows that in the parallel direction, there is a shift of the distribution's peak toward the negative direction (with a mean value of -0.2) compared with the slope-normal distribution

(mean value of -0.05). Both directions show a larger variation of force peak values in the positive direction (upward in the normal direction and up-slope in the parallel direction). In general, the instrumented unit reacted to random waves with a wider range of upward forces than downward. This may be due to the relatively consistent downward pressure on the unit due to the descending water surface level with most water acting on the unit hydrostatically, compared to the complex, turbulent flow field generated through the armour layer and filter layer. It appears the force resulting from the applied wave is more predictable, within a narrower band, for waves descending below the still water level than the more variable force resulting from waves ascending above it.

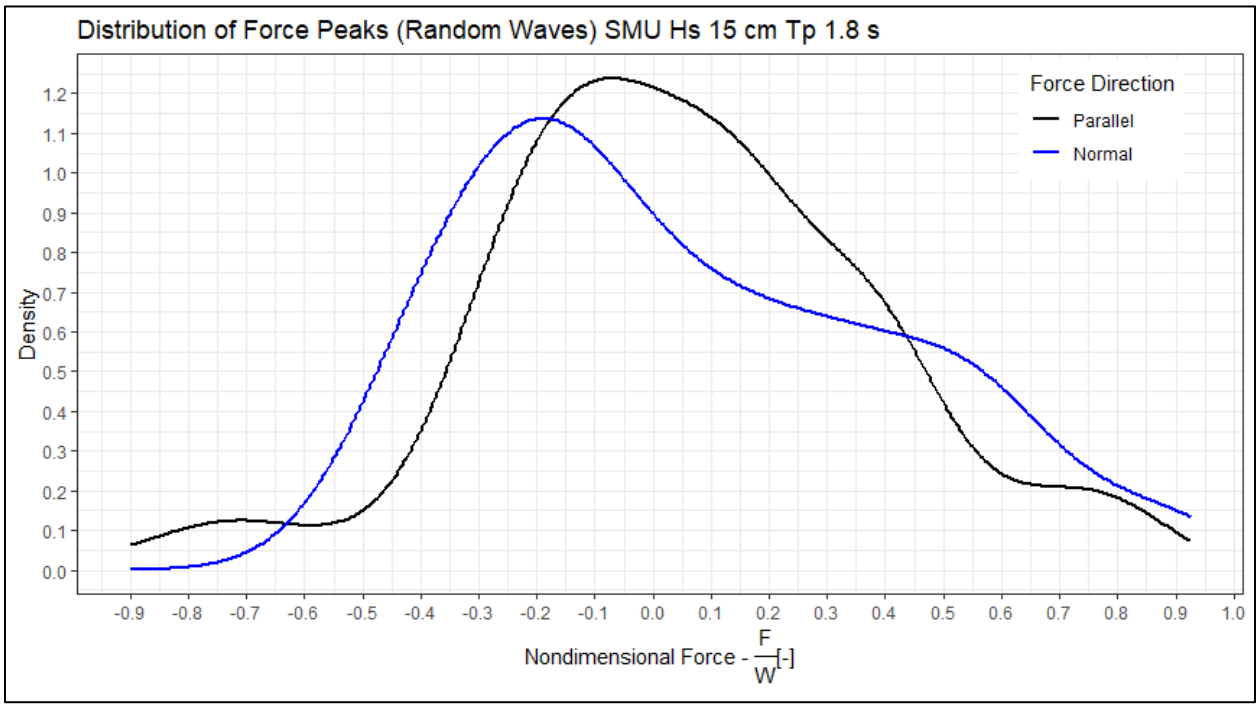

Figure 4-17: Distribution of force peaks, embedded instrumented unit, slope-parallel and slope-normal

The cumulative distribution functions (CDF) of this data is shown in Figure 4-18. Like the density function in Figure 4-17, the CDF shows similar results as discussed in the preceding paragraph.

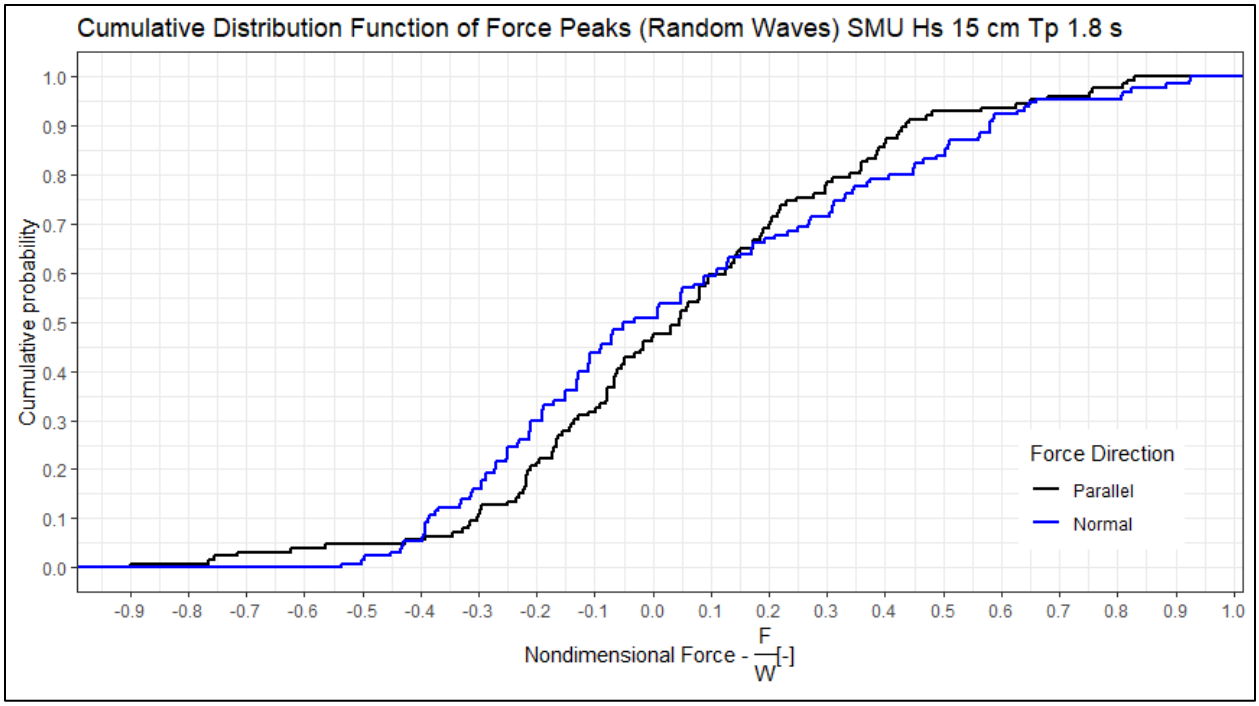

Figure 4-18: Cumulative distribution function of force peaks (random waves), embedded instrumented unit, Hs = 0.15 m, Tp = 1.8 s

From the CDF for this test, the following extreme values were extracted (Table 4-1). These extreme values are still below the critical threshold required to initiate motion in the armour unit, though the force is within 10% of the critical value in the upward normal direction, and within 20% of the critical value in the upward parallel direction.

Table 4-1: Extreme values for fully armoured random wave testing

	Parallel Force Fx/Wx	Normal Force Fz/Wz
1%	-0.762	-0.500
5%	-0.418	-0.415
95%	0.644	0.654
99%	0.814	0.912

For purposes of selecting a suitable statistical distribution of this data, the skewness and kurtosis of the F_x and F_z random wave peak data was plotted on a Cullen and Frey graph (also known as a Pearson graph). The observed F_x data is plotted closest to the expected location of the normal distribution; therefore, this statistical distribution was chosen as the best fit for the data (Figure 4-19). The F_z data plotted in this manner has a higher skewness, suggesting either a normal or beta distribution (Figure 4-19).

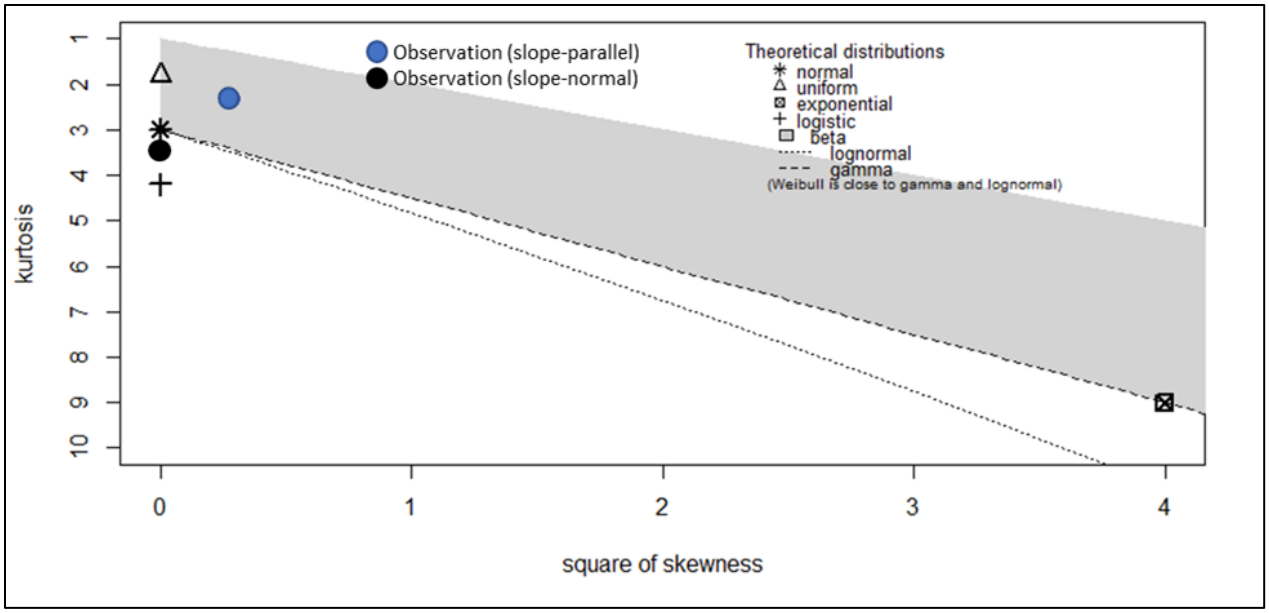

Figure 4-19: Cullen and Frey graph for slope-parallel and slope-normal directions

The adequacy of the normal distribution fit for the slope-parallel direction is shown in Figure 4-20 (left). These plots show that the normal distribution fits this data well, particularly in the central region. The tails of the data have a slight deviation from the quantile-quantile line, though the probability-probability plot shows a good fit. It is possible that with a longer testing run for random waves, i.e. with more force peaks to analyze, the tails may show less variation from the expected distribution.

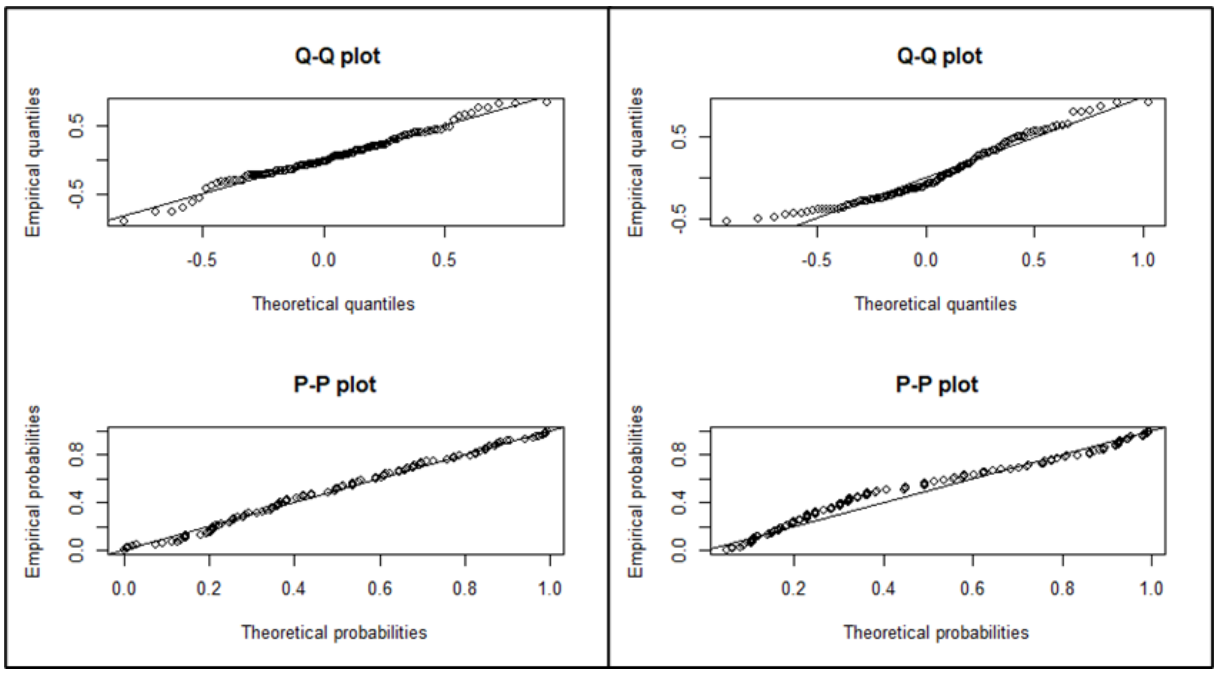

Figure 4-20: Normal distribution, fit of slope-parallel force data (left), Normal distribution, fit of slope-normal force data (right)

The fit of the normal distribution to the slope-normal force data (Figure 4-20, right) shows more deviation than the slope-parallel direction. There, even in the central section where there are the most data points, the quantile-quantile as well as probability-probability plots diverge from their expected values. The increased skewness of the slope-normal data can be seen in the density plot compared with the slope-parallel force peak data.

Again, these statistical results of the random wave testing would be improved by additional testing to produce a larger dataset to statistically fit. More data would reduce the influence of outliers and would produce a result with higher reliability.

4.5 Influence of Wave Height and Stability Number

Shown in Figure 4-21 are force hodographs, tracing the path of the rotating force vector in the vertical plane, for three regular wave height tests. As noted by Cornett (1995) for rock-armoured structures, the "general influence of wave height is to alter the magnitude, but not the character of the hydrodynamic forcing of the armour". As wave height increases, the energy imparted onto the instrumented unit increased in all directions, with a greater increase in the upward normal direction compared to the downward. The increase in force load on the instrumented unit with wave height is not uniform in all directions and observed is a counter-clockwise curling tip of the maximum upward force. The implication of this is that not only the magnitude of the force loading is a function of wave height, but the direction of the maximum load may be as well. The instrumented unit remains submerged during all testing (though the slight reversal at the tip of the 0.2 m hodograph may be due to momentary emergence of the uppermost extremity of the unit). This force peak coincides with up-slope-parallel force for the smallest waves and becomes more down-slope dominated as the waves increase in height.

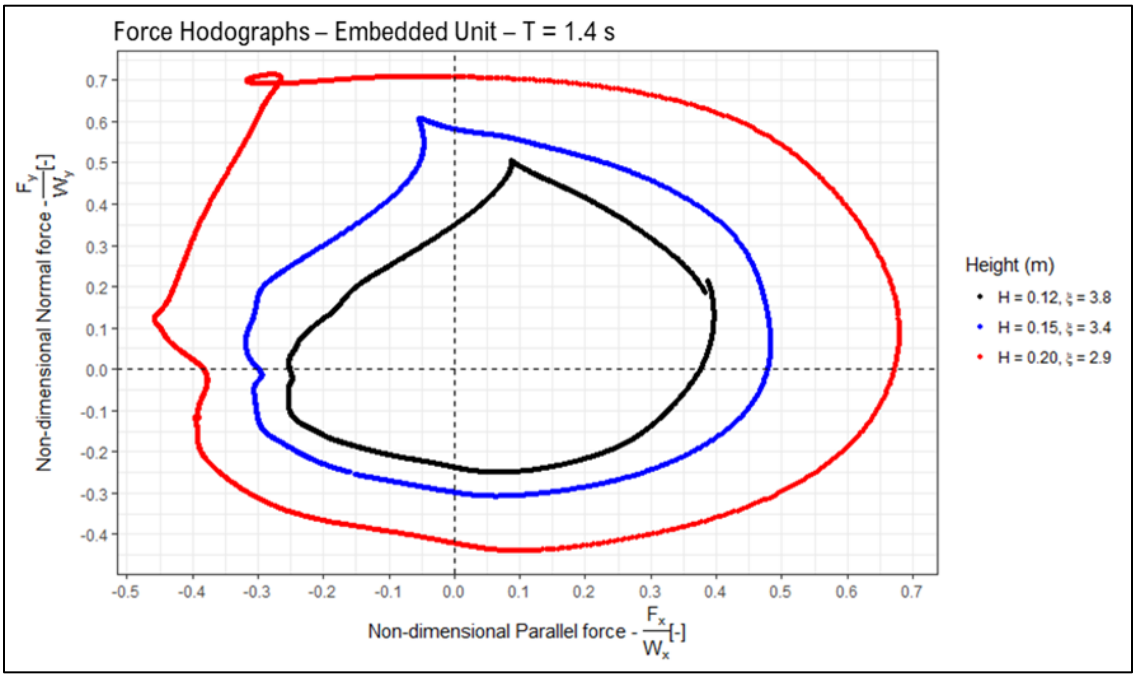

Figure 4-21: Influence of wave height on force loading of instrumented armour unit

In the design of concrete armoured rubble-mound structures, the stability number is a key parameter. This parameter is defined as $\frac{H_s}{\Delta D_n}$, where H_s is the significant wave height, Δ is the relative buoyant density of the concrete and the water ($\rho_c/\rho - 1$), and D_n is the nominal armour unit diameter ($D_n = \left(\frac{M_{50}}{\rho_c}\right)^{\frac{1}{3}}$. The design stability number for a core-loc structure is 2.78 (van der Meer, 1999), and it is at that value that, with a conservative safety factor, structural failure is expected to begin. The testing regime performed did not reach this level, though some insights may be drawn regarding the stability number.

Figure 4-22 shows the maximum upward normal force vs the stability number for all regular wave tests, including the fully armoured tests and isolated unit tests. These maximum force values were found by averaging the peaks during a 10 second period during which the instrumented armour unit was exposed to regular wave action. The stability numbers are a function of wave height and show three groups of tests, corresponding to 0.12 m, 0.15 m, and 0.20 m wave height tests. This data shows an expected increase in upward normal force as stability number increases. The spread of data increased significantly between the fully armoured testing and isolated unit testing. Upward normal forces become higher as stability number increases, and more predictable for the fully armoured condition compared to the isolated condition.

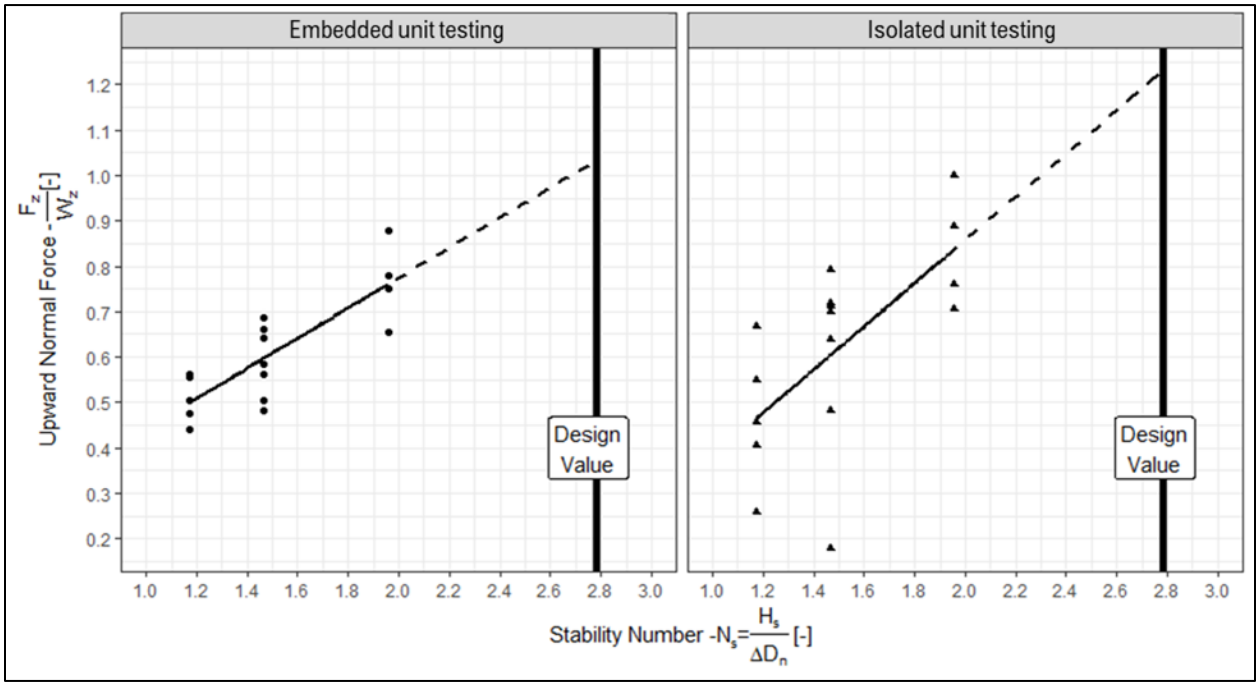

Figure 4-22: Maximum upward normal force vs stability number

Figure 4-23 shows maximum upward parallel force vs stability number. As expected, the upward average maximum parallel force increases with the increase in stability number. The effect of sheltering is much more pronounced in the parallel direction compared with the normal direction. The lack of sheltering in the isolated unit testing significantly increases the maximum parallel forces that the isolated unit is exposed to.

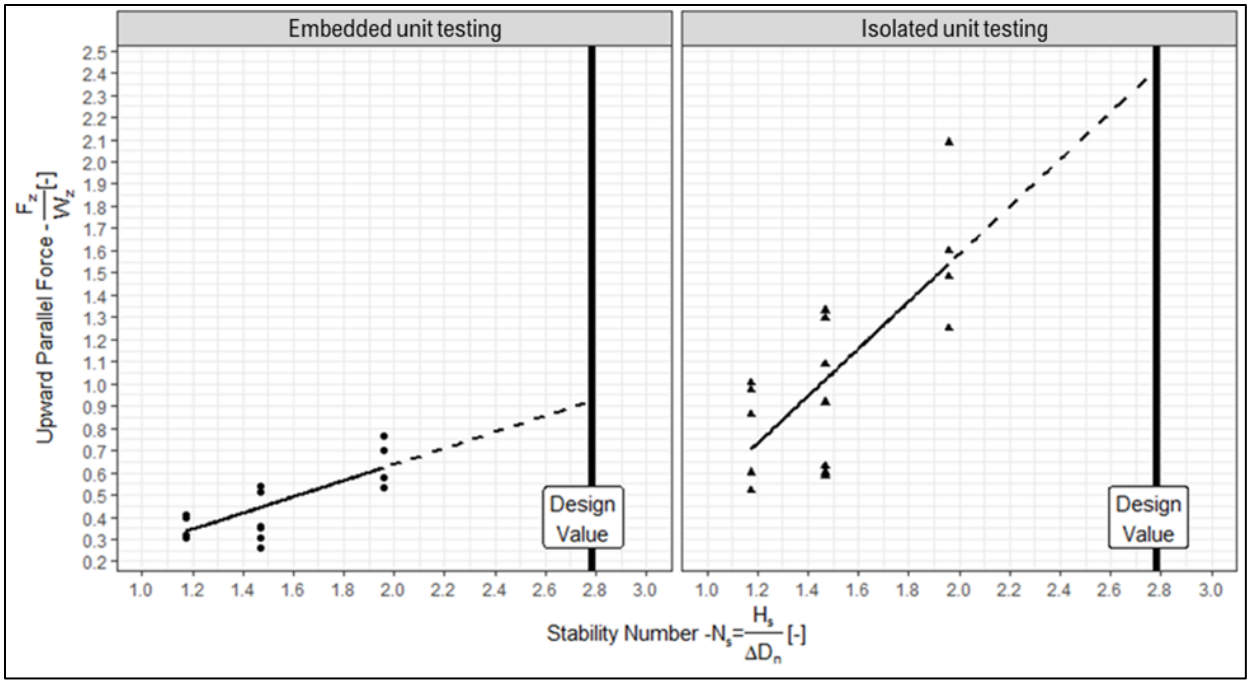

Figure 4-23: Maximum upward parallel force vs stability number

Testing at the design stability number was beyond the capability of the testing equipment, but a linear extrapolation of the embedded testing data to the design value predicts a value of approximately 1 in both the upward-normal and upward-parallel directions. This unity is the value at which destabilizing upward force is equal to the stabilizing gravity force. Motion at this force level would not be likely to initiate due to the interlocking design of single-layer concrete armour units. Reedijk et al. determined the pull-out force capable of dislodging the single-layer Xbloc unit embedded within an armour layer to be between 4 and 10 times the force of gravity. This data suggests that at the design stability number that gravitational stability of the Core-loc unit may be overcome and motion is restrained by interlocking between units.

4.6 Influence of Period and Wave Steepness

In Figure 4-24 force hodographs are shown depicting three wave cycles in the fully armoured armour layer scenario, varying in wave period. These hodographs do not exhibit the type of omni-directional increase in force as the H_s-varied hodographs do (Figure 4-21). Force magnitudes do not alter greatly in most directions due to the effect of period, with the exception of the downslope force ($-F_x$), where a force reduction is observed during exposure to longer period waves.

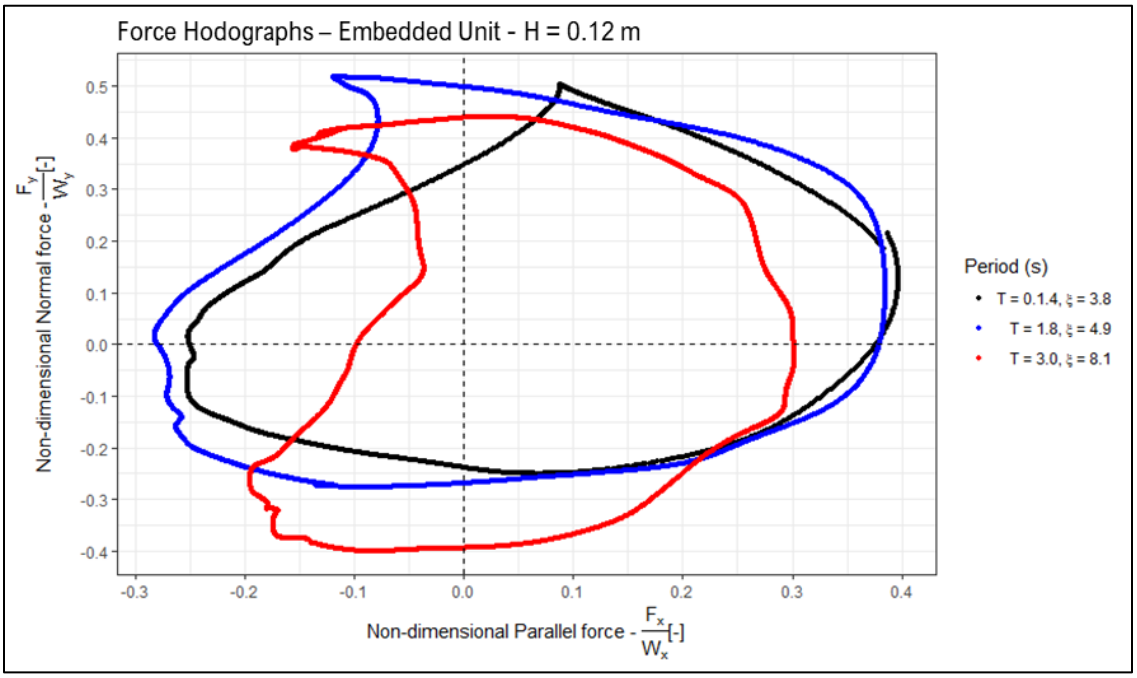

Figure 4-24: Influence of wave period on force loading of instrumented armour unit (Embedded unit scenario)

The reduction in downslope force coincides with the downrush of water as it crosses the still water level. The small secondary slope-parallel force peak can be seen in Figure 4-25. Potential physical causes of this secondary peak include the longer runup duration associated with a longer wave period, causing an increase in phreatic surface elevation within the filter layer. As more water is retained in the pore space of the filter layer, less water is available for immediate downrush, attenuating the force on the individual instrumented unit, as the trapped water descends after the wave crest has passed. This larger volume of water in the pore space will also have its energy reduced by the filter layer stones as well as the armour layer itself, reducing the parallel force on the instrumented unit but having little effect on the normal force.

The largest influence that period has on the hydrodynamic loading of the instrumented armour unit is in the characteristics of the secondary force peak between the main peaks, with the peak increasing in size as period increases.

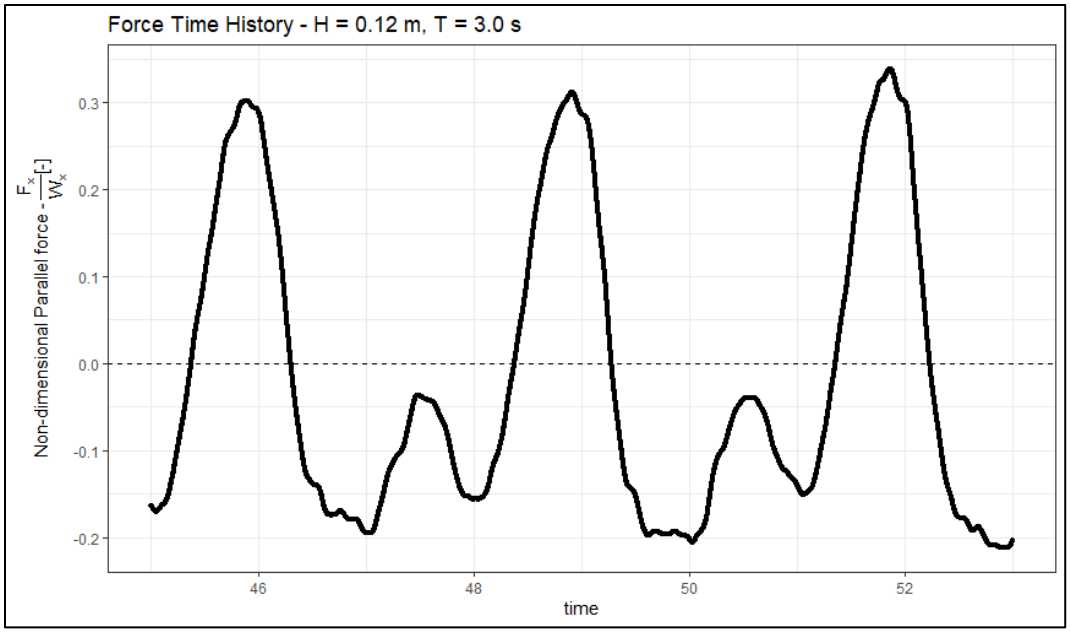

Figure 4-25: Parallel force history showing secondary wave (H = 0.12 m, T = 3.0 s)

In the case of the isolated armour unit (Figure 4-26), the effect of period is more pronounced. For shorter wave periods, the hodograph is oval shaped with low normal forces and high parallel forces. In the 1.4 s hodograph, no secondary peak is observed. Increasing the period increases the normal force acting on the unit. A secondary peak is only observed in the 3.0 s wave, and similar to the fully armoured layer, coincides with the downrush as the water crosses the still water level.

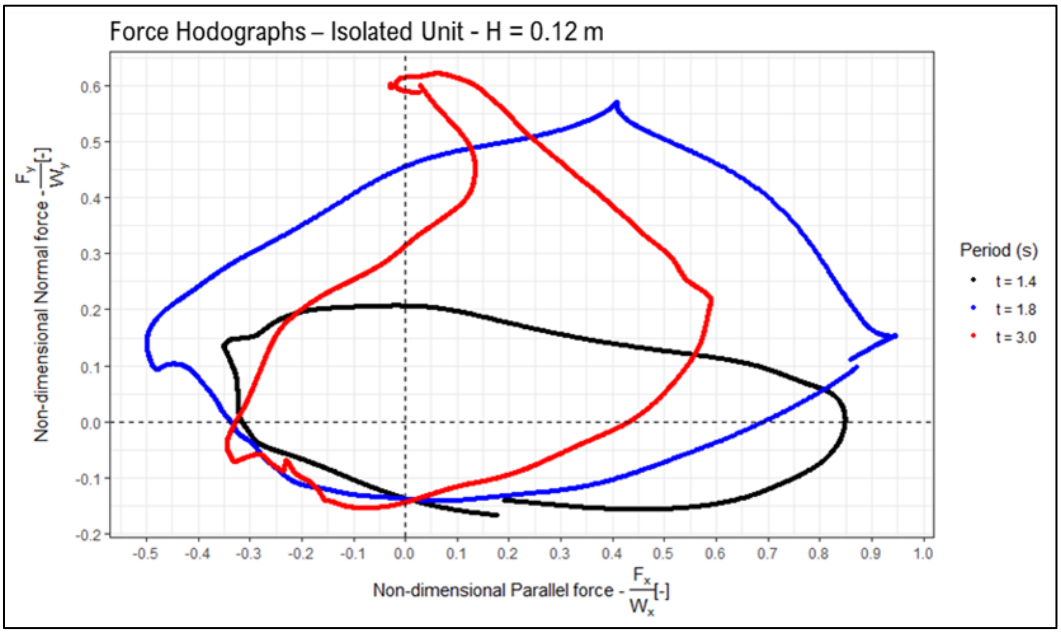

Figure 4-26: Influence of wave period on force loading of instrumented armour unit (Isolated armour unit scenario)

A comparison of hodographs of the embedded armour unit and an isolated armour unit are shown in Figure 4-27. This comparison shows a large reduction in parallel force acting on the unit as a result of armouring, but also shows a large increase in upward normal force acting on the unit. This is likely due to the turbulent redirection of flow as a result of the armour layer and would result in a lowering of the unit's stability.

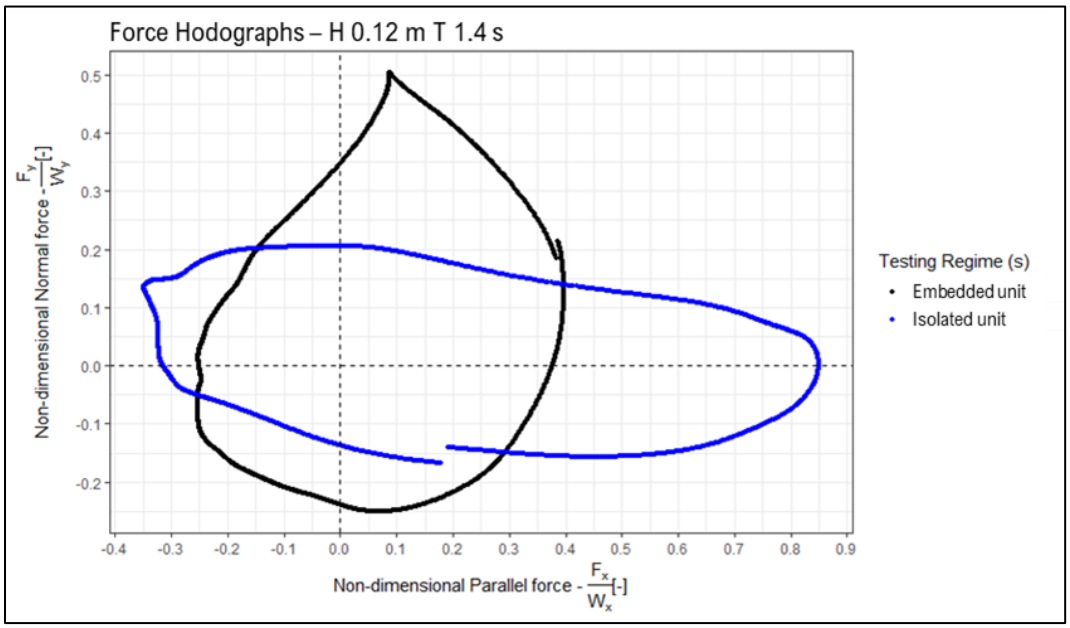

Figure 4-27: Influence of armouring on force loading of instrumented armour unit (H = 0.12 m, T = 1.4 s)

There is also a small increase in negative normal force which would increase unit stability during downrush. This effect is caused by a decreased velocity downslope of the wave as it runs down due to the energy dissipated in the armour layer, causing a piling of water above the unit.

A caveat with these results is that the characteristics of the flow redirection would not necessarily be similar to these results in all armour layers, since the placement of armour units is pseudo-random (within a set of prescribed rules). Armour units are also not deployed independently and are always part of an armour layer, so the isolated unit conditions would not be found in practice.

4.6.1 Influence of Wave Steepness on Force Peaks

Non-dimensional wave steepness is defined as the ratio of wave height to wavelength (H/L). In breakwater design, the steepness is closely related to the surf similarity parameter, or Iribarren number. This non-dimensional number is defined as $\xi = \frac{tan\alpha}{\sqrt{\frac{H}{L_0}}}$, where α is the structure's slope angle, H is the wave height, and L_0 is the deep water wavelength. In this series of experiments, the structural slope angle (α) remains constant, therefore the surf similarity parameter is solely dependent on wave steepness.

The following figures (Figure 4-28 - Figure 4-30) show the relationship between the maximum recorded forces of each scenario tested, and the corresponding wave steepness.

The maximum force imparted to the instrumented unit increases approximately linearly with steepness, (best exemplified by the trendlines of Figure 4-29, though clear in Figure 4-29 and Figure 4-30 as well). This is to be expected, as wave energy increases proportional to wave height[13].

For each force direction the same series of tests were run, and in almost every case force on the instrumented unit was higher in the isolated scenario than in the fully embedded scenario. Maximum force on the embedded unit is attenuated by the sheltering effect of the armour layer.

This sheltering effect is most consistently and most widely noted for the upward parallel force testing. In the upward parallel direction, the force on the armour unit increases more quickly with steepness in the isolated unit scenario. This increase in slope is also observed to a lesser extent in the upward normal and downward parallel directions.

In the slope-parallel direction, sheltering of the unit is much more significant during wave runup than wave rundown, with the largest relative difference of forces between these directions. The largest average maximum forces were also recorded during slope-parallel runup, in excess of twice the stabilizing gravitational force component.

The three steepest tests are outliers in this data. This sudden drop in imparted force may be related to Van der Meer's notional permeability factor (P) (1998), and the critical Iribarren number determined for rock armoured rubble-mound structures. The critical Iribarren number, at which the transition from plunging to surging waves occurs is defined as $\xi_{mc} = \left(6.2p^{0.31}\sqrt{tan\alpha}\right)^{\frac{1}{p+0.5}}$ (van der Meer, 1998). The sudden drop in the data begins at $\xi \cong 4.0$. This corresponds to a steepness of s = 0.035.

Figure 2-12 (Section 2.2.3) shows corresponding values of P for various structures. The tested structure is built of an impermeable core, ~1 D_{na} of filter rock, and 1 D_{na} of interlocked concrete armour units. This permeability factor was determined for rock armour layers, with lower permeabilities than concrete armoured ones. Consequently, none of the example structures are perfect representations, though the $p = 0.1$ structure may be the best representation. A critical Iribarren number of 4.0 corresponds to a permeability factor of ~0.06 or ~0.6.

Data collected during the embedded and isolated unit cases has been interpolated and plotted in Figure 4-28 through Figure 4-30 with a solid trendline showing the linear trend of the data up to the critical Iribarren number for embedded unit testing. The isolated unit trendline is shown with a dashed line. The surrounding grey region around the trendlines indicates the level of uncertainty in the trend fit.

Figure 4-28 shows the relationship between upward slope-parallel force and wave steepness. Upward force increases with wave steepness until approximately $s = 0.035$ ($\xi = 4.0$), after which point the upward force drops dramatically and begins to increase again. This pattern holds as well for downward parallel force (Figure 4-29), as well as for the upward parallel force (Figure 4-30).

[13] $E = \rho g H^2/8$, the sum of energy per unit area of ocean (Reeve, 2018)

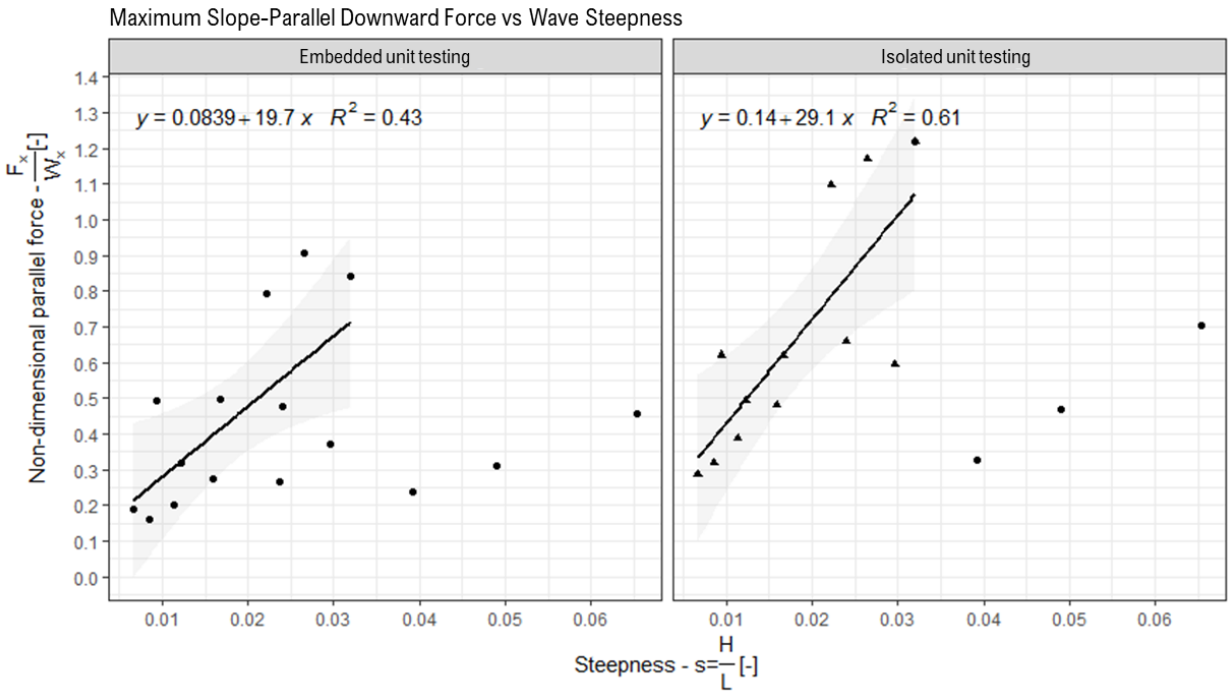

Figure 4-28: Maximum downward parallel force vs wave steepness. Fully armoured scenario (left), and isolated unit scenario (right).

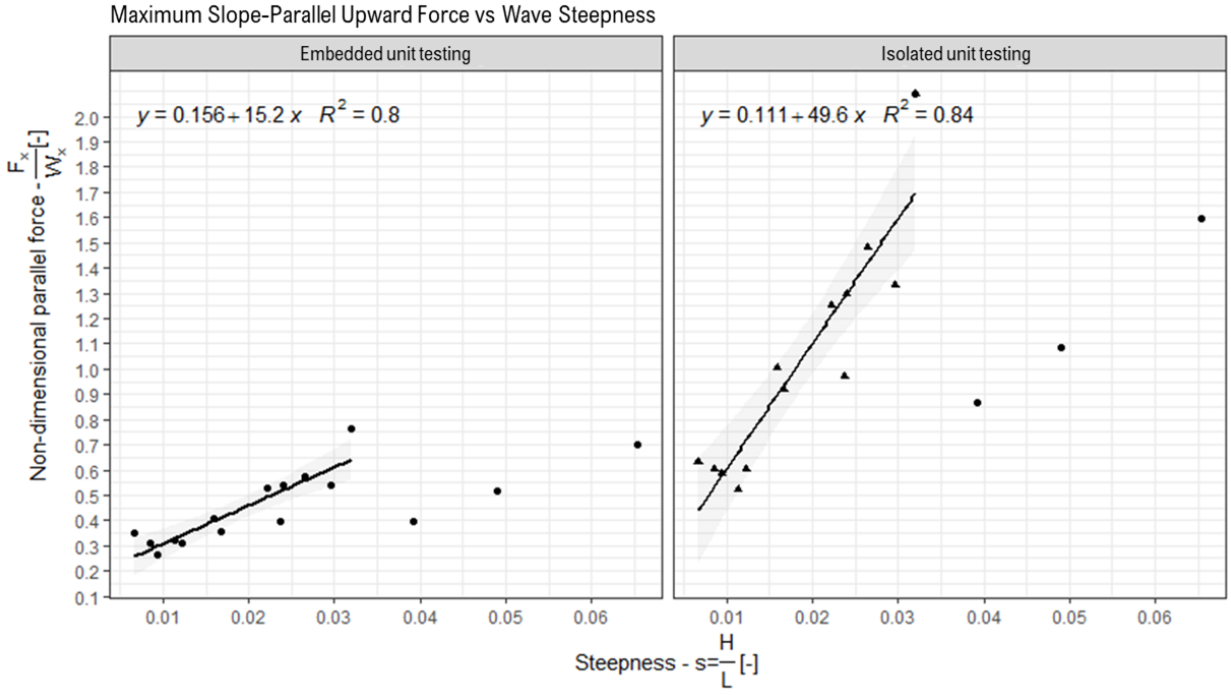

Figure 4-29: Maximum upward parallel force vs wave steepness. Fully armoured scenario (left), and isolated unit scenario (right).

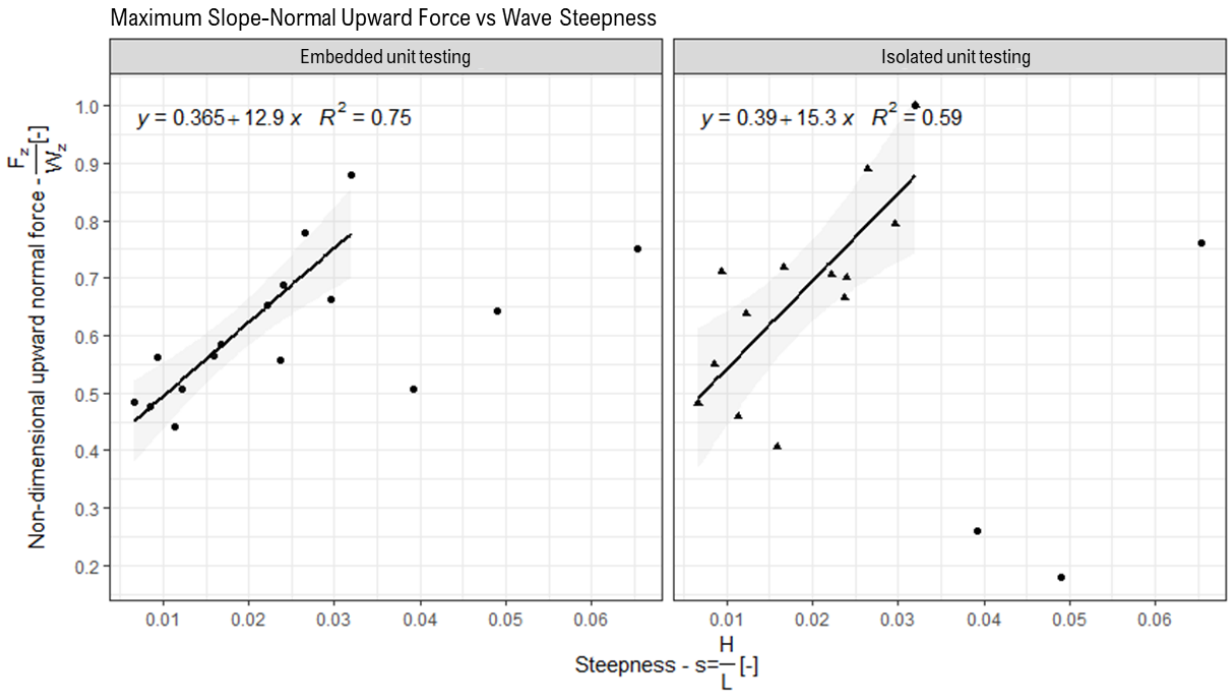

Figure 4-30: Maximum upward normal force vs wave steepness. Fully armoured scenario (left), and isolated unit scenario (right).

5 CONCLUSIONS AND RECOMMENDATIONS FOR FUTURE WORK

This series of tests was focused on the loading of an instrumented Core-loc concrete armour unit in the most critical region of the breakwater – below the still water level where the forces threatening the stability of the armour layer are highest. A summary of results and conclusions:

- Analysis of the force development on the instrumented armour unit found that the maximum slope-parallel and slope-normal forces did not occur simultaneously. The maximum *slope-normal* forces in both the positive and negative directions occur concurrently with extremes in pressure head above the instrumented unit (a combination of primarily hydrostatic but also dynamic pressure). The maximum upward force occurs at the minimum of pressure head, and the maximum downward force occurs at the maximum pressure head. Maximum *slope-parallel* forces however occur as the pressure head is crossing the neutral axis (pressure head equivalent to hydrostatic pressure at rest). Maximum up-slope force as the pressure head is increasing, and maximum down-slope force as the pressure head is decreasing, corresponding to the uprush and downrush phases.

- These loadings are consistent with the expectations of Morison's equation, whereby the inertial force is proportional to flow acceleration in oscillatory flow, and drag force is proportional to flow

velocity. This implies the drag dominance of the slope-parallel direction, and the inertial dominance of the slope-normal direction.

- Significant differences were observed in the loading characteristics of the isolated and embedded armour unit test cases. The presence of the armour layer significantly increased the normal force exerted on the unit and reduced the parallel force. This force redistribution is due in part to an increase in normal force from the redirection of flow within the armour layer which does not occur during an isolated test. Normal force is also affected by an increase in flow away from the armour layer during the downrush as the slope-parallel flow speed is reduced due to the presence of the adjacent armour units. This causes a stagnation of the wave crest during downrush with subsequent increase in water pressure pushing the instrumented unit upward normally away from the filter layer.

- Analysis of the flow above the armour layer shows uprush and downrush velocities in the slope-parallel direction within 10% of each other for both the fully armoured and isolated armour unit scenarios. The magnitudes of the slope-normal velocities during the uprush are significantly higher however in fully armoured testing (increase of approx. 250%). This analysis also depicts the transfer of influence from a parallel dominated flow to normal dominated flow as the pressure increases around the instrumented unit– parallel velocities are highest when pressure head is inflecting. Slope-normal velocities are highest during periods of increasing water-levels with water surface elevation below the SWL.

- Analysis of flow acceleration above the armour layer showed that the distinguishing difference between the slope-normal and slope-parallel directions is that force, flow velocity and flow acceleration are much more symmetrical in the slope-parallel direction, with the flow velocity and force on the unit in particular experiencing large asymmetries. In the slope-normal direction, the occurrence of maxima of force, flow velocity and flow acceleration occur much closer together than in the slope-parallel direction, where the peak velocity precedes the peak force and acceleration.

- Analysis of the statistical distribution of the force peaks in both the slope-parallel and slope-normal direction allow for the rough estimation of extreme values, following a normal distribution. These non-dimensionalized values can be used for the estimation of extreme wave loading from random waves.

- Within the fully armoured testing scenario, increases in incident wave height caused an overall increase in energy in the system, in turn causing an increase in loading of the instrumented armour unit that does not significantly alter the loading response distribution characteristics, but only the magnitude of response.

- Maximum upward normal forces increase as stability number increases at roughly the same rate in embedded and isolated armour unit scenarios. The rate at which maximum upward parallel forces increases is much higher in single unit testing than in fully armoured testing.

- The effect of wave period on instrumented armour unit response is more complex than wave height. Increased wave period did not uniformly affect the magnitude of the maximum force response, though it showed an asymmetrical effect in force hodographs on the slope-parallel force. Longer period waves in this testing formed an interaction between incident and previous waves that show in force hodographs a momentary reverse in slope-parallel force. Longer period waves in this testing formed an interaction between incident and previous waves that show a momentary reverse in slope-parallel force. As wave period increased, the magnitude of this reversal increased. In isolated testing, this effect of period is more pronounced.

- Peak forces exerted on the instrumented unit increased with wave steepness in a mostly linear predictable fashion up to the critical Iribarren number, at which point incident waves transition from plunging to surging waves and a new pattern emerges. Isolated unit testing showed the most divergence between fully embedded testing and solitary unit testing in the upward slope-parallel direction. That direction also exhibited the largest magnitude of force response in isolated testing. In embedded testing, the largest magnitude peak force experienced was in the downward slope-parallel direction, more than twice the submerged weight component. No fully armoured tests produced a unit response in excess of the unit's submerged weight component. Iribarren number

is a function of slope angle and wave steepness, and in this testing, its effect on peak force results would be similar to that of wave steepness.

5.1 Recommendations for Future Work

Potential future work that could result from this series of experiments include:

- These results are applicable to the numerical modelling of rubble mound structures, which has been rapidly advancing in recent years. The data obtained in this study can be used for the calibration and validation of upcoming numerical models, which will aid in design by their prediction of forcing and stability on critical armour units. The testing of isolated units in oscillatory flow is a critical first step in the development of such a model. Larger scale modeling of the loading of isolated armour units is rare in literature. The fully armoured series of testing is valuable for the subsequent phase of numerical model calibration, taking into account the more complex interaction between individual armour units and turbulent flow through the armour layer.
- Increasing the wave height relative to the characteristic length of the CAU. This could be done either through use of a larger wave flume with the same instrument, or through the use of a miniaturized instrumented unit. This would allow for imparted forces in excess of the design forces, and for an examination of the forcing of the unit in failure type conditions.
- A wider variety of sea state conditions, permeabilities, slope angles, and CAU types would allow further aspects of the design methodology to be investigated.
- The miniaturization of the instrumented armour unit would be beneficial for future hydraulic testing, in that this would allow its use with standard model-size concrete armour units, reducing the need for a large wave flume and the manufacture of custom armour units. The instrumented unit could also be improved by the addition of accelerometers for use on testing CAU reaction after armour layer failure and initiation of motion. Wireless communication ability for post-test data transfer would improve results by removing potential flow interference due to connection cable and allow the natural movement of the instrumented armour unit.
- Further testing regimes could include three-dimensional basin type testing, which allows for more complex incident wave fields (such as oblique waves) and the investigation of three-dimensional breakwater geometry (such as roundheads).

- The investigation of the instrumented unit after the initiation of motion would provide valuable data, not only for the potential improvement of design methodology, but also for use in numerical model calibration.
- Random wave analysis would benefit from longer testing times for more robust data analysis.
- Additional loading types other than incident water waves would give valuable insight into breakwater design. For example, ice loads along with incident waves increase complexity of loading and are an area of relatively little engineering knowledge. Similarly, ship strike or debris impact loading would be a valuable area of further investigation.

6 REFERENCES

Altomare, C., Crespo, A. J. C., Rogers, B. D., Dominguez, J. M., Gironella, X., & Gómez-Gesteira, M. (2014). Numerical modelling of armour block sea breakwater with smoothed particle hydrodynamics. Computers and Structures, 130, 34–45. https://doi.org/10.1016/j.compstruc.2013.10.011

Brouwer, M. (2013). The influence of the under layer on the stability of single layer armour units Master of Science Thesis. November. uuid:6b142495-00d3-4ed4-a73e-65c74e30c577

Barends, F. B. J., & Holscher, P. (1988). Modelling interior process in a breakwater. 49–58. https://doi.org/10.1680/dob.13513.0005

Bruun, P. E. R., & Gunbak, A. L. I. R. (1977). STABILITY OF SLOPING STRUCTURES IN RELATION TO ξ=tanα/√(H/L0) RISK CRITERIA IN DESIGN. Coastal Engineering, 1.

Burcharth, H. F. (1993). The Design of Breakwaters. Aalborg University.

CIRIA, CUR, & CETMEF. (2007). The Rock Manual, The use of rock in hydraulic engineering. In CIRIA.

CLI. (2011). CORE-LOC TM Technical Specifications CORE-LOC Technical Specifications Presentation Note.

Cornett, A. (1995). A Study of Wave-Induced Forcing and Damage of Rock Armour on Rubble-Mound Breakwaters. University of British Colombia.

Cornett, A., & Mansard, E. (1995). Wave stresses on rubble-mound armour. Proceedings of the Coastal Engineering Conference, 1, 986–1000.

d'Angremond, K., van der Meer, J. W., & van Nes, C. P. (1995). Stresses in tetrapod armour units induced by wave action. In Proceedings of the Coastal Engineering Conference (Vol. 2, pp. 1713–1726).

Dentale, F., Donnarumma, G., & Carratelli, E. P. (2014). Simulation of flow within armour blocks in a breakwater. Journal of Coastal Research, 30(3), 528–536. https://doi.org/10.2112/JCOASTRES-D-13-00035.1

DAI YB, & KAMEL AM. (1969). Scale Effect Tests for Rubble-Mound Breakwaters. U S Waterways Experiment Station-Research Report H-69-2, 135.

Dominic Reeve, Chadwick, A., & Fleming, C. (2018). Coastal Engineering Processes, Theory and Design Practice 3rd ed.

Eden, D. (2019). Forces and Pressures on Core-Loc Armour Units in Rubble Mound Breakwaters Measured via Instrumented "Smart-Units" (Issue April). University of Ottawa.

Guler, H. G., Ergin, A., & Ozyurt, G. (2014). A comparative study on the stability formulas of rubble mound breakwaters. Proceedings of the Coastal Engineering Conference, 2014-Janua(1988), 1–11.

Hald, Tue, Burcharth, H. F. (2000). AN ALTERNATIVE STABILITY EQUATION FOR ROCK ARMOURED RUBBLE MOUND BREAKWATERS. Coastal Engineering, 1921–1934.

Hald, T. (1998). Wave Induced Loading and Stability of Rubble Mound Breakwaters [Aalborg University]. http://vbn.aau.dk/files/55248437/Wave_Induced_Loading_and_Stability_of_Rubble_Mound_Breakwaters.pdf

Helgason, E., Burcharth, H. F., & Beck, J. B. (2000). Stability of rubble mound breakwaters using high density rock. Coastal Engineering, 1935–1945.

Hofland, B., Arefin, S. S., van der Lem, C., & VAN GENT, M. R. A. (2018). Smart Rocking Armour Units. Proceedings of the 7th International Conference on the Application of Physical Modelling in Coastal and Port Engineering and Science (Coastlab18), July.

Hudson, R. Y. (1959). Laboratory Investigation of Rubble-Mound Breakwaters. Journal of the Waterways and Harbors Division, 85(3), 93–122.

Kamphuis, J. W. (2010). Introduction to Coastal Engineering and Management. World Scientific Publishing.

Latham, J. P., Anastasaki, E., & Xiang, J. (2013). New modelling and analysis methods for concrete armour unit systems using FEMDEM. Coastal Engineering, 77, 151–166. https://doi.org/10.1016/j.coastaleng.2013.03.001

Latham, J. P., Munjiza, A., Mindel, J., Xiang, J., Guises, R., Garcia, X., Pain, C., Gorman, G., & Piggott, M. (2008). Modelling of massive particulates for breakwater engineering using coupled FEMDEM and CFD. Particuology, 6(6), 572–583. https://doi.org/10.1016/j.partic.2008.07.010

Le Méhauté, B. (2000). Froude-Cauchy Similitude. LR Lloyd's Register, 100(July), 1–35.

Maciñeira, E. G., & Burcharth, H. F. (2016). Stability of cube armoured roundheads exposed to long crested and short crested waves. Coastal Engineering, 112, 99–112. https://doi.org/10.1016/j.coastaleng.2016.03.002

Manu, Rao, S., Shirlal, K. G., Prashanth, J., & Rao, K. B. (2011). Physical model studies on stability of concrete armoured breakwaters. ISH Journal of Hydraulic Engineering, 17(December), 51–60. https://doi.org/10.1080/09715010.2011.10515060

Melby, J.A., Turk, G. F. (1997). CORE-LOC Concrete Armor Units.

Melby, J. A., & Trunk, G. F. (1994). The core-loc: optimized concrete armor. Proceedings of 24th Conference on Coastal Engineering, Kobe, Japan., 1426–1438.

Morison, J. R., Johnson, J. W., & Brien, M. P. O. (1953). EXPERIMENTAL STUDIES OF FORCES ON PILES. Coastal Engineering, 4, 340–370.

Reeve, D., Chadwick, A., & Fleming, C. (2018) Coastal Engineering: Processes, Theory and Design Practice. CRC Press.

Sakakiyama, Tsutomu, Kajima, R. (1990). Scale Effect of Wave Force on Armor Units. Coastal Engineering.

Santos, J. A. (2019). Delft University of Technology Measuring Wave Run-Up , Overtopping And Damage Of Rubble-Mound Breakwaters In Scale Model Tests.

Sawaragi, T., Ryu, C., & Iwata, K. (1983). Considerations of the Destruction Mechanism of Rubble Mound Breakwaters Due To the Resonance Phenomenon. Proc. of the 8th Int. Harbour Congress, 3.197-3.208.

Simpalean, A. R. (2019). Experimental Investigations of Core-Loc Armour Units (Issue January). University of Ottawa.

Tørum, A. (1994). Wave-Induced Forces on Armor Unit on Berm Breakwaters. 120(3), 251–268.

Troch, P., De Rouck, J., & Van Damme, L. (1998). Instrumentation and prototype measurements at the Zeebrugge rubble mound breakwater. Coastal Engineering, 35(1–2), 141–166. https://doi.org/10.1016/S0378-3839(98)00026-X

Turk, G.F., Melby, J. A. (1997). Dynamic Structural Response of CoreLoc. USACE Waterways Experiment Station.

United States Army Corps of Engineers. (2011). Coastal Engineering Manual: Part VI Chapter 5 Fundamentals of Design. 1100(Part VI), 378.

Van Den Bosch, I., Ten Oever, E., Bakker, P., & Muttray, M. (2012). Stability of interlocking armour units on a breakwater crest. Proceedings of the Coastal Engineering Conference, 1–10.

Van der Meer, J.W., Allsop, N. W. H., Bruce, T., De Rouck, J., Kortenhaus, A., Pullen, T., Schüttrumpf, H., Troch, P., & Zanuttigh, B. (2016). EurOtop 2016: Manual on wave overtopping of sea defences and related structures An overtopping manual largely based on European research, but for worldwide application. 264. http://www.overtopping-manual.com/index.html

Van der Meer, Jentsje W. (1987). Stability of breakwater armour layers - design formulae. Coastal Engineering, 11(3), 219–239. https://doi.org/10.1016/0378-3839(87)90013-5

Van der Meer, Jentsje W. (1999). Design of concrete armour layers. Proceedings of the International Conference Coastal Structures ’99 : Santander, Spain, 7-10 June 1999, Volume 1, 213–221.